



*nanomaterials*



Review

---

# Impacts of the Catalyst Structures on CO<sub>2</sub> Activation on Catalyst Surfaces

---

Ubong J. Etim, Chenchen Zhang and Ziyi Zhong

Special Issue

Bifunctional Metal Oxides as Heterogeneous Catalysis for CO<sub>2</sub> Adsorption and Conversion

Edited by

Dr. Poernomo Gunawan and Prof. Dr. Ziyi Zhong



<https://doi.org/10.3390/nano11123265>



Review

# Impacts of the Catalyst Structures on CO<sub>2</sub> Activation on Catalyst Surfaces

Ubong J. Etim<sup>1</sup>, Chenchen Zhang<sup>1,2</sup> and Ziyi Zhong<sup>1,\*</sup>

<sup>1</sup> Department of Chemical Engineering, Guangdong Technion-Israel Institute of Technology (GTIIT), Shantou 515063, China; ubong.etim@gtiit.edu.cn (U.J.E.); chenchen.zhang@gtiit.edu.cn (C.Z.)

<sup>2</sup> Wolfson Faculty of Chemical Engineering, Technion-Israel Institute of Technology (IIT), Haifa 32000, Israel

\* Correspondence: ziyi.zhong@gtiit.edu.cn

**Abstract:** Utilizing CO<sub>2</sub> as a sustainable carbon source to form valuable products requires activating it by active sites on catalyst surfaces. These active sites are usually in or below the nanometer scale. Some metals and metal oxides can catalyze the CO<sub>2</sub> transformation reactions. On metal oxide-based catalysts, CO<sub>2</sub> transformations are promoted significantly in the presence of surface oxygen vacancies or surface defect sites. Electrons transferable to the neutral CO<sub>2</sub> molecule can be enriched on oxygen vacancies, which can also act as CO<sub>2</sub> adsorption sites. CO<sub>2</sub> activation is also possible without necessarily transferring electrons by tailoring catalytic sites that promote interactions at an appropriate energy level alignment of the catalyst and CO<sub>2</sub> molecule. This review discusses CO<sub>2</sub> activation on various catalysts, particularly the impacts of various structural factors, such as oxygen vacancies, on CO<sub>2</sub> activation.

**Keywords:** CO<sub>2</sub> conversion; CO<sub>2</sub> activation; metal oxide nanoparticles; oxygen vacancies



**Citation:** Etim, U.J.; Zhang, C.; Zhong, Z. Impacts of the Catalyst Structures on CO<sub>2</sub> Activation on Catalyst Surfaces. *Nanomaterials* **2021**, *11*, 3265. <https://doi.org/10.3390/nano11123265>

Academic Editor:  
Francesc Viñes Solana

Received: 14 October 2021  
Accepted: 23 November 2021  
Published: 30 November 2021

**Publisher's Note:** MDPI stays neutral with regard to jurisdictional claims in published maps and institutional affiliations.



**Copyright:** © 2021 by the authors. Licensee MDPI, Basel, Switzerland. This article is an open access article distributed under the terms and conditions of the Creative Commons Attribution (CC BY) license (<https://creativecommons.org/licenses/by/4.0/>).

## 1. Introduction

The presence of CO<sub>2</sub> in high concentrations in the atmosphere leads to a myriad of harmful consequences, including climate change and sea-level rise. Therefore, CO<sub>2</sub> emission mitigation has become a top priority of various governments globally, and research interest in recent years is being dedicated to deriving the positive impact of the CO<sub>2</sub> levels through efficient capture and utilization. An economically viable approach to mitigating the monstrous effect of CO<sub>2</sub> and reducing its presence in the environment is to transform it into value-added products. The conversion of CO<sub>2</sub> to fuels and chemicals has attracted increasing research attention globally, and great achievements have been recorded in the production of C<sub>1</sub> products, such as methanol, methane, and formic acid [1–3].

CO<sub>2</sub> is a chemically inert molecule due to its kinetically stable nature; thus, its conversion by reduction to economically viable products relies on its activation to kinetically vibrant species [4]. The stable nature of CO<sub>2</sub> and high activation barrier (1.9 eV) implies that its transformation over catalyst surfaces should create a unique environment for facilitating activation pathways [5–9]. It is possible to apply either homogeneous or heterogeneous catalysis to transform CO<sub>2</sub> into value-added products, the latter through thermo-, electro-, or photocatalysis, to induce the catalytic reactions [10,11]. Each of these processes comes with its shortcomings and benefits. The electro-/photocatalytic processes have advantages in tuning the reaction products but are difficult to scale up [12]. Given the intricacy of the accompanying reaction mechanisms and the dynamics of catalysis under reaction conditions, particularly for the heterogeneous system, there is still a lack of very fundamental understanding of the chemistry of CO<sub>2</sub> reduction. In the presence of small but reactive molecules such as hydrogen or water, CO<sub>2</sub> can be transformed into stable products over heterogeneous catalysts with more favorable thermodynamics. The catalyst must possess activity for activating CO<sub>2</sub> in addition to enabling effective conversion reactions. Adsorption and activation are two important steps that occur during the CO<sub>2</sub> reduction

on catalyst surfaces. The adsorption (physisorption and chemisorption) of CO<sub>2</sub> on the surface of heterogeneous catalysts has become a subject of growing research interest in recent years [13].

The activation of CO<sub>2</sub> on the heterogeneous catalyst surface yields CO<sub>2</sub>-derived species that eventually convert to useful products. Several CO<sub>2</sub>-derived species, including carboxylate and carbonates, have been identified, irrespective of which approach is adopted for CO<sub>2</sub> conversion [6]. The generation of specific activated carbon species determines the kind and selectivity of the product(s). Co-reactants such as water contribute to the overall reduction reaction by promoting adsorption and subsequent activation. As with most chemical conversion technologies, the choice of catalyst is also an important factor, which must have suitable selectivity and activity for activating CO<sub>2</sub> under relatively mild conditions. Many studies reported in the literature tried to understand how to promote the chemisorption and subsequent activation of CO<sub>2</sub> by focusing on catalysts preparation and structures. Specifically engineered or surface-modified catalysts have shown improved performance for CO<sub>2</sub> activation. Catalysts (metal oxides) with rich surface defects or high concentrations of oxygen vacancies have been particularly effective for CO<sub>2</sub> activation. Oxygen vacancies can greatly influence the interaction of CO<sub>2</sub> with the surface and enhance the adsorption of CO<sub>2</sub> molecules. Thus, oxygen vacancies play important roles in CO<sub>2</sub> conversion. Surface defects can be created in metal oxide catalysts either during reactions or incorporated by external methods. Understanding the nature of CO<sub>2</sub> in the activated form and the catalyst characteristics will be important in developing novel strategies for activating CO<sub>2</sub>. An appreciable understanding of the reaction of CO<sub>2</sub> on pure metal surfaces is well documented; however, less is known about the reactivity of CO<sub>2</sub> on metal oxide surfaces, e.g., how the surface defects contribute to the mechanism of CO<sub>2</sub> activation. The central aim of this work is to discuss the CO<sub>2</sub> activation mechanism on metal oxide surfaces, particularly the roles of the surface defects in the activation process.

### 1.1. CO<sub>2</sub> Conversion to Chemicals: Challenges, Thermodynamics, and Kinetics

The development of environmentally viable technologies for the utilization of CO<sub>2</sub> as a chemical feedstock remains a great challenge because of its thermodynamic stability (CO<sub>2</sub> possesses a highly stable  $\pi$ -conjugated structure) and kinetic inertness. Regarding the energy requirement, reactions involved in CO<sub>2</sub> conversion can be classified into two major categories: The first category involves adding CO<sub>2</sub> to a reaction where the other reactants with higher Gibbs free energy supply energy; such reactions produce the likes of carboxylates and lactones, carbamates, urea, isocyanates, and carbonates. These reactions are energetically favorable and often can be run without any catalyst. The second category is the CO<sub>2</sub> reduction reaction, through which important industrial chemicals such as formate, oxalates, carbon monoxide, formaldehyde, methanol, and methane can be obtained. Table 1 presents an overview of the standard enthalpies ( $\Delta H^\circ_{298K}$ ) and Gibbs free energies ( $\Delta G^\circ_{298K}$ ) for different products formed from CO<sub>2</sub> conversion reactions. These reactions require an external energy source to activate the strong C=O bond in CO<sub>2</sub> and a catalyst to lower the energy barrier. It will be energy-demanding if CO<sub>2</sub> is used as a single reactant (Table 1, Equation (1)). However, it becomes thermodynamically easier if another substrate molecule, such as H<sub>2</sub>, with higher Gibbs free energy, is introduced as a co-reactant (Table 1, Equations (2)–(10)). Another difficulty is that the final products derived from CO<sub>2</sub> are mostly in the liquid phase (e.g., formic acid, methanol, and higher hydrocarbons). As these reactions involve a phase change from gaseous reactants into liquid products, they are thus entropically unfavorable.

The unfavorable thermodynamic character of CO<sub>2</sub> stems from its highly stable chemical nature. Both  $\Delta S$  and  $\Delta H$  ( $-393.5 \text{ kJ}\cdot\text{mol}^{-1}$ ), which govern the thermodynamics, are unfavorable for CO<sub>2</sub> conversion as a result of the very strong C=O bond with a higher dissociation energy ( $\sim 750 \text{ kJ}\cdot\text{mol}^{-1}$ ) [14,15]. Thus, highly active catalysts are necessary for the activation of CO<sub>2</sub>. Good catalysts should be able to break the kinetic barriers and enable the chemical conversion of CO<sub>2</sub> under relatively mild reaction conditions [16]. While

efforts have been demonstrated in this regard, leading to fair knowledge of the reaction mechanisms, more research inputs are still needed to comprehend the principles governing the catalytic transformation of CO<sub>2</sub> into value-added chemicals that can drive the industrial scale utilization.

**Table 1.** Standard enthalpies ( $\Delta H^\circ_{298\text{K}}$ ) and Gibbs free energies ( $\Delta G^\circ_{298\text{K}}$ ) for different products formed via CO<sub>2</sub>.

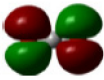

Equation	Reaction	$\Delta H^\circ_{298\text{K}}$ (kJ·mol <sup>-1</sup> )	$\Delta G^\circ_{298\text{K}}$ (kJ·mol <sup>-1</sup> )
(1)	$2\text{CO}_2 \rightarrow 2\text{CO} + \text{O}_2$	293.0	257.2
(2)	$\text{CO}_2 + \text{H}_2 \rightarrow \text{CO} + \text{O}_2$	41.2	28.6
(3)	$\text{CO}_2 + 3\text{H}_2 \rightarrow \text{CH}_3\text{OH} + \text{H}_2\text{O}$	-49.5	3.5
(4)	$2\text{CO}_2 + 6\text{H}_2 \rightarrow 2\text{C}_2\text{H}_5\text{OH} + 3\text{H}_2\text{O}$	-86.7	-32.4
(5)	$\text{CO}_2 + 4\text{H}_2 \rightarrow \text{CH}_4 + 2\text{H}_2\text{O}$	-165.0	-113.5
(6)	$2\text{CO}_2 + 7\text{H}_2 \rightarrow \text{C}_2\text{H}_6 + 4\text{H}_2\text{O}$	-132.1	-78.7
(7)	$3\text{CO}_2 + 10\text{H}_2 \rightarrow \text{C}_3\text{H}_8 + 6\text{H}_2\text{O}$	-125.0	-70.9
(8)	$4\text{CO}_2 + 13\text{H}_2 \rightarrow \text{n-C}_4\text{H}_{10} + 8\text{H}_2\text{O}$	-121.6	-66.9
(9)	$2\text{CO}_2 + 6\text{H}_2 \rightarrow \text{C}_2\text{H}_4 + 4\text{H}_2\text{O}$	-64.0	-28.7
(10)	$3\text{CO}_2 + 9\text{H}_2 \rightarrow \text{C}_3\text{H}_6 + 6\text{H}_2\text{O}$	-83.6	-42.1
(11)	$4\text{CO}_2 + 13\text{H}_2 \rightarrow \text{n-C}_4\text{H}_8 + 8\text{H}_2\text{O}$	-90.3	-45.2

Thermodynamics data adapted with permission from the authors of [17]. Copyright 2016 Elsevier B.V.

### 1.2. General Properties of CO<sub>2</sub> Molecule: Molecular Structure and Bonding Properties

CO<sub>2</sub> is a linear non-polar molecule in its ground state possessing two equivalent C–O double bonds, and its main properties are summarized in Table 2 [18–21]. Its high oxidation state of carbon (+4) makes it a thermodynamically stable molecule, requiring a high energy input for activation and reaction for producing value-added products. The activation of CO<sub>2</sub> typically involves altering the molecular properties, such as the C–O bond length and O–C–O angle. According to the molecular orbital diagram of CO<sub>2</sub> (Figure 1a), there are a total of 16 valence electrons distributed among the three atoms (one carbon and two oxygen atoms) in the molecule. The carbon atom exhibits an electrophilic character, conveying an exception to the overall energetics of the CO<sub>2</sub> molecule, and thus the nucleophilic and electrophilic reactions are preferred on the C- and O-atoms, respectively. In other words, activation of CO<sub>2</sub> can be achieved both nucleophilically and/or electrophilically through the carbon or oxygen atom, respectively [22]. For example, nucleophilic compounds such as water and hydroxides prefer to react at the carbon center; the carbon atom could also gain electrons from a catalyst surface. On the other hand, oxygen atoms in the CO<sub>2</sub> molecule with lone pairs of electrons can donate them; thus, CO<sub>2</sub> molecules can simultaneously donate or accept electrons, leading to mixed coordination (i.e., binding on both C and O atoms). In the presence of a substrate such as water, the charge on the carbon atom can increase according to a DFT study using a polarizable continuum model with a linear geometry [7], which can boost the carbon atom reactivity of CO<sub>2</sub>. Non-bonding orbitals are located on the 1s shells of the C and O atoms and do not participate in CO<sub>2</sub> bonding [23,24]. The introduction of an electron into the antibonding orbital  $2\pi_u$ , as shown in Figure 1b, results in the formation of the CO<sub>2</sub> radical anion (CO<sub>2</sub><sup>•-</sup>) or CO<sub>2</sub><sup>δ-</sup>, which can be stabilized by changing the structure from the linear to the bent form [23]. For the anionic CO<sub>2</sub> molecule, the carbon atom is nucleophilic, and the molecule has a bent geometry (Figure 1c).

**Table 2.** Properties of CO<sub>2</sub> molecule.

Property	Boiling Point (°C)	Density Gas (g/L)	Dipole Moment	Bond Polarity	$\Delta H_f$ (298 K) (kJ·mol <sup>-1</sup> )	Bond Energy (kJ·mol <sup>-1</sup> )	C–O Bond Distance (Å)	Bond Angle (degree)	Band Gap	Charge	<sup>a</sup> HOMO Structure	<sup>b</sup> LUMO Structure
CO <sub>2</sub>	−78.5 (sublimes)	1.98	0	1.0	−393.5	806	1.16	180	ca. 8 e	C: −0.360 O: +0.19		

<sup>a</sup> Highest occupied molecular orbital, <sup>b</sup> Lowest unoccupied molecular orbital (high energy for ground state CO<sub>2</sub> molecule).

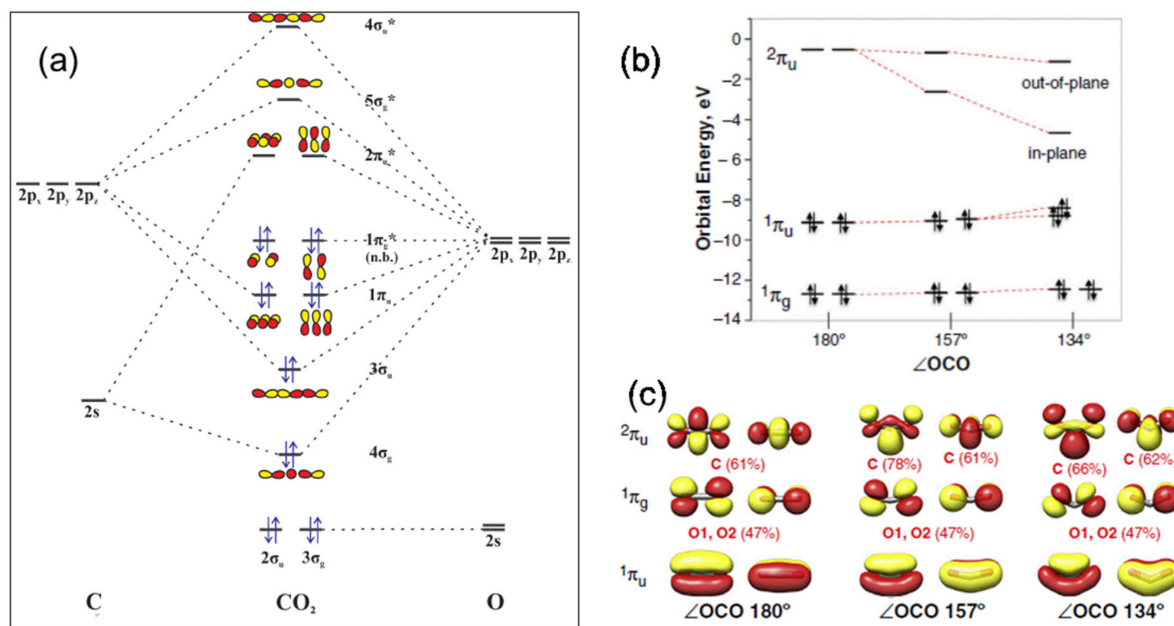


**Figure 1.** (a) Molecular orbital of CO<sub>2</sub> at the ground state. Reproduced with permission from the authors of [23]. Copyright 2016 Elsevier B.V. (b) Walsh diagram for the orbital energies upon CO<sub>2</sub> bending, and (c) molecular orbitals of CO<sub>2</sub> at different OCO angles (carbon and oxygen weights are given in %). Reproduced with permission from the authors of [25]. Copyright 2015 Elsevier B.V.

## 2. CO<sub>2</sub> Activation and Different Modes

CO<sub>2</sub> is an inert molecule, but its reactivity can be increased by activation, which can be measured by the difference in molecular properties (geometry and electronic properties) of the charged species relative to those in the stable ground state [5]. The activation of a stable CO<sub>2</sub> molecule can take one of the following modes:

- bending of the O–C–O angle from 180 degrees,
- elongation of at least one of the two C–O bonds,
- polarization of the charges on C and O, leading to the transfer of charge/electron to CO<sub>2</sub>,
- hydride transfer, or
- redistribution of charges.

Generally, over heterogeneous catalysts, the activation of CO<sub>2</sub> molecule involves a charge transfer (effect iii) from the catalyst to the molecule, which results in elongation of the C–O bond length and reduction in/bending of O–C–O bond angle (effects i and ii). The activation can proceed in the presence or absence of reducing species such as hydrogen [26,27]. Mondal et al. [27], via ab initio DFT calculations, observed the C–O bond in CO<sub>2</sub> to increase from 1.16 Å to between 1.27 and 1.42 Å on Zr clusters. Furthermore, the O–C–O bond angle changed from 180 to between 115 and 136°. These occurred through chemisorption and subsequent activation of the free CO<sub>2</sub> on the surface of the metal cluster

as a result of charge migration from the Zr cluster to the CO<sub>2</sub>, forming partially charged CO<sub>2</sub><sup>δ-</sup> species.

At the molecular level, the CO<sub>2</sub> activation results from partial electron transfer into the LUMO [28]. Based on the molecular orbitals analysis, the reverse charge donation to LUMO of the activated CO<sub>2</sub> is responsible for the CO<sub>2</sub> binding, which determines the degree of CO<sub>2</sub> activation. Consequently, the binding energy originating from the backward donation can be explored to explain the degree of CO<sub>2</sub> activation [29]. However, the binding energy is affected by the coordination number and the deformation of the ligand. Definitive evidence for CO<sub>2</sub> activation is the bending of the linear OCO configuration. The more bent the geometry, the lower the energy level of the in-plane (i.e., to the plane of bending) contribution of the 2π<sub>u</sub> LUMO will be.

CO<sub>2</sub> bending lowers the LUMO's energy to a significant degree, particularly that of the in-plane 2π<sub>u</sub> orbital (Figure 1b), and increases the carbon electron density associated with it, facilitating the transfer of an electron to the molecule. As a result, bending leads to the C–O bond weakening by stretching up to 0.11 Å in comparison with the linear state. This may lead to the dissociation of CO<sub>2</sub> on the catalyst surface into CO and O species. Unlike the HOMO that possess the characteristics of the O p-orbital, the LUMOs exhibit mainly the C p-orbital character. These features enhance the CO<sub>2</sub> reduction (electron accepting) ability.

However, some of the above indicators or differences in other properties may not sufficiently explain the activation of the CO<sub>2</sub> molecule. It has been shown that bending CO<sub>2</sub> molecules to smaller O–C–O angles (less than 180 degrees) and an electron transfer to the π\*-antibonding orbital correlate more with strong adsorption, leading to the formation of undesired carbon species such as carbonates [30]. CO<sub>2</sub> activation on metal oxide surface as studied using an Artificial Intelligence (AI) model revealed the binding of an O atom to a surface cation, resulting in an increase in the C–O bond length and weakening of the bond strength. This confirms only the C–O bond elongation as a valid indicator of CO<sub>2</sub> activation [30].

The transfer of electrons to CO<sub>2</sub> always precedes a key step—adsorption (chemisorption or physisorption), and the structural properties of the activated CO<sub>2</sub> species are evident after adsorption of the CO<sub>2</sub> molecule. In many examples, the interaction that results upon chemisorption leads to the formation of CO<sub>2</sub><sup>δ-</sup>. This carbon species present different structures depending on the mode of adsorption [31,32], including oxygen coordination, carbon coordination, and mixed coordination (Figure 2). Coordination through the oxygen atom results in two possible structures of bidentate species as shown in Figure 2a. The formation of a carbonate-like species is evident in the carbon binding mode. Structures of both species can be observed in the combined coordination mode. These different binding modes play a crucial part in determining the reaction pathways as a result of the different possible intermediates that can form [32].

The other chemisorbed CO<sub>2</sub> species is the CO<sub>3</sub><sup>2-</sup>, which is direct evidence of the transfer of charge from surface oxygen to the CO<sub>2</sub> and a molecule bending to form a [O–CO<sub>2</sub>]<sup>2-</sup> complexes [33].

The chemisorption of CO<sub>2</sub> is a critical step in CO<sub>2</sub> conversion reactions [34–36]. For example, the dissociation into CO and O or hydrogenation to form different products such as methane or methanol follows the adsorption of CO<sub>2</sub>. However, the adsorption process must avoid producing inactive surface species (e.g., carbonates) that poison catalysts [26]. From both experimental and theoretical investigations, the activation of CO<sub>2</sub> over a heterogeneous catalyst surface involves its adsorption followed by charge transfer (electron) from the catalyst active site to the CO<sub>2</sub> molecule [35,37,38]. Upon accepting an extra electron, the molecular CO<sub>2</sub> forms the radical anion, CO<sub>2</sub><sup>-</sup> or CO<sub>2</sub><sup>δ-</sup> [31]. This perturbation of the molecular state results in weakening of the C–O bond and reduction in O–C–O bond angle (bending) [34,39]. CO<sub>2</sub> activation was observed from the infrared vibrational spectra of the CO<sub>2</sub> molecule adsorbed onto Ti<sub>8</sub>C<sub>12</sub> [35]. A peak that was obviously lacking in the gaseous state CO<sub>2</sub> molecule was observed. CO<sub>2</sub> is adsorbed and activated by dissociating into CO

and O. In some CO<sub>2</sub> transformation reaction mechanisms, CO has been identified as an important intermediate in the reaction pathway.

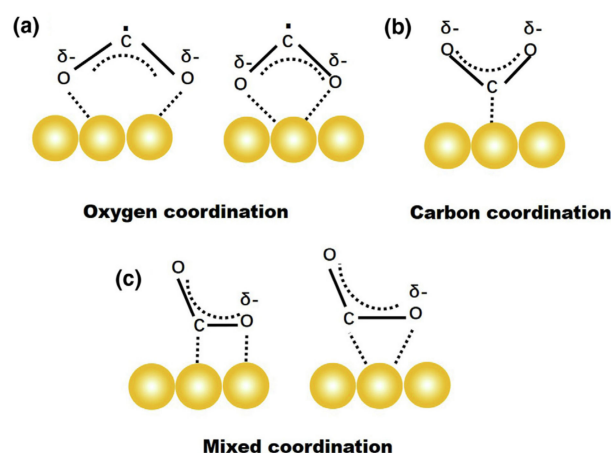
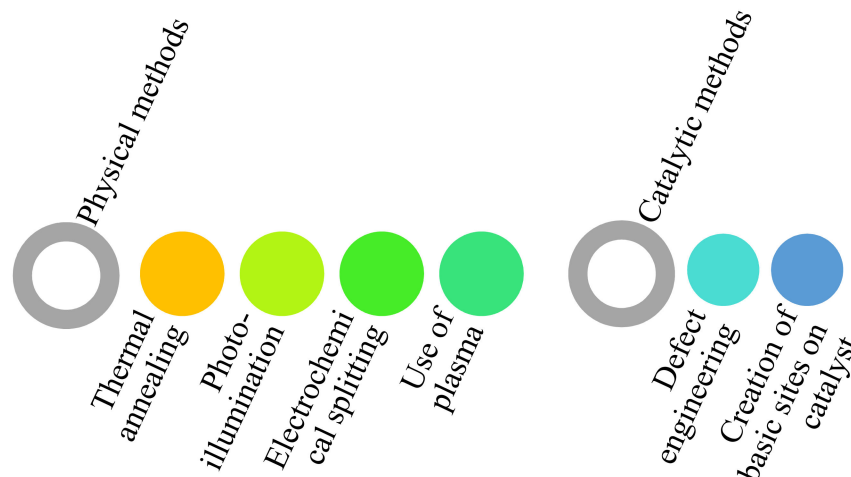


**Figure 2.** Possible structures of CO<sub>2</sub><sup>δ−</sup> on heterogeneous catalyst surface: (a) oxygen coordination, (b) carbon coordination and (c) mixed coordination. Reproduced with permission from the authors of [31]. Copyright 2016 The Royal Society of Chemistry.

The adsorption and activation of CO<sub>2</sub> molecules can be enhanced by adopting the strategies presented in Scheme 1.



**Scheme 1.** Strategies for enhancing CO<sub>2</sub> activation of oxide-based catalyst surface.

### 2.1. Photocatalytic Activation of CO<sub>2</sub>

Solar-driven catalytic (photo)reduction of CO<sub>2</sub> with H<sub>2</sub>O at low temperature (room temperature) and pressure (atmospheric pressure) is an approach for economically utilizing large amounts of CO<sub>2</sub> emitted [40]. CO<sub>2</sub> photoreduction mainly involves the following elementary steps:

- i. Photon absorption and excited carrier generation.
- ii. Activation of CO<sub>2</sub> to form an anion radical, CO<sub>2</sub><sup>•−</sup>, or other intermediates by the photoexcited electrons.
- iii. Dissociation of the C–O bond, involving the participation of protons and electron transfer, generating different products.
- iv. Desorption of reduced products from the active sites [41,42].

During the photoreduction process in the presence of a photocatalyst, an electron–hole pair is generated upon photo-illumination of the catalyst surface. The generated electrons

transfer to the stable  $\text{CO}_2$  molecule and activate it to intermediates species that can be much easily converted to a variety of chemical and fuel products, including  $\text{CO}$ ,  $\text{CH}_4$ ,  $\text{CH}_3\text{OH}$ , and  $\text{HCOOH}$ . However, water, which is typically used as the reducing agent in  $\text{CO}_2$  photoreduction reaction, results in low photocatalytic efficiency [40,43]. Some of the reasons for the observed low efficiency on  $\text{TiO}_2$  photocatalyst include:

- i. the one-electron transfer to form  $\text{CO}_2^-$  is thermodynamically unfavorable as it requires a very negative reduction potential of  $-1.9$  V NHE;
- ii. the photoexcited holes (or OH radicals) easily oxidize water to oxygen, or oxidize the intermediates and products converted from  $\text{CO}_2$  to undesirable products (reverse reactions); and
- iii. the electron–hole pairs recombination rate is much faster.

Almost no photocatalyst can provide sufficiently high energy to transfer a single photoexcited electron to a neutral state  $\text{CO}_2$ . This remains the most important obstacle to the photoreduction of  $\text{CO}_2$ . Consequently, the multielectron process is often adopted; however, this leads to slow reaction kinetics. The above limitations can be checked by stabilizing the LUMO of  $\text{CO}_2$  close to or lower than the conduction band minimum (CBM) of the semiconductor; this especially can decrease the strongly negative potential [44]. In the photoreduction process, it is possible to regulate light irradiation to tune the  $\text{CO}_2$  conversion as desired in comparison with the conventional thermal reaction. Thus, the photo-assisted heterogeneous catalytic reaction can proceed with quite low energy consumption for product formation and a much faster response for the changes in the reaction condition.

The photoreduction of  $\text{CO}_2$  also involves important steps, namely, adsorption, activation of  $\text{CO}_2$ , and dissociation of the  $\text{C}=\text{O}$  bond. Although the adsorption precedes the activation step followed by the dissociation step, they all work synchronously to realize the overall process, and these steps are often paid less attention in the literature. The transfer of charge (photogenerated electrons) to the  $\text{CO}_2$  molecule from the photocatalyst surface occurs during the activation step. At the metal-oxide interface, the ease of electron transfer depends on the electron affinity of  $\text{CO}_2$  and its interaction with the catalyst surface [45]. In addition, the adsorption and activation properties of  $\text{CO}_2$  on the surface of photocatalyst greatly affect the activity and product selectivity. Generally, the activation and subsequent reduction of  $\text{CO}_2$  involves the participation of protons and electrons transfer (single or multiple electrons). This generates  $\text{CO}_2^-$  by one-electron transfer to  $\text{CO}_2$ , which is an important activated intermediate in  $\text{CO}_2$  reduction reactions [40]. A more feasible pathway involves multiple electrons and a corresponding number of protons. Therefore, controlling the transfer of electrons and protons is crucial for the activation of  $\text{CO}_2$  [46]. Understanding the  $\text{CO}_2$  activation mechanism is essential to guide the improvement and development of effective photocatalysts to promote  $\text{CO}_2$  reduction efficiency [47]. We herein briefly discuss the activation of  $\text{CO}_2$  through the photocatalytic reduction mechanism. The adsorption of  $\text{CO}_2$  on photocatalysts through interactions with surface atoms can activate  $\text{CO}_2$  by transferring an electron from excited photocatalysts to the  $\text{CO}_2$ , although adsorption and the interactions between  $\text{CO}_2$  and the photocatalyst surface sometimes are not strong enough to sufficiently lower the barrier and enable the transfer of conduction band electrons. In this case, efforts are directed at improving the photocatalytic efficiency by fabricating photocatalysts with various features to enhance the chemisorption of  $\text{CO}_2$  [46].

Researchers have studied many strategies to promote adsorption and activation of  $\text{CO}_2$  on metal oxides. Both theoretical and experimental studies have revealed that these processes are significantly influenced by the crystal phase of  $\text{TiO}_2$  photocatalysts and their surface defects [48–51]. Graphene-laden catalysts have been observed with high photocatalytic activity. In addition to increasing  $\text{CO}_2$  adsorption, there are reports about the increasing separation efficiency of photogenerated electrons and holes of graphene containing photocatalysts. Reduced graphene (rGO)-adorned Pt/ $\text{TiO}_2$  photocatalysts with enhanced photogenerated charges separation and  $\text{CO}_2$  adsorption was reported by Zhao et al. [52]. The surface hydroxyl and abundant  $p$  electron of rGO provide adsorption and activation sites for  $\text{CO}_2$ . Doping photocatalysts with alkaline-earth or transition



metal oxides can provide more surface basic sites for CO<sub>2</sub> adsorption and activation, thus improving reaction kinetics and product selectivity [53,54]. For example, 1.0 wt% MgO–Pt–TiO<sub>2</sub> gave a superior photocatalyst performance in reducing CO<sub>2</sub> into CH<sub>4</sub> in the presence of H<sub>2</sub>O in comparison with Pt–TiO<sub>2</sub> [55]. MgO presence provided more surface basic sites for chemisorption of CO<sub>2</sub>. Insertion of defects or vacancies in photocatalysts can provide more sites for CO<sub>2</sub> adsorption and activation. Zhao et al. [56] constructed O vacancies in ZnAl-LDH nanosheets for photocatalytic reduction of CO<sub>2</sub>. The resulting Zn<sup>+</sup>–V<sub>O</sub> complexes served as trapping sites for adsorption of CO<sub>2</sub> and H<sub>2</sub>O that boosted the photocatalytic CO<sub>2</sub> reduction activity. Incorporating an appropriate co-catalyst can enhance CO<sub>2</sub> activation. Pt/Cu<sub>2</sub>O-modified TiO<sub>2</sub> exhibited high activity for the selective photocatalytic reduction of CO<sub>2</sub> into CH<sub>4</sub>. Deposited Pt can capture photogenerated electrons and generate H<sub>2</sub> and CH<sub>4</sub>, while the Cu<sub>2</sub>O can enhance the CO<sub>2</sub> chemisorption and inhibit H<sub>2</sub>O [57]. In general, on the surface of photocatalysts, these strategies can be adopted to activate CO<sub>2</sub> molecules essential for CO<sub>2</sub> conversion. Photocorrosion of oxide photocatalysts can generate in situ photoinduced oxygen vacancies to activate a defect reaction for splitting CO<sub>2</sub> under mild reaction conditions that eliminate the need for high temperature and water presence. Wang et al. [58] used an amorphous semiconductor photocatalyst with weak lattice constraint via the photocorrosion mechanism to facilitate the generation of oxygen vacancies, which can react with oxygen atoms of CO<sub>2</sub>, splitting it into C and O<sub>2</sub>. Such a defect reaction can be sustained by continuous photogenerated hole oxidation of surface oxygen atoms of the photocatalyst to form an oxygen vacancy and O<sub>2</sub>. On the other hand, the photogenerated electrons would reduce the carbon species of CO<sub>2</sub> to solid carbon. A major challenge is how to generate a high concentration of oxygen vacancies on the photocatalyst surface [58].

Recently, photoinduced electrons have been shown to benefit the activation of stable CO<sub>2</sub> molecules for the photoreduction process [44,59]. Hot electrons generated upon light irradiation enhanced the CO<sub>2</sub> conversion. The enhancement was related to the change in the HOMO–LUMO energy gap of the CO<sub>2</sub> adsorbed on the metal surface. According to DFT calculations, CO<sub>2</sub> can strongly bind to Ru surface, and the energy bandgap is reduced from 8.5 eV to 2.4 eV in free CO<sub>2</sub> and CO<sub>2</sub> adsorbed to the Ru surface, respectively. The CO<sub>2</sub> dissociation into CO is promoted with light irradiation because it lowers the reaction energy for CO<sub>2</sub> reduction. Total energy consumption of 37% was required for the light-irradiated process compared to the case without light irradiation at a CO<sub>2</sub> conversion rate of 15% [59]. On the rutile TiO<sub>2</sub> (110) surface investigated theoretically, photo-excited electron induced CO<sub>2</sub> reduction through a process that involves the formation of a transient CO<sub>2</sub><sup>•−</sup> with bent geometry through the photoexcitation of one electron to the LUMO of CO<sub>2</sub> as shown in Figure 3, and summarized as follows: (1) photoexcitation generates CO<sub>2</sub><sup>•−</sup>, (2) transient CO<sub>2</sub><sup>•−</sup> excites the bending and antisymmetric stretching vibrations that stabilize the CO<sub>2</sub> LUMO, (3) CO<sub>2</sub> traps hot electrons and forms a new CO<sub>2</sub><sup>•−</sup>, and (4) CO<sub>2</sub><sup>•−</sup> dissociates on oxygen vacancy [44]. The excitation of the bending and antisymmetric stretching vibrations can sufficiently decrease the energy of the CO<sub>2</sub> LUMO to below that of the CBM of TiO<sub>2</sub>. Although this was demonstrated with TiO<sub>2</sub>, it is believed that conclusion can be widely applied to other metal oxides as well as to other semiconductors.

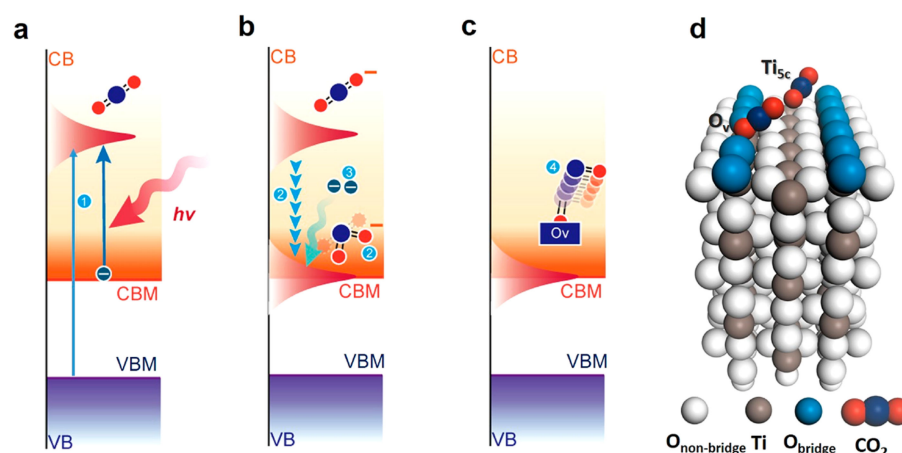


**Figure 3.** CO<sub>2</sub> photoactivation on the TiO<sub>2</sub> surface (a–c). CB: conduction band; CBM: conduction band minimum. Schematic of the CO<sub>2</sub> molecule adsorbed in the oxygen vacant site and Ti<sub>5c</sub> sites on the TiO<sub>2</sub> (110) surface (d). Reproduced with permission from the authors of [44]. Copyright 2020 American Chemical Society.

## 2.2. Electrocatalytic Activation of CO<sub>2</sub>

Electroreduction of CO<sub>2</sub> is another appealing approach for CO<sub>2</sub> valorization. The principles of operation, striking features, and the challenges of this process have been discussed in the literature [10,12,60–62]. The electrochemical CO<sub>2</sub> reduction is a multielectron and multiproton process involving several transfer pathways that result in different products [63], and this is of immense advantage over the single electron process in terms of electrochemical potential requirements [62]. As in the thermo- and photo-catalytic processes, the electrocatalytic reduction involves the adsorption and activation of CO<sub>2</sub> on the catalyst surface to product precursors. Following adsorption of CO<sub>2</sub> on the electrocatalytic surface is the electron transfer and/or proton migration that initiates the C=O bond cleavage and subsequent formation of C–O and/or C–H bonds [64]. The adsorbed product species then desorb and diffuse from the catalyst surface. From both theoretical and experimental studies, the adsorption and activation steps are the most critical of the CO<sub>2</sub> electroreduction process not only due to the high thermodynamic stability of the neutral CO<sub>2</sub> molecule, but also the requirement of a large amount of energy for breaking the kinetic barrier [62], considering the strongly negative redox potential (−1.90 V) compared with SHE [65]. As the rate-determining step, the chemisorption and subsequent activation of CO<sub>2</sub> on the electrocatalyst surface would form CO<sub>2</sub><sup>•−</sup> intermediate that can further be reduced to the \*CO, \*COH, \*CH<sub>2</sub> product precursors, or effect C–C coupling to form multi-carbon products [65–68]. Consequently, understanding the CO<sub>2</sub> activation mechanisms over electrocatalysts is necessary for a proper comprehension of the electroreduction transformation to different products, and for improving its performance. To this end, researchers have focused on how to achieve efficient CO<sub>2</sub> activation on electrocatalysts. This includes electrocatalyst engineering and surface modification [69]. Such catalysts need to be tailored with electron-donating centers for the efficient chemisorption of CO<sub>2</sub> molecules.

The proper design of the electrocatalyst active phase can improve the activation of the neutral CO<sub>2</sub> molecule. Xiao et al. [69] conducted a detailed study of the CO<sub>2</sub> adsorption on Cu electrocatalyst employing different catalyst models. It was found that only the catalyst with a combination of surface Cu<sup>0</sup>/Cu<sup>+</sup> sites promoted CO<sub>2</sub> activation, favoring kinetics and thermodynamics. The Cu<sup>0</sup> sites bind to activated CO<sub>2</sub>, whereas Cu<sup>+</sup> sites dilute the negative charge by binding to water molecules in the electrolyte solution. This translated into the observed increase in the onset potential and peak Faradaic efficiency for CO production [69].

The combination of experiments and theoretical calculations on the surface and electronic structure of Cu electrocatalyst revealed that the presence of a thin suboxide species

below the Cu surface could bind the CO<sub>2</sub> in the physisorbed configuration at 298 K; in the presence of H<sub>2</sub>O, this suboxide is essential for further converting to the chemisorbed CO<sub>2</sub> and subsequently toward CO<sub>2</sub> reduction products such as formate and CO [70]. Indeed, it has been suggested that the CO<sub>2</sub> might dissociate more easily on pre-oxidized Cu surfaces [71], but evidence to support this is scarce. The results of the CO<sub>2</sub> reduction to CO with annealed Cu<sub>2</sub>O revealed a linear Tafel plot over the range of overpotentials from 0.05 to 0.3 V with a slope of 116 mV/decade. The slope of this plot was in agreement with the rate-determining initial electron transfer to CO<sub>2</sub> to form a surface adsorbed CO<sub>2</sub><sup>•−</sup> intermediate. The difference in Faradic Efficiency (FE) between the reduced Cu electrode and that of the polycrystalline Cu suggested that the Cu surface formed by reducing thick Cu<sub>2</sub>O layers could form the CO<sub>2</sub><sup>•−</sup> intermediate [71]. This presents the need for understanding the surface structures of electrocatalytic Cu particles for the CO<sub>2</sub> activation and subsequent reduction to different products.

Engineering oxygen vacancy/surface defects in CO<sub>2</sub>-reduction catalysts has proven an indispensable method for generating and transferring surface electrons to CO<sub>2</sub> molecules [72–74]. Gu et al. [73] reduced copper oxide nanodendrites with rich surface oxygen vacancies and obtained partially reduced Cu oxide catalyst with Lewis base sites for enhanced CO<sub>2</sub> adsorption and subsequent electroreduction. Furthermore, strong binding of \*CO and \*COH intermediates to CuO<sub>x</sub> surface was observed. Theoretical calculations and catalytic test results showed that oxygen vacancy can provide a surface for binding, and as a result, the partially reduced CuO<sub>x</sub> nanodendrites had a high electrocatalytic activity for C<sub>2</sub>H<sub>4</sub> production. ZnO nanosheets rich in oxygen vacancies exhibited a current density of −16.1 mA cm<sup>−2</sup> with a FE of 83% for CO production at −1.1 V versus RHE in the CO<sub>2</sub> electrochemical reduction [74]. According to DFT calculations, introducing oxygen vacancies increased the charge density of ZnO around the valence band maximum, resulting in the enhanced activation of CO<sub>2</sub>. In addition, mechanistic studies revealed that introducing oxygen vacancies into ZnO nanosheets increased the binding strength of CO<sub>2</sub> and facilitated CO<sub>2</sub> activation [74]. The electrochemical properties of InO<sub>x</sub> electrocatalysts (P-InO<sub>x</sub> NRs, O-InO<sub>x</sub> NRs, and H-InO<sub>x</sub> NRs) in CO<sub>2</sub>-saturated NaHCO<sub>3</sub> solution were investigated. It was found that H-InO<sub>x</sub> NRs exhibited the best performance, generating a current density of 26.6 mA·cm<sup>−2</sup> at −1.05 V versus RHE. This catalyst had the highest oxygen vacancy concentration compared with others. The current densities for HCOO<sup>−</sup> at various overpotentials for the different InO<sub>x</sub> catalysts are presented in Figure 4a. The Tafel plot of O-InO<sub>x</sub> NRs, P-InO<sub>x</sub> NRs, and H-InO<sub>x</sub> NRs gave slopes of 150.2, 117.0, and 57.9 mV/decade, respectively, pointing to the different adsorption strength of the catalysts for CO<sub>2</sub> molecules. H-InO<sub>x</sub> yielding the least slope value indicates the pre-equilibrium transfer step (CO<sub>2</sub> + H<sup>+</sup> + e<sup>−</sup> + \* → HCOO\*) rather than a chemical H<sup>+</sup> transfer step as the rate-determining step [72]. The availability of hydroxyl groups on the surface of the electrocatalyst can enhance its adsorption properties. Huang et al. [64] functionalized the MOF surface with OH<sup>−</sup> moieties and used it for the electrochemical reduction of CO<sub>2</sub>. They observed single-crystal to single-crystal structural transformation between the MOF and MOF-CO<sub>2</sub>, activating it to HCO<sub>3</sub><sup>−</sup>, an important intermediate in the electrocatalytic reduction process [75]. Theoretical calculations revealed the formation of the HCO<sub>3</sub><sup>−</sup> species from the geometries of CO<sub>2</sub> adsorption at both the O- and C-atoms. In addition, the OH-incorporated MOF sample exhibited high FE for CO, achieving approximately 100% at −0.6 V versus RHE, surpassing the 96% (−0.6 to −0.9 V) in most MOF-based catalysts [64].

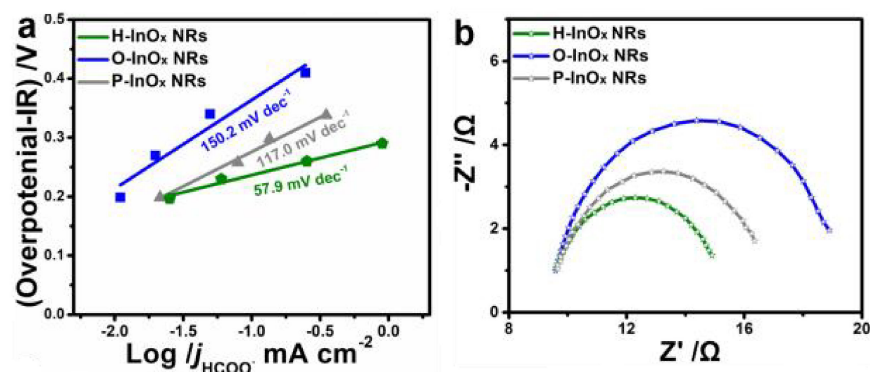


**Figure 4.** (a) Tafel plots and (b) Nyquist plots of  $\text{HCOO}^-$  for the electrocatalytic reduction of  $\text{CO}_2$  on  $\text{InO}_x$  catalysts. Reproduced with permission from the authors of [72]. Copyright 2019 John Wiley & Sons, Inc.

### 2.3. Activation of $\text{CO}_2$ by Homogeneous Catalysts

In an aqueous solution of transition metal salts, a  $\text{CO}_2$  molecule can be activated by forming a transition metal- $\text{CO}_2$  complex via direct coordination [4,22,76–78]. This can be considered a combination of  $\pi$  electrons transfer to the metal and the oxidative addition of the C–O bond to the metal (Scheme 2) [22]. For a multi-metal complex,  $\text{CO}_2$  can also be activated by bridging between metals in the complex. The successful formation of the metal- $\text{CO}_2$  complexes is key to  $\text{CO}_2$  activation. Upon forming the metal- $\text{CO}_2$  bond, the activation energy for further reactions is sufficiently lowered, thus accelerating the reactions rates in various  $\text{CO}_2$  transformation processes. A number of factors, including the central metal itself, ligand set, and metal oxidation state, have been identified to affect the activation of  $\text{CO}_2$  on metal complexes [22].



**Scheme 2.** Activation of  $\text{CO}_2$  by transition metal complexes.

Infrared spectroscopy (IR) has emerged as an excellent tool for the structural investigation of metal- $\text{CO}_2$  interactions in complexes, such as  $\text{M}^+(\text{CO}_2)_n$  or  $\text{M}^-(\text{CO}_2)_n$  [79–83]. Review articles discussing the spectroscopic studies of the various types of  $\text{CO}_2$  interactions with metal complexes are available in the literature, which readers are directed to. A recent review on the subject was authored by Paparo and Okuda in 2017 [84].

We briefly discuss recent studies on the conversion of  $\text{CO}_2$  to chemicals and fuel via the formation of  $\text{CO}_2$ -activated complexes. Catalytic reduction of  $\text{CO}_2$  to methanol and other products has been observed with transition metal complexes [22]; it is possible to develop highly active catalysts based on early transition metal complexes. It was found that anionic metal clusters ( $\text{M}_n^-$ ) with 1, 2, and 6 atoms formed the activated complex ( $\text{M}_n-\text{CO}_2$ ) $^-$  for Cu, Ag, and Au [4]. The activation was a result of a strong interaction between the  $\text{CO}_2$  moiety and  $\text{M}_n^-$  via the formation of a partial covalent M–C bond with a full delocalization of the electronic charge due to electron transfer from the HOMO of  $\text{M}_n^-$  to the LUMO of  $\text{CO}_2$  as in metal- $\text{CO}_2$   $\pi$ -backbonding. This can easily be understood from the perspective of the orbital geometry and energetics following orbital mixing (orbital interaction between HOMO of  $\text{M}_n^-$  and LUMO of  $\text{CO}_2$ ) [4,29].

### 3. Activation of $\text{CO}_2$ on Heterogeneous Catalyst Surface

The interaction of  $\text{CO}_2$  molecules with metal-based surfaces has attracted intense research attention for a long time. Reduction of  $\text{CO}_2$  by  $\text{H}_2$  has been studied on some

transition metals (e.g., Cu, Co, and Ni) and metal oxide catalysts (e.g., TiO<sub>2</sub>, CeO<sub>2</sub>, and In<sub>2</sub>O<sub>3</sub>). The catalytic surfaces for the activation of CO<sub>2</sub> include metal sites, metal-oxide interfaces, and oxygen vacancies. For facile CO<sub>2</sub> activation and conversion, efforts should be made to know, design, and optimize functional sites in heterogeneous catalysts, which involves constructing surface sites with a charge density gradient capable of reorganizing the electronic structures of CO<sub>2</sub> and polarizing the adsorbed species [85].

Metal-based catalysts are capable of effectively activating the CO<sub>2</sub> even in the absence of hydrogen [27]. These include pure metal surfaces, doped or promoted metal surfaces, and supported metal nanoparticles. On supported metal surfaces, CO<sub>2</sub> activation occurs mainly through acceptance of charge from the metal; the oxide support plays a big part in the activation process through different mechanisms such as acid sites interactions and provision of oxygen vacant sites [86]. The metal surface is also important in the dissociation of H<sub>2</sub> in CO<sub>2</sub> hydrogenation reactions [6].

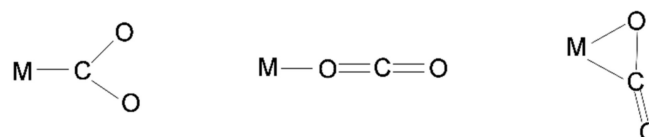
### 3.1. CO<sub>2</sub> Activation on Representative Pure Metals

Metal nanoparticles sit on a metal oxide serve as active sites for the electron transfer. Transition metals such as Cu, Ni, and Fe are particularly energetic for activating CO<sub>2</sub>. Their surfaces possess high binding abilities to CO<sub>2</sub>. DFT calculations evidenced that on Pt, Rh, Ni, Cu, Ag, and Pd (111) surfaces, the affinity toward oxygen is different for the metals, which selects their reaction pathways for the CO<sub>2</sub> activation in the RWGS reaction. Pt, Ag, and Pd tend to favor the COOH-mediated mechanism, whereas Rh, Ni, and Cu dissociate CO<sub>2</sub> into CO and O. This difference underlines the variation in the CO<sub>2</sub> dissociation barrier of the different metal groups. Thus, the nature of interaction between the adsorbed O and the surface is critical for determining the CO<sub>2</sub> dissociation barrier [87]. In the activation of CO<sub>2</sub> via the charge transfer mode, which is the prevalent on metal surfaces, the partial and full charge transfer leads to the formation of CO<sub>2</sub><sup>δ-</sup> and CO<sub>2</sub><sup>-</sup>, respectively. The degree of charge transfer can be analyzed on metal surfaces after adsorption. Physisorption and chemisorption of CO<sub>2</sub> on single crystal surfaces of various metals have been studied by means of DFT calculations [88]. Physisorption imposes difficulty in transferring charge due to the weak interaction of adsorbed CO<sub>2</sub> with the surface. It was found that, approximately −0.06 electron charge transferred from the surface of metals listed in Table 3 (little or no dependence on the kinds of metals) as a result of the location of adsorbed CO<sub>2</sub> (~3 Å) above the surface [88]. On the contrary, chemisorption states are highly dependent on both the metal itself and adsorption sites. Chemisorbed CO<sub>2</sub> molecules often have a bent structure with O–C–O angle varying between 121 and 140° compared with the nearly linear coordination of the physisorbed CO<sub>2</sub> molecules, and their extent depends on the kind of metal surface. In other words, the degree of CO<sub>2</sub> activation varies with metal surfaces. A similar behavior can be observed for the amount of charge transferred (Table 3). According to Wang et al. [89], who investigated CO<sub>2</sub> chemisorption on nine transition metal surfaces (Fe, Co, Ni, Cu, Rh, Pd, Ag, Pt, and Au), the adsorption strength is affected by both the *d*-band center of the metal surface and the charge transfer, which control the activation of C=O bond. It is possible to promote chemisorption by adjusting the properties of the catalysts, such as the catalyst surface area, surface defects, basic sites and the addition of promoters [31].

**Table 3.** DFT-calculated adsorption energies, geometries, and charge transferred to CO<sub>2</sub> on single crystal surfaces of metals. Data extracted with permission from the authors of [88]. Copyright 2016 American Chemical Society.

Metal	Physisorption		Chemisorption	
	Binding Energy (kJ·mol <sup>-1</sup> )	OCO Angle/°	Binding Energy (kJ·mol <sup>-1</sup> )	Net Charge/e
Fe (110)	-23	121	-90	-1.11
Ir (111)	-33	128	-34	-0.47
Pd (111)	-32	140	-17	-0.35
Ru (0001)	-31	123	-61	-0.83
Rh (111)	-32	135	-35	-0.46
Ni (111)	-26	136	-20	-0.50
Co (0001)	-25	139	-30	-0.64
Pt (111)	-21	131	-3	-0.36

Generally, the DFT study of the CO<sub>2</sub> activation on transition metal surfaces suggests different barriers for CO<sub>2</sub> dissociation on different monometallic or bimetallic surfaces [88]. The coordination of CO<sub>2</sub> with metals can take different modes, e.g., with the electron-deficient C atom as the electron acceptor and the C=O bonds or O atoms as the electron donor as shown in Scheme 3 [85]. Electron-rich metal surfaces such as Ni (110) and Cu (100) generally activates CO<sub>2</sub> by attaching to the carbon atom [90,91]. In the process, electrons in the d<sub>z<sup>2</sup></sub> orbital of the metal transfer to the unpopulated antibonding π\* orbital of the CO<sub>2</sub> molecule. Consequently, negatively charged surfaces are efficient for CO<sub>2</sub> activation via the charge transfer mode. Such charged surfaces can be generated through inserting strong metal-support interaction, bimetallic and ligand effects, etc. [85]. Electron-deficient metal surfaces, such as Ti, Cr, V, and Mn, favor the end-on coordination with CO<sub>2</sub> [92]. In this mode, the bending or distortion of the linear CO<sub>2</sub> molecule is difficult [85]. For metal centers with combined binding behavior, i.e., possessing both an electron acceptor site and an electron donor site, CO<sub>2</sub> adsorption generally prefers the bridge sites. More efficient activation can result through this mechanism and lead to bending of the linear CO<sub>2</sub> molecule from different sites [85].



Electron rich metals

Electron deficient metals

**Scheme 3.** CO<sub>2</sub> coordination modes at the transition metal center.

Investigations by DFT calculations revealed the characteristic adsorption and activation of CO<sub>2</sub> on Rh, Pd, Pt, Ni, Fe, Cu, Re, Al, Mg, and Ag metals [87,93]. Strong evidence has been provided for the formation of CO<sub>2</sub><sup>-</sup> according to spectroscopic results. Depending on the type of metal, CO<sub>2</sub> can also dissociate into CO and O or be transformed into CO<sub>3</sub><sup>2-</sup> and CO. The activation of CO<sub>2</sub> on Pt, Rh, Ni, Cu, Ag, and Pd followed different elementary steps as a result of the different levels of interaction of the metals with adsorbed oxygen in the RWGS reaction. Metals with high affinities toward oxygen presented lower activation barriers, leading to facile hydrogenation reactions [87]. The presence of preadsorbed oxygen was responsible for forming carbonates of different structures [87,93]. On most metal surfaces, CO<sub>2</sub> activation is highly surface orientated, pressure- and particle size-dependent [89,94–96]. Yu et al. [96] demonstrated through spin-polarized DFT calculations that adsorption and dissociation of CO<sub>2</sub> was dependent on the Co particle size. They showed that Co<sub>55</sub> nanoclusters had the highest CO<sub>2</sub> dissociation activity in comparison to

Co<sub>13</sub> and Co<sub>38</sub>. However, Co<sub>13</sub> activated CO<sub>2</sub> with the smallest O–C–O angle (123°) against 137° for both Co<sub>38</sub> and Co<sub>55</sub> nanoclusters.

Cu-based materials have gained much attention in the CO<sub>2</sub> conversion process due to their wide applicability in the different conversion processes and low cost [12,97]. Despite these and other massive studies, the activation of CO<sub>2</sub> on Cu catalysts is still an issue due to the poor understanding of its mechanism. Studies have shown that CO<sub>2</sub> interacts weakly on low-index Cu surfaces under UHV conditions [98,99]. However, a recent study found Cu (100) surface to be more active in dissociating CO<sub>2</sub> than Cu (111), producing oxygen [91]. Ambient pressure X-ray photoelectron spectroscopy (APXPS) and DFT calculations revealed the activation of CO<sub>2</sub> on Cu surfaces. APXPS showed that CO<sub>2</sub> adsorbed as CO<sub>2</sub><sup>δ−</sup> on Cu (111) surface under a pressure of 0.01 mbar at 300 K (Figure 5). With an increase in pressure to 1 mbar, adsorbed CO<sub>2</sub><sup>δ−</sup> partially transformed into carbonate as a result of the disproportionation reaction between CO<sub>2</sub> molecules. Subsequent annealing at 400 K or higher temperatures led to the dissociation of CO<sub>2</sub><sup>δ−</sup> and carbonate and the formation of a chemisorbed oxygen-covered surface. On Cu (110) surface, the CO<sub>2</sub><sup>δ−</sup> gradually dissociated into CO and chemisorbed oxygen under the same CO<sub>2</sub> pressure at room temperature. On both surfaces, atomic oxygen was generated that catalyzed the self-deactivation of CO<sub>2</sub> adsorption. The DFT results, which collaborated the experimental findings, further indicated that the Cu (110) surface was more active than the Cu (111) surface in breaking C–O bonds [95]. Comparing the adsorption of CO<sub>2</sub> on Cu (111), (100), and (110) surfaces, it was found that CO<sub>2</sub> molecules aligned parallel to Cu (111) and (100), whereas a vertical configuration was more stable for the adsorbed CO<sub>2</sub> on Cu (110) with one of two oxygen atoms towards the surface. The degree of CO<sub>2</sub> activation followed the order: Cu (110) > Cu (100) > Cu (111) [89]. A decrease in the activation energies for CO<sub>2</sub> dissociation has been observed when Cu surfaces have step or kink defects in comparison with the flat surface. However, chemisorption of CO<sub>2</sub> has been reported on Cu stepped surfaces [98–101].

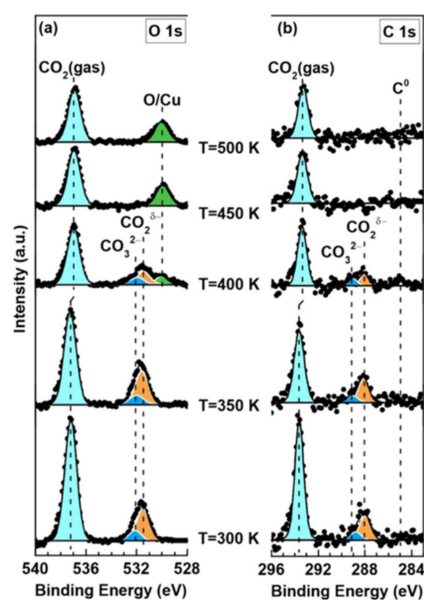


**Figure 5.** Ambient pressure XPS spectra of Cu (111) obtained in under 1 mbar CO<sub>2</sub> at 300 K and at 350, 400, 450, and 500 K; (a) O 1s and (b) C 1s. Reproduced with permission from the authors of [95]. Copyright 2020 American Chemical Society.

Ni-based catalysts can dissociate and convert CO<sub>2</sub> into value-added products, such as methane; thus, a fundamental understanding of the interaction between CO<sub>2</sub> and Ni surface at the atomic level is crucial to design even more efficient Ni-based catalysts. According to theoretical studies, the surface orientation of Ni influences the activation of CO<sub>2</sub> by altering the energetics for subsequent C–O bond breakage [102]. Ab initio

calculations using slab models have shown that CO<sub>2</sub> reactions on model Ni are surface sensitive, with reactivity in the following trend: Ni (110) > Ni (100) > Ni (111) [102,103]. Experimental investigations revealed the capability of Ni (110) surface to molecularly adsorb and subsequently dissociate CO<sub>2</sub> at room temperature [104]. By using in situ APXPS, carbonate was identified as the dominating surface intermediate at room temperature upon CO<sub>2</sub> adsorption on Ni (111) and Ni (100) surfaces [105–107]. However, where there are multiple dissociation products, their distribution depends on the surfaces. Carbonate, CO, and graphitic carbon were all observed on both Ni (111) and Ni (100) surfaces under a CO<sub>2</sub> pressure of 0.2 Torr. Ni (111) was predominantly covered with carbonate, whereas adsorbed CO\* and graphitic carbon were prevalent on the Ni (100) surface as indicated in Figure 6a–d [107]. The CO<sub>2</sub> adsorption and dissociation on ideal Ni (111) and stepped Ni (211) surfaces are shown in Figure 6e. It can be seen that CO<sub>2</sub> adsorption is endothermic by 20 kJ·mol<sup>-1</sup> on the Ni (111) surface, whereas it is exothermic by 40 kJ·mol<sup>-1</sup> on the Ni (211) surface [108].

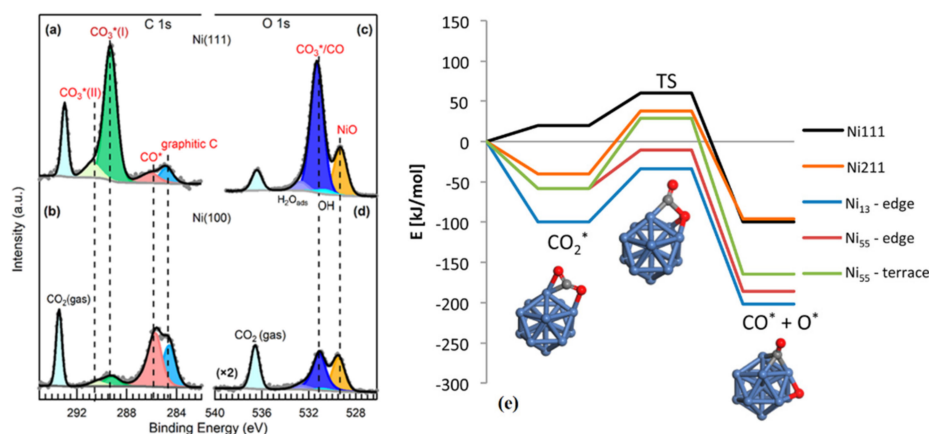


**Figure 6.** Ambient pressure XPS spectra of (a,b) C 1s, and (c,d) O 1s Ni (111) and Ni (100), respectively. CO<sub>2</sub> adsorption was performed under 0.2 Torr CO<sub>2</sub> at room temperature. Reproduced with permission from [107]. Copyright 2019 American Chemical Society; (e) Energy profile diagram for the CO<sub>2</sub> activation on Ni (111) and Ni (211) surfaces, edges of Ni<sub>13</sub> particle, and edges and terraces of the Ni<sub>55</sub> particle and the activation geometries on the Ni<sub>13</sub>. Reproduced with permission from [108]. Copyright 2016 American Chemical Society.

Based on the experimental results of the ultrahigh vacuum (UHV), Auger electron spectroscopy (AES), temperature-programmed desorption (TPD), and high-resolution electron energy loss spectroscopy (HREELS), it is difficult for CO<sub>2</sub> to adsorb on a clean Pt (111) surface between 110 and 300 K, but the dissociation capability can be improved by doping alkali metals such as potassium [109,110]. Conversely, it was reported that Pt foil treated with CO<sub>2</sub> in the gas phase during in situ UHVXPS experiments at 77 K formed chemisorbed CO species [111]. In collaboration with the latter assertion, on the clean Pt (111) surface, CO<sub>2</sub> dissociated into adsorbed CO and O at both room and elevated temperatures [112]. The production of adsorbed CO increased upon the introduction of H<sub>2</sub> (hydrogenation reaction). This observation was obvious for the CO<sub>2</sub> adsorption at all temperatures and led to the deoxygenation (consumption of oxygen) of the surface, resulting in cleaning the sites for further CO production and desorption from the surface at elevated temperatures. The Pt surface was active in the RWGS reaction. At a low pressure, the RWGS was initiated at 300 °C; on the contrary, at a high pressure (H<sub>2</sub>:CO<sub>2</sub> of 150 mtorr: 15 mtorr), a low temperature (200 °C) favored the initiation of the RWGS reaction, and the conversion of CO<sub>2</sub> continued to increase with increasing temperatures [112]. Moreover, under a pressure of 40 mtorr of pure CO<sub>2</sub> and at temperatures below 150 °C, graphitic carbon has been also observed as a product of the Boudouard reaction. IR spectroscopy revealed the size-dependent nature of CO<sub>2</sub> adsorption on Pt clusters. On small Pt clusters



anions ( $\text{Pt}_n^-$ ,  $n = 4-7$ ),  $\text{CO}_2$  was highly activated but remained molecularly adsorbed on  $\text{Pt}_4^-$ . On large clusters, dissociative adsorption was observed [13].

The  $\text{CO}_2^{\delta-}$  state of adsorbed  $\text{CO}_2$  molecule has been observed on Co (100) and Co (110) surfaces upon  $\text{CO}_2$  dissociation based on the energetics, geometries, vibrational frequencies, and charge transfer analysis [113].

### 3.2. $\text{CO}_2$ Activation on Bimetallic/Alloyed Catalyst Surfaces

Bimetallic surfaces are highly unique and active for a wide range of  $\text{CO}_2$  transformation reactions due to the electronic and geometric alterations within the structure. These alterations could be observed as a change in the morphology of metal, adsorption mode and configuration, and chemical ordering with varying composition and particle size [8,34]. This can help to control the adsorption properties to attain desired adsorption coverages. Numerous studies have appeared in the open literature discussing both activation of  $\text{CO}_2$  and the subsequent conversion of  $\text{CO}_2$  to fuels and chemicals on bimetallic catalysts. Ko et al. [88] studied the  $\text{CO}_2$  activation and adsorption by performing DFT calculations on a range of bimetallic alloy surfaces. The dissociation energy barriers of  $\text{CO}_2$  were screened by combining Bronsted–Evans–Polanyi (BEP) relation, scaling relation, and surface mixing rule. It was found that  $\text{CO}_2$  dissociated into CO and O, which sum of their adsorption energies was linearly related to both the energy for  $\text{CO}_2$  dissociation and that for  $\text{CO}_2^{\delta-}$  adsorption. The activation of  $\text{CO}_2$  proceeded through a direct dissociation ( $\text{CO}_2 \rightarrow \text{CO} + \text{O}$ ) mechanism in three successive elementary steps: physisorption of  $\text{CO}_2$  from the gas phase on the metal surface, chemisorption of  $\text{CO}_2^{\delta-}$  from the physisorbed  $\text{CO}_2$ , and direct dissociation of  $\text{CO}_2^{\delta-}$  into CO and O.

The predicted activation energies for the  $\text{CO}_2$  dissociation on bimetallic alloy surfaces are shown in Figure 7, with the row and column indicating the host and solute metals of the bimetallic alloys, respectively. The alloying effect would lead to reduction for surface reactions when the solute metals are placed in the bulk region. In the figure, the activation energy ( $E_a^{\text{act}}$ ) decreases from right to left and from bottom to top, thus alloys with relatively low activation energies ( $\sim 0.75$  eV) are Fe-, Ru-, Co-, Ni-, Rh-, and Ir-based alloys, whereas Pd-, Pt-, and Cu-based alloys possess high activation energies ( $\sim 1.51$  eV). Still, some metals, including Ru-, Co-, Ni-, Rh-, Ir-, and Cu-based alloys, have activation energies in between the extremes (0.76–1.50 eV). This picture makes sense for fabricating bimetallic catalysts for  $\text{CO}_2$  conversion reactions by manipulating the activation energies [88].

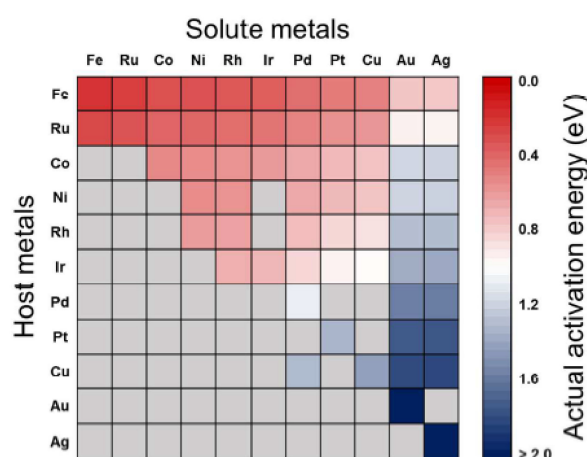


**Figure 7.** Screening for  $E_a^{\text{act}}$  for  $\text{CO}_2$  dissociation on pure metals and bimetallic alloys. Gray cells indicate the bimetallic alloys which are not preferred to the surface segregation of solute atoms.  $E_a^{\text{act}}$  were estimated by combining BEP relation, scaling relation, and surface mixing rule. Reproduced with permission from the authors of [88]. Copyright 2016 American Chemical Society.

The mechanisms of  $\text{CO}_2$  dissociation on bimetallic clusters ( $\text{Pt}_3\text{Ni}_1$ ,  $\text{Pt}_2\text{Ni}_2$ , and  $\text{Pt}_1\text{Ni}_3$ ) were investigated and characterized by the activation barrier [21]. Compared with the

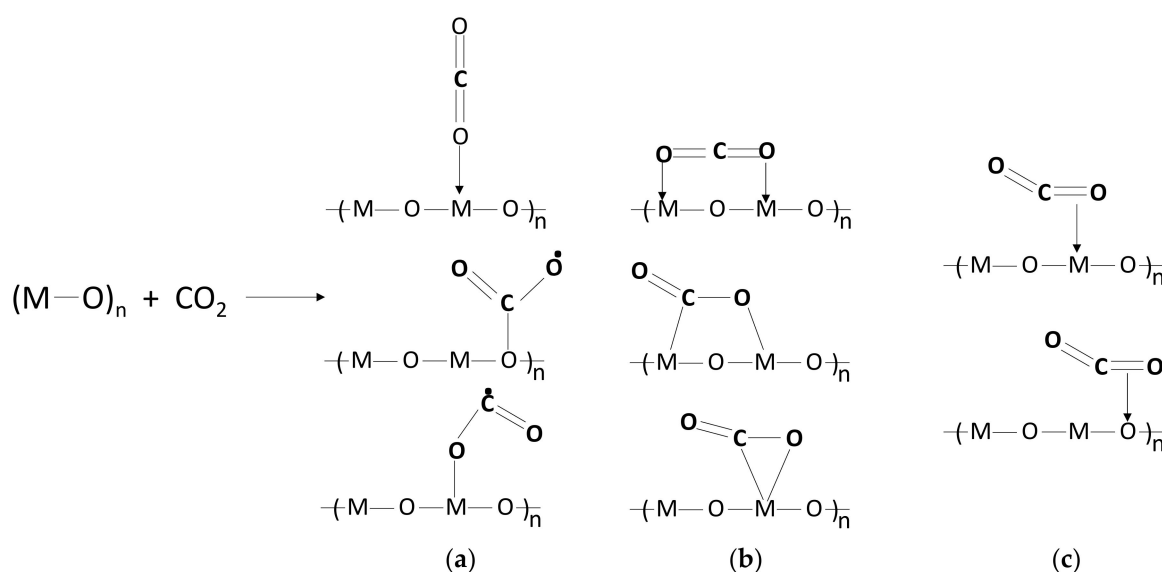
single metallic clusters ( $\text{Pt}_4$  and  $\text{Ni}_4$ ), results showed the activation barrier to be between those of the monometallic clusters. Increasing Ni atoms in the bimetallic clusters moderately raised the activation barrier, which means that such a bimetal combination could have a significant negative impact on the activity of Pt for  $\text{CO}_2$  reaction. In the presence of  $\text{H}_2$ ,  $\text{CO}_2$  dissociation became less difficult for all metallic clusters [21].

Results from an ab initio study of chemisorption and activation of  $\text{CO}_2$  on Pt-based transition-metal nanoalloys on 55-atom nanoclusters ( $\text{Pt}_n\text{TM}_{55-n}$ ), where  $n = 0, 13, 42, 55$ , and  $\text{TM} = \text{Fe}, \text{Co}, \text{Ni}, \text{Cu}, \text{Ru}, \text{Rh}, \text{Pd}, \text{Ag}, \text{Os}, \text{Ir}, \text{Au}$ , indicated a linear correlation between the interaction energy, charge transfer from the nanoclusters toward  $\text{CO}_2$  and the bent  $\text{CO}_2$  angle [8]. It was further realized that the interaction energy was enhanced for larger angles and molecular charge. With 55 atoms for Cu, Ag and Au in the Pt alloy, a change from physisorption to chemisorption was observed, whereas the strong interaction energy of  $\text{CO}_2$  with  $\text{Os}_{55}$ ,  $\text{Ru}_{55}$ , and  $\text{Fe}_{55}$  can be decreased by alloying with Pt [8]. It was concluded that certain metals (Fe, Co and Ni) activate  $\text{CO}_2$  more strongly as monometals than in an alloyed form due to weaker adsorption energy in the latter.

### 3.3. $\text{CO}_2$ Adsorption and Activation on Metal Oxide Surfaces

#### 3.3.1. Metal Oxide

Various metal oxides ( $\text{MO}_x$ ) or ( $\text{M}_x\text{O}_y$ ) are investigated as supports or directly as catalysts for  $\text{CO}_2$  conversion, including  $\text{In}_2\text{O}_3$ ,  $\text{CeO}_2$ ,  $\text{ZnO}$ ,  $\text{ZrO}_2$ ,  $\text{TiO}_2$ , and  $\text{CeO}_2$ . Metal oxide surfaces consist of both metal ( $\text{M}^{n+}$ ) and oxygen ( $\text{O}^{2-}$ ) ions, which are effective sites for  $\text{CO}_2$  activation. The activation can occur by coordination to one or two adjacent metal sites through the terminal oxygen atoms or C atom of the  $\text{CO}_2$  molecule, forming monodentate or bidentate carbonate species, as illustrated in Scheme 4a,b [114]. Interaction of the C atom is on the surface oxygen sites of the metal oxide. The  $\text{CO}_2$  activation can also occur via the  $\sigma$ -bond and  $\pi$ -bonds activation on metal ions and oxygen ions, respectively, as observed upon chemisorption on metal oxides applied as catalyst supports (as shown in Scheme 4c) [115]. Due to the large surface areas, switchable redox properties, and rich oxygen vacancies, metal oxides can act as adsorption and activation sites for small molecules, including  $\text{O}_2$ ,  $\text{H}_2$ , and  $\text{CO}_2$  [116]. The surface oxygen vacancies interact with the carbon and/or oxygen atoms of  $\text{CO}_2$  through which electron transfer from the oxide defective site to adsorbed  $\text{CO}_2$  becomes feasible. One example is  $\text{In}_2\text{O}_3$ , which is rich in oxygen vacancies and has shown a high activity for  $\text{CO}_2$  activation and methanol synthesis by hydrogenation [116]. On oxide surfaces, generally,  $\text{CO}_2$  interactions can vary from physisorption to chemisorption, the extent that affects the structure and reactivity of the adsorbed  $\text{CO}_2$  and the kinetics and mechanisms of surface catalytic reactions [114]. The surface structure is important for  $\text{CO}_2$  adsorption and activation [117]; thus, the interaction of  $\text{CO}_2$  with metal oxides can be structure-dependent. It was found that  $\text{CO}_2$  adsorption on  $\text{Zn}_2\text{GeO}_4$  (001) was higher than that on  $\text{Zn}_2\text{GeO}_4$  (010) surface [117]. The interaction with (010) surface led to bidentate carbonate species, whereas on the (001) surface, stronger interaction with  $\text{CO}_2$  resulted in a bridged carbonate-like species. The strongest adsorption based on calculated  $\text{CO}_2$  adsorption energies were around the surface oxygen vacancy site on both surfaces. Analysis of the LDOS and Mulliken charge for adsorbed  $\text{CO}_2$  on perfect  $\text{Zn}_2\text{GeO}_4$  surfaces revealed that  $\text{CO}_2$  formed a  $\text{CO}_2^{\delta-}$  species upon receiving electrons from the surface.  $\text{CO}_2$  molecule was found to be activated on the CuO surfaces ((011), (111), and (-111)), with strong adsorption only on the (011) surface. The CuO (111) and CuO (-111) surfaces showed relatively weak adsorption.  $\text{CO}_2$  activation was characterized by structural transformations and charge transfer that resulted in the formation of bent  $\text{CO}_2^{\delta-}$  species with an elongation of the C–O bonds [94].



**Scheme 4.** Possible modes of  $CO_2$  adsorption on metal oxide surfaces: (a) monodentate, (b) bidentate (c)  $\pi$ -coordination. Reproduced with permission from the authors of [114]. Copyright 2017 The Royal Society of Chemistry.

The ability of metal oxides to bind and activate  $CO_2$  depends greatly on several factors, including their preparation methods, physiochemical properties, redox properties, and electronic and geometric structures [108,114,118]. The preparation methods were found to impact the properties of  $CeO_2$  nanostructures for the photocatalytic reduction of  $CO_2$  [119]. A high surface area was obtained for catalysts synthesized through the sunlight-assisted combustion process, in addition to possessing a small particle size, high concentration of oxygen vacancies, and a narrow bandgap. Compared to that prepared from the conventional combustion process with a spongy-like structure, a porous network consisting of small and uniform pores was also obtained for the sunlight-assisted process. The superior catalytic properties could be attributed to the combustion process aided by solar irradiation during the synthesis process. As demonstrated with the  $CeO_x/Cu$  catalyst, the important roles of metal oxide ions were revealed on the catalytic cycle of  $H_2O$  and  $CO_2$  activation. The Cu phase reduced into  $Cu^0$  that promoted  $Ce^{4+}$  reduction into  $Ce^{3+}$ .  $H_2O$  and  $CO_2$  activation occurred on the  $Ce^{3+}$  sites. Without the presence of Cu,  $Ce^{3+}$  would lead to oxidation into  $Ce^{4+}$ . However, in contact with  $Ce^{4+}$ ,  $Cu^0$  reacted to form  $Cu^+$  and  $Ce^{3+}$ , sustaining ceria in the more active state. The cycle is closed when  $Cu^+$  reduced to  $Cu^0$  [120]. This synergistic effect afforded the catalysts with high reactivity in the RWGS reactions. The chemisorption of  $CO_2$  molecules on  $CeO_2$  at RT as studied using in situ DRIFTS indicated adsorption at both the  $Ce^{3+}$  and  $Ce^{4+}$  sites, although adsorption was also found at the oxygen sites that resulted in carbonates and bicarbonates species [121]. In the same study, the  $CO_2$  chemisorption on  $TiO_2$  under similar reaction conditions and instrumentation was observed at both  $Ti^{3+}$  and  $Ti^{4+}$  sites, exhibiting O–C–O vibrations at  $1667$  and  $1248\text{ cm}^{-1}$  and  $2339$ – $2345\text{ cm}^{-1}$ , respectively [121]. The  $CO_2$  molecules adsorbed at  $Ti^{3+}$  sites formed  $CO_2^-$  species, which concentration increased with the amount of oxygen vacancies present. Like with  $CeO_2$ ,  $CO_2$  chemisorption at the oxygen sites formed carbonates and bicarbonates species. It was observed that the interaction between  $TiO_2$  and  $CO_2$  molecules is somewhat weak compared with that of  $CeO_2$ . Such weak interactions can be improved by doping  $TiO_2$  with  $CeO_2$ .  $CeO_2$  doping can improve the interaction of  $TiO_2$  with  $CO_2$  as a result of the introduction of  $Ce^{3+}$ , which strengthens the bonding of  $CO_2$  with catalyst surfaces and enhances the production of bidentate carbon species that can readily be transformed to surface  $CO_2^-$  in the presence of  $H_2O$  under sunlight irradiation. The formation of adsorbed species of  $CO_2$  over  $CeO_2/TiO_2$  could be attributed to the binding of  $CO_2$  species to Ti/Ce atoms that have reductive capabilities under photo-irradiation. Furthermore, the  $Ce^{3+}$  availability from  $CeO_2$  facilitates photogenerated charge

separation; thus, the CO<sub>2</sub> adsorption and enhanced charge separation can be tuned for increased activity of CeO<sub>2</sub>/TiO<sub>2</sub> catalyst [122]. The surface area of a material positively correlates with its adsorption capacity. It was found that the Bi<sub>12</sub>O<sub>17</sub>Cl<sub>2</sub> nanotubes had higher adsorption capacity for CO<sub>2</sub> (~4.3 times) than bulk Bi<sub>12</sub>O<sub>17</sub>Cl<sub>2</sub> due to the higher BET specific surface area of the former. As a result, the effective adsorption of CO<sub>2</sub> on Bi<sub>12</sub>O<sub>17</sub>Cl<sub>2</sub> nanotubes than bulk Bi<sub>12</sub>O<sub>17</sub>Cl<sub>2</sub> favored the photocatalytic process [123]. In addition, the high surface area correlated with strong adsorption. Weak chemisorption of CO<sub>2</sub> has been reported for CeO<sub>2</sub> nanostructures with low exposed surface area [121]. Mesoporous structured photocatalyst displayed improved activity for CO<sub>2</sub> reduction into CH<sub>4</sub> due to the presence of high specific surface area and mesostructure that enhanced adsorption of CO<sub>2</sub> [124]. Highly mesoporous In(OH)<sub>3</sub> synthesized via a sol-gel hydrothermal treatment exhibited ~20-fold higher efficiency for CO<sub>2</sub> reduction in comparison with that lacking mesopores [125]. It is reported that the methanol activity of the In<sub>2</sub>O<sub>3</sub> catalyst could also be improved by increasing the (111) surface area [126].

### 3.3.2. Characteristic Adsorption of Representative Metal Oxides

Ceria (CeO<sub>2</sub>) has shown catalytic activity in the reduction of CO<sub>2</sub> to liquid fuels and chemicals. It has rich oxygen vacancies and a high oxygen storage/release capacity. Several studies demonstrating the interaction of CO<sub>2</sub> with high-surface-area ceria catalysts have been reported. As noted in [127], CO<sub>2</sub> dissociates into CO and an oxygen-containing surface species on the surface Ce<sup>3+</sup> ions, which are considered active sites for CO<sub>2</sub> activation due to formation of carbonates or inorganic carboxylates. Graciani et al. reported a highly active CeO<sub>x</sub>/Cu nanoparticles catalyst for methanol synthesis from CO<sub>2</sub> [128]. The catalyst activated CO<sub>2</sub> as CO<sub>2</sub><sup>δ-</sup> and exhibited a faster methanol production rate than Cu/ZnO, on which CO<sub>2</sub> was chemisorbed as CO<sub>3</sub><sup>2-</sup>. A study on the CO<sub>2</sub> adsorption sites of CeO<sub>2</sub> (110) surface using DFT was carried out by Cheng et al. [129]. Reduced and stoichiometric ceria (110) surfaces were compared. Results revealed that CO<sub>2</sub> adsorption on the reduced ceria (110) surface was thermodynamically favored than on the stoichiometric ceria (110) surface. Furthermore, the most stable adsorption configuration consisted of CO<sub>2</sub> adsorbed parallel to the reduced ceria (110) surface at the oxygen vacancy. Upon adsorption, the CO<sub>2</sub> molecule distorted out of the plane and formed carbonates with the remaining oxygen anion at the surface [129]. It was suggested that the structural changes in the catalyst after CO<sub>2</sub> adsorption were due to charge transfer between the surface and adsorbate molecule. The formation of two different adsorbate species: a carbonate and a weakly bound and linear physisorbed species, were observed upon exposure of reduced CeO<sub>2-x</sub> (110) substrates to CO<sub>2</sub> at low temperatures. There was no evidence for the formation of CO<sub>2</sub><sup>δ-</sup>. Furthermore, based on angle-dependent C K-edge NEXAFS spectra, the most preferred orientation of the adsorbate was lacking. The physisorbed CO<sub>2</sub> species and carbonate species were completely desorbed at 250 and 500 K, respectively. The authors remarked that it is most unlikely that the activation of CO<sub>2</sub> on the reduced CeO<sub>2-x</sub> (110) surface was via breaking the C=O bond to form CO and O. However, on fully oxidized CeO<sub>2</sub> (110), CO<sub>2</sub> adsorbed as a carbonate which was completely decomposed and desorbed as CO<sub>2</sub> at 400 K [130]. CO<sub>2</sub> adsorbed on the CeO<sub>2</sub> (111) surface formed a monodentate carbonate species found to be most stable on CeO<sub>2</sub> at low coverages [131]. Increasing the CO<sub>2</sub> coverage destabilized the formed species, indicating a mixed adsorption mechanism with both carbonate and linear adsorbed CO<sub>2</sub> species. Although CeO<sub>2</sub> has been studied for CO<sub>2</sub> reduction reactions, the insights into CO<sub>2</sub> adsorption, activation, and reaction on ceria surfaces are not yet fully understood.

TiO<sub>2</sub> possesses good photocatalytic properties for many chemical reactions, including CO<sub>2</sub> reduction. Since its first demonstration in the photoelectrochemical CO<sub>2</sub> reduction to formic acid and formaldehyde by Inoue et al. [132], TiO<sub>2</sub>-based materials have attracted great research interests in CO<sub>2</sub> photoreduction reactions. The adsorption properties of CO<sub>2</sub> on both the rutile and anatase phases of TiO<sub>2</sub> have been widely studied using various surface science techniques [133–136]. Sorescu et al. [137] investigated the adsorption and

dissociation of CO<sub>2</sub> on an oxidized anatase (101) surface using dispersion-corrected DFT and found CO<sub>2</sub> to adsorb at a fivefold coordinated Ti site in a tilted configuration. Based on in situ FTIR experiments, the CO<sub>2</sub> adsorption formed CO<sub>3</sub><sup>2-</sup> and CO<sub>2</sub> bonded to Ti, with absorption bands at 1319, 1376, 1462, 1532, 1579, and 2361 cm<sup>-1</sup>. The band at 2361 cm<sup>-1</sup> was assigned to adsorbed CO<sub>2</sub> with Ti–O–C–O adsorption configuration [138]. The 1319 and 1579 cm<sup>-1</sup> bands were assigned to bidentate carbonate, while the band at 1461 cm<sup>-1</sup> was due to monodentate or free carbonate. Under the vacuum condition, the intensities of all of the bands were reduced at 35 °C. The bidentate carbonate was the predominant species for CO<sub>2</sub> on TiO<sub>2</sub>. The scanning tunneling microscopy (STM) enabled the study of the dissociation of CO<sub>2</sub> adsorbed at the oxygen vacancy of TiO<sub>2</sub> (110) at the single-molecule level [139]. It was found that the electrons injected from the STM tip into the adsorbed CO<sub>2</sub> caused its dissociation into CO and O, and the released O was observed to heal the oxygen vacancy. According to experimental analysis, ~1.4 eV above the conduction band minimum of TiO<sub>2</sub> is needed for the electron induction process to dissociate CO<sub>2</sub>. The formation of a transient negative ion by the injected electron is an important step in the CO<sub>2</sub> dissociation, and this can only be possible above the threshold voltage. TiO<sub>2</sub> modified with metal oxide nanoclusters possess enhanced activity to adsorb and convert CO<sub>2</sub> [26,140]. The Bi<sub>2</sub>O<sub>3</sub>-TiO<sub>2</sub> heterostructures obtained by modifying TiO<sub>2</sub> with Bi exhibited low coordinated Bi sites in the nanoclusters and a valence band edge consisting mainly of Bi–O states due to the presence of the Bi lone pair. Upon interaction of CO<sub>2</sub> with the reduced heterostructures, CO or CO<sub>2</sub><sup>-</sup> were observed mainly through electron transfer to CO<sub>2</sub>, and the Bi<sub>2</sub>O<sub>3</sub>-TiO<sub>2</sub> heterostructures became oxidized in the process with adsorbed CO<sub>2</sub> in carbonate form [140]. In a related study, clean or hydroxylated extended rutile and anatase TiO<sub>2</sub> surfaces modified with Cr nanoclusters presented an upshift valence band edge related to the existence of Cr 3d–O 2p interactions, which promoted the CO<sub>2</sub> activation. [26]. The activated CO<sub>2</sub> molecule reduced its O–C–O angle to 127–132° and increased the C–O bond length 1.30 Å. It was concluded that the strong CO<sub>2</sub>–Cr–O interaction induced the structural distortions.

Iron oxides (FeO<sub>x</sub>) are an important component of catalysts for the conversion of CO<sub>2</sub> to hydrocarbons (liquid fuels). The adsorption and activation of CO<sub>2</sub> on FeO<sub>x</sub> have been investigated by researchers [141–143]. It is suggested that Fe<sup>2+</sup> and Fe<sup>3+</sup> cations are crucial for CO<sub>2</sub> adsorption. Using TPD, Pavelec et al. [141] observed a weak interaction between CO<sub>2</sub> and Fe<sub>3</sub>O<sub>4</sub> (001) surface. On this surface, CO<sub>2</sub> molecules existed in the physisorbed state as they desorbed at a low temperature (115 K). However, strong CO<sub>2</sub> adsorption was observed on the defects and surface Fe<sup>3+</sup> sites. Weak CO<sub>2</sub> adsorption has also been observed on Fe<sub>3</sub>O<sub>4</sub> (111) as investigated by various experimental techniques [144]. At different CO<sub>2</sub> dosages and temperatures (between 120 and 140 K), TPD experiments suggested CO<sub>2</sub> adsorb very weakly on a regular Fe<sub>3</sub>O<sub>4</sub> (111) surface. However, CO<sub>2</sub> chemisorption was also observed but at relatively long CO<sub>2</sub> exposure times [144,145] via binding to under-coordinated oxygen sites [145]. The formation of chemisorbed species such as carboxylates and carbonates was facilitated by surface imperfections. Conclusively, FeO<sub>x</sub> exhibit weak interaction with CO<sub>2</sub> molecules, and studies are recommended in this direction to adjust its CO<sub>2</sub> adsorption strength.

ZrO<sub>2</sub> has been demonstrated as an active catalyst or catalyst support for the CO<sub>2</sub> hydrogenation reactions to a variety of products. In a study on CO<sub>2</sub> hydrogenation on Cu/ZrO<sub>2</sub> interface using the first-principles kinetic Monte Carlo simulations by Tang et al. [146], the authors showed that CO<sub>2</sub> prefers to adsorb on the bare ZrO<sub>2</sub> nanoparticles surface rather than at the Cu/ZrO<sub>2</sub> interface. This led to the bending of the CO<sub>2</sub> molecule with a calculated adsorption energy of 0.69 eV. The stretching of the C–O bonds and charge transfer from the ZrO<sub>2</sub> surface to the antibonding 2π<sub>u</sub> orbital of CO<sub>2</sub> were also observed. On the bare ZrO<sub>2</sub> surface, bidentate bicarbonate (HCO<sub>3</sub>) was formed upon CO<sub>2</sub> adsorption based on observable IR frequencies at ~1225, ~1620, and ~3615 cm<sup>-1</sup> [147].

### 3.3.3. Oxygen Vacancies and Their Roles in CO<sub>2</sub> Activation

Many metal oxides, particularly the reducible ones (e.g., TiO<sub>2</sub>, CeO<sub>2</sub>, and In<sub>2</sub>O<sub>3</sub>), contain certain number oxygen vacancies, depending on the preparation and treatment conditions. The formation of oxygen vacancies can alter the physicochemical and electronic properties, improve surface adsorption, and generate additional active centers of metal oxides [148]. As reported in the literature, the generation of oxygen vacancies in catalytic materials is linked with enhanced light harvesting, charge separation and transfer in photochemical reactions, charge (electron) production and transfer in thermochemical reactions, and charge density increase in electrochemical reactions. During CO<sub>2</sub> conversion by the mentioned approaches, surface oxygen defects on metal oxides can significantly influence the interaction of CO<sub>2</sub> with the surface and enhance the adsorption compared to the perfect surface due to modification of adsorption and binding properties [117]. In theory, removing O atoms in metal oxides leads to the formation of oxygen defects/voids that can activate CO<sub>2</sub> due to the unsaturated chemical bond in the metal oxide and the unshared pair electrons of CO<sub>2</sub> [72]. This reconfigures the coordination environment and delocalizes charge, facilitating the conversion of reaction intermediates [149]. The backward transfer of electrons from the defect to the adsorbed molecule alters the d-band center of the oxide catalyst, causing further interaction with the adsorbed CO<sub>2</sub> and resulting in the reduction of activation energy barrier and enhanced CO<sub>2</sub> reduction [72]. In summary, oxygen vacancies have valuable input to the overall reaction mechanism, thermodynamics, and kinetics.

#### How to Generate Oxygen Vacancies

Theoretical studies predict that reducible metal oxides with oxygen vacancies possess high CO<sub>2</sub> adsorption and activation properties and can improve selectivity toward a characteristic reaction product [58,73,74,139,150–152]. Thus, the presence of oxygen vacancies in proper concentration can improve the catalytic performance of oxide-based catalysts. While oxygen vacancies in a catalyst sample can be detected by various techniques [153], X-ray photoelectron spectroscopy (XPS) is a good technique for confirming and measuring the relative oxygen vacancy concentration [119,154,155]. The ratio of the peak areas of lattice oxygen (O<sub>lat</sub>) to adsorbed oxygen (O<sub>ads</sub>), i.e., O<sub>lat</sub>/O<sub>ads</sub> area ratio, obtained from the XPS can be used to estimate the relative concentrations of oxygen vacancy. A low oxygen vacancy concentration would exhibit a high O<sub>lat</sub>/O<sub>ads</sub> ratio [154,155]. Oxygen vacancies can be formed during catalytic reactions [85] or be deliberately introduced in metal oxides during synthesis [153].

The formation of oxygen vacancies during reactions can be enabled by reaction conditions, via thermal desorption of lattice oxygen or reduction by reactive molecules (H<sub>2</sub> or CO) [152,156–158]. Their generation through the former process is highly endothermic, while it is exothermic when initiated in the presence of H<sub>2</sub> or CO; it is more exothermic using CO than H<sub>2</sub> [152]. As an example, the surface reduction of In<sub>2</sub>O<sub>3</sub> with H<sub>2</sub> at above 500 K reordered the surface and formed defective sites [157]. During CO<sub>2</sub> hydrogenation on oxide supported metal catalysts, H<sub>2</sub> that dissociates on the metal site spills over and attacks the oxide at the metal-oxide interface, generating oxygen vacancies [156]. It was revealed in CO<sub>2</sub> methanation over Ru/CeO<sub>2</sub> catalyst, using operando XAENS, IR, and Raman that Ru species reduced to metallic Ru, which provided the ability to dissociate H<sub>2</sub>. The dissociated H atom attacked the Ce–O bond on the CeO<sub>2</sub> surface, generating surface OH, Ce<sup>3+</sup>, and oxygen vacancies [156]. The hydrogen spillover effect of metallic Ru would facilitate the attacking of Ce–O bond by H atoms. Pd/In<sub>2</sub>O<sub>3</sub> catalyst with highly dispersed Pd NPs (~3.6 nm in size) and predominately exposed (111) facets showed a better ability to dissociatively adsorb hydrogen and supply it for creating oxygen vacancy. The interfacial sites were also active for enhanced CO<sub>2</sub> adsorption and hydrogenation [158].

Catalytic activities of irreducible metal oxides such as Al<sub>2</sub>O<sub>3</sub>, ZnO, and MgO can be improved by introducing oxygen vacancies in them. Methods including doping, plasma-assisted techniques, photo-irradiation of synthesis reaction, high-temperature annealing

under inert environment, and wet and solid-state chemical reactions have been reported to create oxygen vacancies in metal oxides [74,119,153]. Doping suitable elements, both metallic (Cu, Fe, La, etc.) and non-metallic (C, N, S, P, etc.), is a proven method for introducing oxygen vacancies in metal oxides, which can be carried out either during synthesis or by post-synthesis treatment. For example, doping of non-metallic elements in  $\text{TiO}_2$  has been reported as an effective approach to producing oxygen vacancies [153]. Wang et al. [159] increased the oxygen vacancy concentration in  $\text{CeO}_{2-x}$  by doping Cu to it. Cu doping stabilized the pre-existed vacancies in  $\text{CeO}_{2-x}$  and resulted in improved and sustained photocatalytic activity in  $\text{CO}_2$  reduction. Co-doping or self-doping has also been reported. In co-doping, any two or more combinations of metals, metal/non-metal or non-metal/non-metal, can effectively dope and create oxygen vacancies [160,161]. Self-doping, on the other hand, occurs intrinsically within the metal oxide structure. Such structural doping can be achieved by other oxygen vacancies creation methods such as treatment with plasma,  $\text{H}_2$  or via redox reactions [162].

Solid-state and wet chemical redox reactions can produce metal oxides with sufficient oxygen vacancies, applying various treatments or reactions [153,163]. In the solid-state process, the reaction uses gaseous or solid reductants such as graphene,  $\text{H}_2$ ,  $\text{NH}_3$ , S,  $\text{CaH}_2$ , NaH, and LiH at high temperatures. The wet reaction is carried out in the liquid phase in the presence of a suitable reducing agent such as  $\text{NaBH}_4$  at room temperature or by using the hydrothermal process. The mechanism involves decreasing the oxidation states of the metal cations during the redox reactions, leading to the formation of oxygen vacancies. In addition, oxygen vacancies can be created in metal oxides by decreasing the particle size of the bulk material [56,164]. Guo et al. [164] introduced oxygen vacancies in  $\text{Bi}_2\text{Sn}_2\text{O}_7$  nanoparticles by decreasing the nanoparticle size to  $\sim 4$  nm via the solution chemistry synthesis technique. The formation of oxygen vacancies was confirmed by an obvious increase in the visible light absorption according to the UV–visible spectroscopy results. The obtained oxidic nanoparticles with abundant oxygen vacancies exhibited an 8-fold enhanced photocatalytic performance compared with the bulk  $\text{Bi}_2\text{Sn}_2\text{O}_7$  in  $\text{CO}$  production from  $\text{CO}_2$  in pure water. Layered double hydroxide (LDH) nanosheets were synthesized via the templated hydrothermal methods (inverse microemulsion technique or controlled hydrolysis) [56]. These methods decreased the thickness of the Zn-containing LDH nanosheets from  $5 \mu\text{m}$  to  $40$  nm, with platelet thicknesses of  $\approx 2.7$  nm. A combination of several characterization results (EXAFS, positron annihilation spectrometry, ESR, and DFT calculations) concluded that oxygen vacancies were created with decreasing LDH thickness. The created oxygen vacancies formed coordinatively unsaturated Zn with the nanosheets represented as  $\text{Zn}^+-\text{V}_\text{o}$  complexes that serve as trapping sites for the efficient adsorption of  $\text{CO}_2$  and  $\text{H}_2\text{O}$  molecules, promoting photoinduced charge separation, thus significantly improving the catalytic activity for  $\text{CO}_2$  photoreduction. These illustrations demonstrate the possibility of engineering metal oxide catalysts with abundant oxygen vacancies for enhanced activity for  $\text{CO}_2$  reduction.

Thermal treatment of metal oxides in reducing gases ( $\text{H}_2$ , Ar or vacuum) at a high temperature is a proven strategy to generate or enrich oxygen vacancies in metal oxides. The process ejects some lattice oxygen from the crystal and effects a change in the bulk phase. This method is very easy and efficient because the oxygen vacancy concentration can be easily tuned by simply controlling either the annealing temperature or reducing gas flow rate during treatment [163,165]. Ye et al. [154] applied a zeolite imidazolate framework-8 (ZIF-8)-derived ZnO as the carrier and synthesized carbon-modified CuO/ZnO catalyst with high oxygen vacancy content for  $\text{CO}_2$  hydrogenation to methanol. They revealed that the pyrolysis temperature of ZIF-8 affected the surface oxygen defects of ZnO, and the CuO/ZnO catalyst (pyrolyzed at  $400^\circ\text{C}$ ) achieved the best  $\text{CO}_2$  conversion and methanol selectivity due to the presence of more oxygen vacancies and carbon modification. Oxygen vacancies were engineered in bulk  $\text{Bi}_{24}\text{O}_{31}\text{Cl}_{10}$  by thermal annealing at  $250^\circ\text{C}$  under an inert atmosphere consisting of  $\text{H}_2/\text{Ar}$  ( $10/90$  v/v) [148]. In the process,  $\text{H}_2$  interacted with the lattice oxygen, forming oxygen vacancies, which created a new level near the conduction

band minimum, enabling a fast charge transfer and high carrier density (Figure 8a,b). As shown in Figure 8e, the existence of oxygen vacancies led to a reduction in the energy barrier for the  $^*COOH$  intermediates formation during  $CO_2$  photochemical reduction. The photocatalytic activity of  $Bi_{24}O_{31}Cl_{10}$  for photoreduction of  $CO_2$  to CO was enhanced. CO was generated at a rate of  $0.9 \text{ mmol h}^{-1} \text{ g}^{-1}$ , which is 4 times higher compared with that of bulk  $Bi_{24}O_{31}Cl_{10}$  [148]. A controlled thermal process was adopted to prepare different indium oxide  $InO_x$  nanoribbons (NRs) with tunable O-vacancy: P- $InO_x$  NRs, O- $InO_x$  NRs, and H- $InO_x$  NRs. The H- $InO_x$  NRs rich in O-vacancy showed enhanced performance for the electrocatalytic  $CO_2$  conversion to HCOOH with the selectivity up to 91.7% [72].

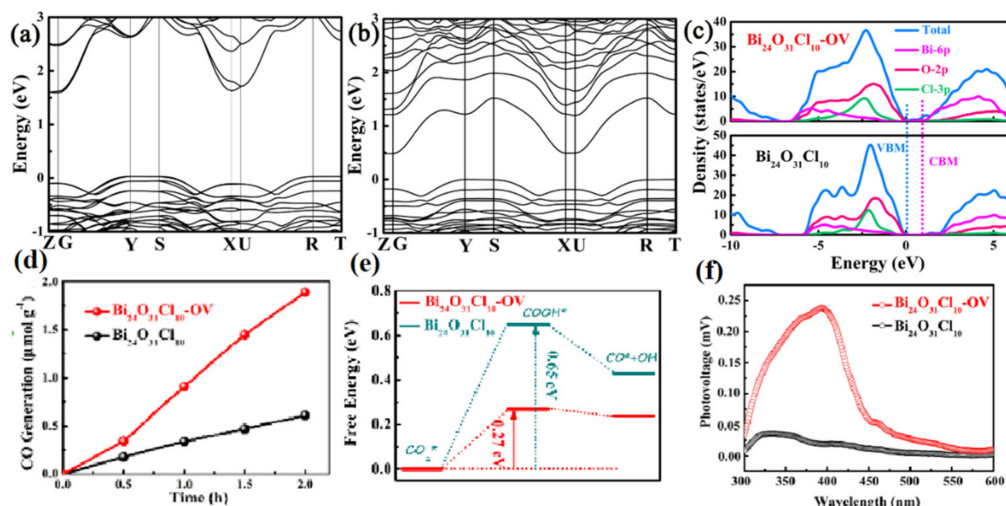


**Figure 8.** Calculated electronic band structures of (a)  $Bi_{24}O_{31}Cl_{10}$ , (b)  $Bi_{24}O_{31}Cl_{10}-OV$ , and (c) the corresponding DOS plots. (d) CO evolution rate of  $Bi_{24}O_{31}Cl_{10}$  and  $Bi_{24}O_{31}Cl_{10}-OV$ . (e) Free-energy diagram for  $CO_2$  reduction to CO on  $Bi_{24}O_{31}Cl_{10}-OV$ . (f) Surface photovoltage spectroscopy showing carrier separation behavior. Reproduced with permission from the authors of [148]. Copyright 2019 John Wiley & Sons, Inc.

In the plasma method, the material is subjected to high-energy ion (such as  $Ar^+$ ,  $N_2^+$ ,  $H_2O^+$ ) bombardment [166]. Metal oxides bombardment with these high-energy ions generates oxygen vacancies on the surface. An advantage is that the plasma treatment is fast and can effectively etch the oxide to expose more surface sites and selectively remove oxygen from the surface to produce oxygen vacancies. Geng et al. [74] introduced oxygen vacancies in ZnO nanosheets via  $H_2$  plasma treatment for the electrochemical reduction of  $CO_2$ . This induced the formation of a new defect level around the valence band maximum, where abundant localized electrons accumulation caused increasing charge density. The new electronic structure promoted the activation of  $CO_2$ , and the ZnO nanosheets with rich oxygen vacant sites ( $V_o$ -rich ZnO nanosheets) exhibited a current density for CO production of  $-16.1 \text{ mA cm}^{-2}$  with a Faradaic efficiency of 83% at  $-1.1 \text{ V}$  versus RHE. The oxygen vacancies concentration can be controlled by the plasma treatment time.

The photochemical reactions for generating oxygen vacancies involve directing a photo source to the synthesis reaction system, as shown in Figure 9 [119]. Hezam et al. [119] used sunlight as the energy source to effect exothermic combustion reaction between  $Ce-(NO_3)_3 \cdot 6H_2O$  and  $C_2H_5NO_2$ . The presence of the light source improved the oxygen vacancies generation in  $CeO_2$  compared with  $CeO_2$  synthesized in the conventional way, without sunlight.



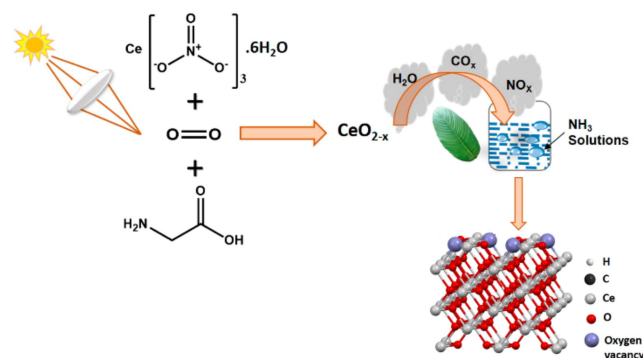


**Figure 9.** Photo-assisted solution combustion synthesis of  $\text{CeO}_2$  with rich oxygen vacancies. Redrawn with permission from the authors of [119]. Copyright 2019 American Chemical Society.

### The Roles of Oxygen Vacancies

#### (1) $\text{CO}_2$ adsorption and dissociation, creation of binding and active sites

In the adsorption and dissociation of  $\text{CO}_2$  on the anatase  $\text{TiO}_2$  (101) surface, by dispersion-corrected DFT calculations, Sorescu et al. [137] found that  $\text{CO}_2$  adsorbed at a fivefold coordinated Ti site in a skewed configuration on an oxidized surface. The presence of a bridging oxygen defect allowed for the creation of strong binding configurations. Lee et al. [139] found that  $\text{CO}_2$  was preferentially adsorbed at the oxygen vacancy defects on the  $\text{TiO}_2$  (110) surface. During the  $\text{CO}_2$  reduction process, one oxygen atom of  $\text{CO}_2$  filled an oxygen vacancy, decreasing the surface concentration. Oxygen vacancies provided active sites and increased the  $\text{CO}_2$  adsorption energy, promoting  $\text{CO}_2$  adsorption and activation on the photocatalyst surface. It was also found that subsurface oxygen vacancy enhanced the binding of  $\text{CO}_2$  molecules to the surface, and the  $\text{CO}_2$  dissociation from the defect sites was exothermic with a barrier of less than 21 kcal/mol [70].  $\text{CO}_2$  adsorbed directly at the oxygen vacant sites of  $\text{Zn}_2\text{GeO}_4$  dissociated into CO and O [117]. As the oxygen vacancies can be healed by oxygen atoms released during the dissociation process, the dissociative adsorption of  $\text{CO}_2$  on the oxide followed a stepwise mechanism that could be described as:  $\text{CO}_2 + \text{V}_o \rightarrow \text{CO}_2^{\delta-} / \text{V}_o \rightarrow \text{CO}_{\text{ad}} + \text{O}_{\text{sur}}$ , where  $\text{V}_o$  is the oxygen vacancy.

Huygh et al. [150] studied the adsorption and activation of  $\text{CO}_2$  on the fully oxidized and reduce anatase  $\text{TiO}_2$  (001) surfaces using DFT calculations with long-range dispersion energy corrections (Figure 10a,b). They found the monodentated carbonate-like structure to be the most stable adsorption configuration for the fully oxidized surface.  $\text{CO}_2$  dissociation was not observed on the stoichiometric anatase  $\text{TiO}_2$  (001) surface. The introduction of oxygen-vacant defects gave rise to new highly stable adsorption configurations with stronger C–O bond activation. These reactions caused the formation of a CO molecule, which will easily desorb, and the reduced surface became oxidized.

By DFT slab calculations, Pan et al. [151] studied the effects of hydration and oxygen vacancy on  $\text{CO}_2$  adsorption on the  $\beta\text{-Ga}_2\text{O}_3$  (100) surface. Adsorption of  $\text{CO}_2$  on the perfect dry  $\beta\text{-Ga}_2\text{O}_3$  (100) surface was slightly endothermic, with an adsorption energy of 0.07 eV, which resulted in a carbonated species. The presence of oxygen vacancies promoted the adsorption and activation of  $\text{CO}_2$ . On the most stable  $\text{CO}_2$  adsorption configuration, one of the oxygen atoms of the adsorbed  $\text{CO}_2$  occupied the oxygen vacancy site with low adsorption energy (−0.31 eV). Feng et al. [167] synthesized a series of  $\text{GaZrO}_x$  catalysts by the evaporation-induced self-assembly (EISA) method and proposed the  $\text{Zr}^{3+}\text{-O}_V\text{-Ga-O}$  species ( $\text{O}_V$  represents the oxygen vacancy) on the  $\text{GaZrO}_x$  surface as the active site (Figure 10c). The synergistic effect stems from neighboring Ga–O and  $\text{Zr}^{3+}\text{-O}_V$  sites.  $\text{H}_2$  dissociated on the Ga–O sites to produce Ga–H and OH species, while  $\text{CO}_2$  was trapped by the oxygen vacancies and activated by electron transfer from the  $\text{Zr}^{3+}$  ions. Liu et al. [47] studied the activation of  $\text{CO}_2$  on the defective surface of  $\text{Cu(I)}/\text{TiO}_{2-x}$  using the in situ diffuse reflectance infrared Fourier transformed spectroscopy (DRIFTS). They observed the formation of  $\text{CO}_2^-$  species upon the transfer of an electron to  $\text{CO}_2$ . The anionic  $\text{CO}_2^-$

species further dissociated into CO on a partially oxygen-depleted Cu(I)/TiO<sub>2-x</sub> surface obtained by thermal annealing in a non-reactive atmosphere. The dissociation process was enhanced by the surface Cu<sup>+</sup> species on the catalyst. The defective surface also delivered the electronic charge for the formation of Ti<sup>3+</sup>. It was observed that the dissociation of CO<sub>2</sub><sup>-</sup> in the absence of light related to the surface oxygen vacancies that provided electronic charge and sites for the adsorption of oxygen atoms from CO<sub>2</sub>. DFT studies also confirmed that the adsorption of CO<sub>2</sub> at the oxygen vacancy site over the Zn-terminated ZnO (0001) surface occurs by inserting one of the O atoms of CO<sub>2</sub> into the vacancy, resulting in the formation of a bent CO<sub>2</sub> species [168]. Singh et al. [169] investigated the role of oxygen vacancies and basic site density in tuning methanol selectivity over Cu/CeO<sub>2</sub>, Cu/ZnO, and Cu/ZrO<sub>2</sub> catalysts during CO<sub>2</sub> hydrogenation. The strong basic sites for CO<sub>2</sub> adsorption over catalyst surface were attributed to unsaturated, low coordination oxygen atoms (derived from oxygen vacancies), the oxygen vacancy concentrations of Cu/CeO<sub>2</sub> catalyst was higher than those of Cu/ZnO and Cu/ZrO<sub>2</sub> catalysts, so the Cu/CeO<sub>2</sub> catalyst exhibited more than 90% methanol selectivity at 220 °C and 30 bar. The adsorption capacity of m-ZrO<sub>2</sub> was increased due to the high concentration of oxygen vacancy on its surface, which led to the higher catalytic activity of Cu/m-ZrO<sub>2</sub> compared with that of Cu/t-ZrO<sub>2</sub> [170]. This benefited the activation of CO<sub>2</sub>, thus improving the catalytic activity for methanol synthesis. Martin et al. [171] synthesized In<sub>2</sub>O<sub>3</sub>/ZrO<sub>2</sub> catalyst and observed the catalyst had high activity, high stability, and high selectivity due to the possession of a large number of oxygen vacancies. It was difficult to form oxygen vacancy on the Pt/SiO<sub>2</sub> interface, and also weak CO<sub>2</sub> adsorption was observed due to an obvious lack of the oxygen vacancies. However, CO<sub>2</sub> adsorbed strongly on TiO<sub>2</sub> due to the presence of oxygen vacancies on the TiO<sub>2</sub> surface [172].

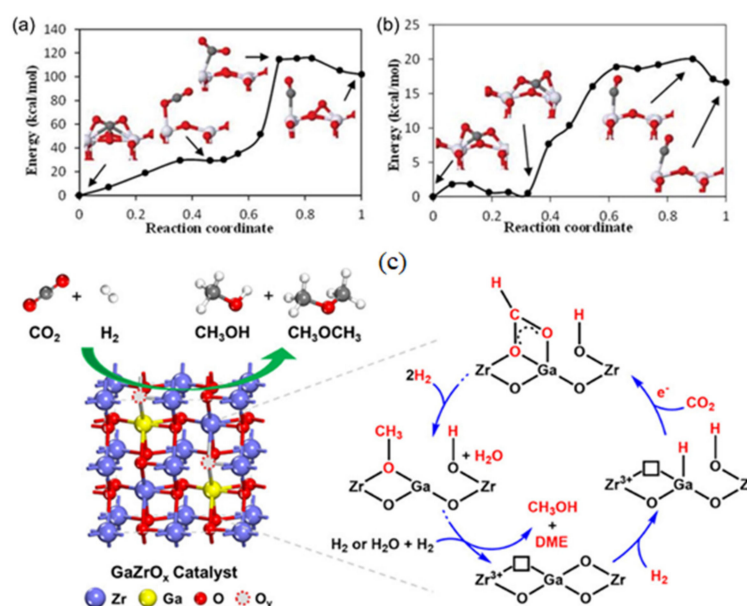


**Figure 10.** CO<sub>2</sub> dissociation minimal energy pathway on (a) stoichiometric anatase (001) surface and (b) reduced anatase (001). Reproduced with permission from the authors of [150]. Copyright 2016 American Chemical Society (c) Proposed mechanism for the hydrogenation of CO<sub>2</sub> to methanol and DME on the GaZrO<sub>x</sub> catalyst. Reproduced with permission from the authors of [167]. Copyright 2021 American Chemical Society.

- (2) Selection of reaction pathway, stabilization of key intermediates and electronic structure modification

CO<sub>2</sub> hydrogenation to methanol on In<sub>2</sub>O<sub>3</sub> surface with an oxygen vacancy was investigated by Ye et al. [152] using periodic DFT calculations. Different kinds of oxygen vacancies were identified with dissimilar energy states. On the surface with the highest

energy, one of the O atoms of the  $\text{CO}_2$  molecule filled in the site upon adsorption. The hydrogenation process that proceeded passed through the  $\text{HCOO}^*$  intermediate. Further hydrogenation of  $\text{HCOO}^*$  formed the C–H bond following the C–O bond scission, resulting in  $\text{H}_2\text{CO}^*$  and hydroxyl. This step was slightly endothermic with a barrier of 0.57 eV but both thermodynamically and kinetically favorable. These observations confirm that the oxygen vacancy on the  $\text{In}_2\text{O}_3$  (110) surface assists  $\text{CO}_2$  activation and hydrogenation and also stabilizes the key intermediates ( $\text{HCOO}^*$ ,  $\text{H}_2\text{COO}^*$ , and  $\text{H}_2\text{CO}^*$ ) involved in methanol formation. The methanol molecules healed the oxygen vacant sites by replenishing them (Figure 11) with the assistance of  $\text{H}_2$ , sustaining the catalytic cycle. Oxygen vacancy catalyzed the formate dissociation to methanol, which was the rate-determining step on Ru/ $\text{CeO}_2$  catalyst. Moreover, the activation temperature for the formate route was much lower than that for the CO route (150 °C vs. 250 °C), which shows the advantage of oxygen vacancy in promoting the rate-determining step [173].

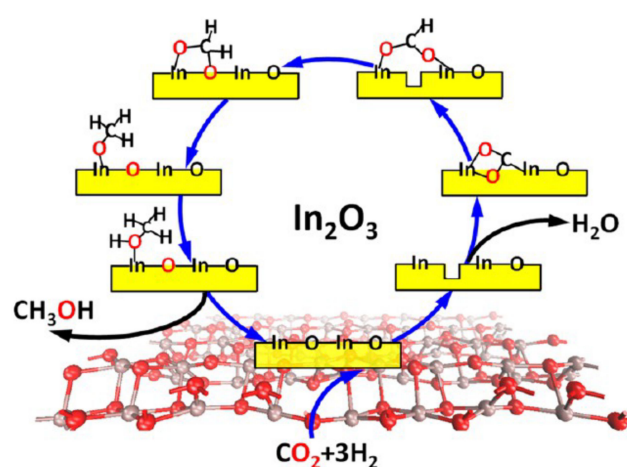


**Figure 11.** Possible oxygen vacancies formation mechanism and their healing in  $\text{CO}_2$  hydrogenation to methanol. Reproduced with permission from the authors of [152]. Copyright 2013 American Chemical Society.

The introduction of oxygen vacancies into ZnO nanosheets created a new defect level around the valence band maximum where abundant localized electrons accumulated. This formed a new electronic structure that benefited the activation of  $\text{CO}_2$  as revealed by the lower Gibbs free energy and lower energy barrier of the rate-determining step than that of the ZnO slab for the formation and activation of  $^*\text{COOH}$  intermediates [74]. The  $\text{Bi}_2\text{Sn}_2\text{O}_7$  NPs with oxygen vacancies possess the ability to back donate an electron and optimize the electronic structure for effective  $\text{CO}_2$  activation as proven by DFT calculations, revealing through the catalytic performance efficient stabilization of the  $^*\text{COOH}$  intermediates, and energy barrier reduction for CO desorption which was the determining step [164]. Abundant oxygen vacancies in  $\text{Bi}_{24}\text{O}_{31}\text{Cl}_{10}$  improved separation of electron–hole pairs, enhanced charge density, and lowered activation energy for the formation of intermediates during the photocatalytic  $\text{CO}_2$  reduction that led to an optimized  $\text{CO}_2$  conversion efficiency [148]. The photocatalytic performance (enhanced light absorption and improved charge carrier separation) of  $\text{CeO}_2$  nanoparticles (12–18 nm) was improved in the presence of higher concentration of oxygen vacancies, which suppressed the electron–hole recombination as studied using photoluminescence, and confirmed with photocurrent measurement results. The surface oxygen vacancies modified the surface state above the valence band, as seen in the upward shift relative to the vacuum (Figure 12). In the photoelectrochemical  $\text{CO}_2$  reduction system, introducing oxygen vacancies into the lattice of a semiconductor catalyst can alter its intrinsic electronic properties and band gap, promote the transfer of electrons and facilitate adsorption and activation of  $\text{CO}_2$  [139].

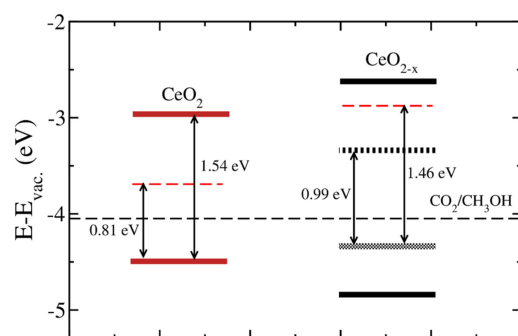


**Figure 12.** Valence band top and conduction band bottom energies of  $\text{CeO}_2$  surface without ( $\text{CeO}_2$ ) and with ( $\text{CeO}_{2-x}$ ) oxygen vacancies. Modified surface state and defect peak are shown with the shaded and striped black blocks, respectively. Reproduced with permission from the authors of [119]. Copyright 2019 American Chemical Society.

### 3.3.4. The Roles of Solvent in $\text{CO}_2$ Transformation

There have been interesting attempts to replace water with other solvents as reductants in photocatalytic  $\text{CO}_2$  reduction. For example, as described in a study by Srinivas et al. [174],  $\text{CO}_2$  reduction with CdS in various solvents (water, methanol, ethanol, and 1-propanol of different dielectric constants of 80, 33, 24.3, and 20.1, respectively) was experimentally investigated. Formate and CO were observed as the major products in various solvents deployed as reductants in the photocatalytic reduction of  $\text{CO}_2$  using  $\text{TiO}_2$  nanocrystals embedded in  $\text{SiO}_2$  matrices as the photocatalyst [175]. The characteristics of the solvent (defined with polarity/dielectric constant) and  $\text{CO}_2$  adsorption/dissolution will determine the selectivity toward the product. Based on the polarity and dielectric constant, solvents with low dielectric constant or low polarity could in situ generate  $\text{CO}_2^-$  anionic radicals that were strongly adsorbed on the surface of the catalyst through the carbon atom because the  $\text{CO}_2^-$  anion radicals were poorly dissolved in the solutions [174,175]. This will lead to the formation of CO as the major product. In solutions with high dielectric constants, such as water, the  $\text{CO}_2^-$  anion radicals are well stabilized in the solvent, resulting in a weak interaction with the photocatalyst surface. In this case, the carbon atom tends to be attracted to a proton, exhibiting a high propensity toward formate formation [175]. However, water is often deployed for the photocatalytic (artificial photosynthesis) and, in some cases, electrocatalytic  $\text{CO}_2$  reduction reactions.

The change in the adsorbed surface species and surface chemical state of catalysts has been correlated with the moisture or humidity change during chemical reactions [107]. Adsorbed water takes part in the reaction chemistry of  $\text{CO}_2$  on metal oxide surfaces. Water molecules involve in the  $\text{CO}_2$  reduction process by providing hydroxyl ions and protons that facilitate the electron transfer [176]; thus,  $\text{H}_2\text{O}$  is beneficial for hydroxylation of the catalyst surface. In addition, the adsorption and dissociation of  $\text{H}_2\text{O}$  to protons on the catalyst surface can activate deep reduction, leading to highly reduced state hydrocarbon products [32]. On the hydroxylated metal/metal oxide surfaces,  $\text{CO}_2$  can bind as bicarbonates and carbonates in monodentate and bidentate modes [114]. Co-adsorbed water was essential for activating  $\text{CO}_2$  by forming surface adsorbed intermediates during methanol synthesis on metal/oxide catalysts [177]. Most photocatalytic  $\text{CO}_2$  reduction reactions proceed in the presence of  $\text{H}_2\text{O}$ . Water participates in the reaction by capturing photogenerated holes to generate  $\text{O}_2$ , thus reducing the recombination rate of photogenerated holes and electrons. Under this condition, the utilization efficiency of photogenerated electrons can be improved [32]. Although water is often used as the reducing agent in photocatalytic process, pure water is hardly used. The use of NaOH-containing water solution is practiced due to undisputed benefits that include: (i) facilitating the dissolution of adsorbed  $\text{CO}_2$  due to its high affinity with caustic NaOH solution, and (ii) slowing the electron-hole pairs recombination, leading to more utilization of surface electrons that facilitates  $\text{CO}_2$

reduction. The OH ions in aqueous basic solutions act as strong hole scavengers and readily form  $\bullet\text{OH}$  radicals [174].

In the absence of co-adsorbed  $\text{H}_2\text{O}$ , the in situ  $\text{H}_2\text{O}$  formation is possible via the following mechanism. In the presence of  $\text{H}_2$  as a reducing agent, over the surface of supported metals/metal oxides,  $\text{H}_2$  dissociates at the metal sites or metal-oxide interface to adsorbed  $\text{H}^*$  atoms, which then migrate to the active sites and react with the surface oxygen atoms of metal oxide or interact with the adsorbed  $\text{CO}_2$  species in a stepwise fashion to form water [178]. Therefore, the hydroxylation of the catalyst surface is still possible when  $\text{H}_2$  is deployed as a reductant, and the facile and efficient activation of hydrogen is necessary. Using DFT,  $\text{CO}_2$  adsorption was investigated on the  $\text{In}_2\text{O}_3$  (110) surface for methanol synthesis to understand the benefits of  $\text{H}_2$  and  $\text{H}_2\text{O}$  presence. Results revealed the hydroxylation of the catalyst surface.  $\text{H}_2$  dissociated homolytically on the oxide surface with a high surface coverage, leading to the formation of water. This induced the formation of surface OH-groups, which reduced under-coordinated In atoms at the surface, giving rise to In ion sites and enhanced the formation of oxygen vacancies observed at high hydrogen coverages [179]. However, the oxygen vacancies formed on  $\text{In}_2\text{O}_3$  (110) surfaces did not facilitate  $\text{CO}_2$  adsorption during the reaction.  $\text{CO}_2$  adsorption was facilitated on hydroxylated surface sites, leading to activation by accepting one electron from the  $\text{In}_2\text{O}_3$  (110) surface [179]. Su et al. [112] observed the promotion of a reaction with adsorbed oxygen which formed  $\text{H}_2\text{O}$  after the introduction of  $\text{H}_2$  during the RWGS, although the adsorbed  $\text{H}_2\text{O}$  desorbed from the surface at high temperatures. It was also found that adsorbed  $\text{CO}$  produced more in the presence of  $\text{H}_2$ .

The effect of  $\text{H}_2\text{O}$  on Ni surfaces pre-exposed to  $\text{CO}_2$  was investigated by Cai et al. [107]. As observed using ambient air XPS measurements (Figure 13c,d), a new peak evolved in the O 1s spectra at 535.3 eV due to the gas-phase  $\text{H}_2\text{O}$ , that transformed to surface hydroxyl and adsorbed water with increased concentrations as revealed by the enhanced peak intensities at 530.9 and 532.6 eV, respectively. It obviously indicates that adsorption and dissociation of  $\text{H}_2\text{O}$  occurred on the Ni surfaces, producing H atom and OH, which further reacted with  $\text{CO}_2$  and other surface species to produce  $\text{CO}_2$  hydrogenation intermediates and product species (formate, methoxy/ $\text{CO}^*$ , and carbonate species) as shown in Figure 13a,b.

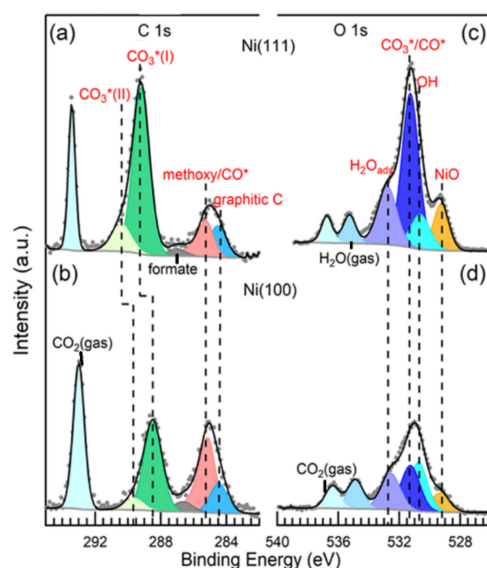


**Figure 13.** Ambient pressure XPS spectra of (a) C 1s, (c) O 1s of Ni (111) and (b) C 1s, (d) O 1s of Ni (100) in 0.2 Torr  $\text{CO}_2$  + 0.2 Torr  $\text{H}_2\text{O}$  at room temperature. Reproduced with permission from the authors of [107]. Copyright 2019 American Chemical Society.

The interaction of CO<sub>2</sub> with a ZrO<sub>2</sub> model surface (a O–Zr–O trilayer grown on Pt<sub>3</sub>Zr (0001)) with and without the presence of H<sub>2</sub>O was measured by in situ near ambient (atmospheric) pressure XPS (NAP-XPS) and infrared reflection absorption spectroscopy (IRAS). No interaction was observed with the ZrO<sub>2</sub> model surface at room temperature upon exposure to pure CO<sub>2</sub> up to  $3 \times 10^{-2}$  mbar. Co-adsorption of CO<sub>2</sub> with H<sub>2</sub>O led to the formation of various carbonaceous surface species. This means that activation of CO<sub>2</sub> occurred near ambient pressures under the humid condition due to surface hydroxylation that led to the formation of surface species identified by the combined NAP-XPS and IRAS measurements [177]. On reduced CeO<sub>x</sub>-TiO<sub>2</sub> composite surfaces, the interaction of CO<sub>2</sub> and H<sub>2</sub>O was thermodynamically favorable at multiple sites. H<sub>2</sub>O molecules were observed to spontaneously dissociate at the oxygen vacant sites, generating surface hydroxyl groups that reacted with CO<sub>2</sub> to form carbonaceous species—carboxylate or bicarbonate species—according to the NEXAFS results [130]. The apparent correlation between CO<sub>2</sub> and water was investigated via infrared experiments performed using regular and deuterated water to pre-cover the surface prior to the CO<sub>2</sub> adsorption. It was found that the degree of hydroxylation of the surface plays a crucial role in CO<sub>2</sub> adsorption on regular (Fe<sub>tet1</sub>) tetrahedrally terminated magnetite (Fe<sub>3</sub>O<sub>4</sub>) surface, leading to the formation of surface bicarbonates [144]. Surface hydroxide sites in hydroxylated indium oxide (In<sub>2</sub>O<sub>3-x</sub>(OH)<sub>y</sub>) acted as Lewis base for CO<sub>2</sub> activation [180]. In the presence of co-adsorbed water, metal oxides (FeO<sub>x</sub>, Al<sub>2</sub>O<sub>3</sub>, and TiO<sub>2</sub>) exhibited high reaction rates for CO<sub>2</sub> adsorption under ambient conditions and, thus, can improve the CO<sub>2</sub> adsorption kinetics [176].

Although the positive effects of moisture have been discussed, an experimental report revealed a 20% decrease in methanol yield under standard methanol synthesis conditions when water was co-fed into an H<sub>2</sub>/CO<sub>2</sub> mixture over In<sub>2</sub>O<sub>3</sub> surface [181]. The co-adsorption of H<sub>2</sub>O suppressed the interfacial interaction between CO<sub>2</sub> and Ni surface [107]. On defective β-Ga<sub>2</sub>O<sub>3</sub> (100) with rich oxygen vacancy, water spontaneously enhanced dissociative adsorption of CO<sub>2</sub> at the oxygen vacancy site, with reaction energy of −0.62 eV. These results indicate that the co-existence of water and CO<sub>2</sub> in the adsorption system imposes competition with CO<sub>2</sub> for the oxygen vacancy sites, which negatively impacts CO<sub>2</sub> chemisorption and conversion [151].

### 3.3.5. General Methods for Modifying Metal Oxide Surface Structure for CO<sub>2</sub> Transformation

Several approaches can be applied to modify the structure of metal oxides for the facile adsorption and dissociation of CO<sub>2</sub> molecules, mainly, through tailoring their physicochemical (e.g., improving surface basicity) [182,183] and electronic properties (e.g., doping and creating defect sites) [182].

- (i) Insertion of acidic and basic surface sites. The basic sites on the catalyst surface can facilitate CO<sub>2</sub> adsorption because CO<sub>2</sub> is an acidic compound whose interaction with the catalyst surface will be enhanced with a basic surface. The basic sites of metal oxide catalysts can be generated by pre-treatment with basic promoters such as La<sub>2</sub>O<sub>3</sub>, K<sub>2</sub>O, Na<sub>2</sub>O, and MgO [183]. Tian et al. [182] reported that introducing potassium into iron oxide catalyst increased the surface basicity. Thus, alkali metals can be incorporated into the metal oxides to tune the concentration of surface basic sites. The basic sites enhance the activation of acidic CO<sub>2</sub> and also help to limit carbon deposition. The overall benefit is improvement in catalytic activity and stability. For example, in the CO<sub>2</sub> dry reforming of methane, the catalytic reaction was initiated by an acid–base interaction [183]. On the In<sub>2</sub>O<sub>3-x</sub>(OH)<sub>y</sub> surface, comprising frustrated Lewis pairs (FLP) (A frustrated Lewis pairs consists of both Lewis acid and Lewis base that cannot combine to form an adduct due to steric hindrance.), the surface hydroxide site acts as Lewis base and the coordinately unsaturated In surface site acts as a Lewis acid to activate CO<sub>2</sub> [180]. The Lewis acid and Lewis base synergistically interact to heterolytically dissociate H<sub>2</sub> adsorbed on the In<sub>2</sub>O<sub>3-x</sub>(OH)<sub>y</sub> surface, forming protonic

surface FLP sites that can capture and convert CO<sub>2</sub> to CO and H<sub>2</sub>O. The surface Lewis basicity can be tuned by the nature of the metal site, which can be controlled by the size, charge, coordination number, geometry, and electronegativity of the metal in a particular oxidation state [114]. Surface basic sites can be characterized using CO<sub>2</sub>-TPD. Typically, desorption at high temperatures signifies the presence of strong basic sites. The CO<sub>2</sub> adsorption strength on metal oxides has been related to the basicity, improving as the concentration increases. However, too strong adsorption may result in the formation of undesirable intermediate species such as surface carbonate and bicarbonate species.

- (ii) Metal oxide doping. Doping metal oxides with metallic elements can optimize their electronic and geometric structures and enhance catalytic performance. Alkali metals doping can modify the electronic structure by increasing the concentration of electron-withdrawing groups such as surface hydroxyl groups or reducing the kinetic barrier for CO<sub>2</sub> dissociation [184]. Moreover, oxides with electron-rich defect centers may interact readily with CO<sub>2</sub> by donating an electron. These, in turn, will facilitate surface reaction activity, boosting catalytic efficiency for CO<sub>2</sub> activation. The list is not exclusive to alkali metals, as some transition metals have the potentials to tune the electronic characteristics of the doped oxide. Doping transition metal oxide to the based oxide can as well tune the concentration of oxygen vacancies
- (iii) Defect engineering. It involves creating or adjusting surface oxygen vacancies or hydroxyl groups in an oxide. The presence of oxygen defective sites can similarly impact the surface electronic property. Evidence has linked the activity of an oxide catalyst with surface defects. For example, it was demonstrated that the activity of MnO<sub>2</sub> in HCHO oxidation correlated with the concentration of surface defects [185]. CeO<sub>2</sub> nanoparticles with a high concentration of oxygen vacancies had high photocatalytic performance in converting CO<sub>2</sub> to methanol (0.702 μmol h<sup>-1</sup> g<sup>-1</sup>) [119]. Furthermore, oxygen vacancies are sites for adsorption and anchoring of CO<sub>2</sub> molecules. Consequently, surface adsorption and reactivity of adsorbates, including H<sub>2</sub> and H<sub>2</sub>O, would be facilitated in the presence of extra electrons in the vicinity of oxygen vacancies. The amount of defective sites in a metal oxide can be controlled by oxidative treatment during the catalyst synthesis and catalytic reactions.
- (iv) Generation of surface hydroxyls. The surface hydroxyl groups participate in CO<sub>2</sub> hydrogenation by incorporating hydrogen atom into CO<sub>2</sub>, facilitating CO<sub>2</sub> activation and accelerating reaction rate. Mechanistic studies evidenced the surface hydroxyl species on SiC quantum dots (QDs) to directly participate in CO<sub>2</sub> hydrogenation through the addition of H atoms of hydroxyl groups into CO<sub>2</sub> to form HCOO\* [186]. The surface hydroxide site on the In<sub>2</sub>O<sub>3-x</sub>(OH)<sub>y</sub> surface acted as a Lewis base that interacted with CO<sub>2</sub> [180].
- (v) Mixed metal oxides or composites catalysts can yield good catalytic performances. Introducing a second oxide component can improve adsorption, increase the effective oxygen vacancies, and present an interfacial surface for reactions (adsorption/activation and desorption). When preparing a mixed-metal oxide catalyst, consideration should be given to factors that can improve catalytic performance, such as elemental composition since catalytic activity can be a function of how elements in the composite are combined. The deposition of sub-monolayer amounts of a second oxide over a host oxide can create nanostructures that can enhance the overall catalytic properties of the composite system [114,187].
- (vi) Forming metallic–non-metallic hybrid catalysts. These kinds of catalysts have high surface areas and improved adsorption properties. Carbon materials, such as carbon nanotubes (CNTs) and graphene oxides (GOs), and metal oxides (e.g., TiO<sub>2</sub>, CeO<sub>2</sub>, Al<sub>2</sub>O<sub>3</sub>, ZrO<sub>2</sub>, In<sub>2</sub>O<sub>3</sub>, Ga<sub>2</sub>O<sub>3</sub>, and NiO) can be grafted to form hybrid nanostructured materials [154,188–190]. Carbon materials possess very high surface areas, whereas metal oxides are endowed with rich oxygen vacancies. Combining materials with these features can result in a unique hybrid material with superior catalytic perfor-

mance toward CO<sub>2</sub> reduction reactions. The high surface area will enhance adsorption complemented by oxygen vacancies, which are also sites for CO<sub>2</sub> activation on oxide catalysts. Modification of CuO–ZnO–ZrO<sub>2</sub> with GO increased the adsorption capacities of both CO<sub>2</sub> and H<sub>2</sub>, resulting in an improved catalytic activity (methanol selectivity) in methanol synthesis than the GO-free catalyst [188]. The electronic structure of the traditional methanol synthesis catalyst (Cu–ZnO–Al<sub>2</sub>O<sub>3</sub>) was altered by adding the N-doped graphene, which provided a synergistic effect for methanol synthesis [189]. Incorporating metal oxides to single-wall CNT electrode can form a hybrid structure with an increase in specific surface area, which also improved electrical conductivity and charge transfer [191,192]. Moreover, doping carbon into photocatalysts can enhance light absorption and improve the photothermal conversion efficiency by reducing the energy for oxygen vacancy formation, thus generating a high concentration of active sites [190]. Therefore, hybrid nanostructured materials with good electronic and charge transfer properties can be explored for both thermochemical and electrochemical reduction of CO<sub>2</sub>.

- (vii) Stabilization of metal oxide surface. Reduced oxides are more susceptible to react with CO<sub>2</sub> [118,193]. Stabilizing the reduced surface can be achieved by creating a conducive environment for reactions such as forming oxide–metal or oxide–oxide interfaces [128,187,194]. The synergistic properties associated with these interfaces can improve the surface chemistry of metal oxides and could be beneficial for synthesizing efficient catalysts for CO<sub>2</sub> transformation.

#### 4. Conclusions

Controlling the emission of CO<sub>2</sub> by converting it to products of economic value is highly attractive. However, CO<sub>2</sub> is a kinetically stable molecule that requires high energy input for the C–O bond breaking. Its proper activation can reduce the high energy barrier substantially, easing conversion by various processes. The CO<sub>2</sub> activation is an important step that precedes the conversion of CO<sub>2</sub> to chemicals and fuels. It can be effected in the presence of a catalyst by decreasing the O–C–O angle from 180 degrees (bending), weakening and elongation of the C–O bonds, polarizing the charges on C and O by charge/electron transfer, and redistribution of charges on the CO<sub>2</sub> molecule. Upon accepting an extra electron from a substrate, the neutral CO<sub>2</sub> molecule forms an anion with a full charge (CO<sub>2</sub><sup>−</sup>) or partial charge (CO<sub>2</sub><sup>δ−</sup>). However, a recent study has proposed that just a charge transfer is insufficient to activate CO<sub>2</sub> molecules on metal oxide catalysts, but the binding of an O atom to a surface metal cation weakens and elongates the molecular C–O bond.

Some metals and metal oxides are efficient catalysts for CO<sub>2</sub> conversion reactions; thus, they should be good for CO<sub>2</sub> activation. In general, metal nanoparticles serve as active sites for electron transfer, with certain factors such as change in morphology of metal particles, nanoparticle size, adsorption mode and configuration, and chemical ordering as the CO<sub>2</sub> activation marker. The interaction of CO<sub>2</sub> with pure metals is rather weak but can be improved by incorporating promoters (e.g., alkali metals) with low electronegativity. Metal oxide nanoparticles are utilized as supports or directly as catalysts for the CO<sub>2</sub> conversion. Their surfaces comprise both metal (M<sup>n+</sup>) and oxygen (O<sup>2−</sup>) ions, which can act as active sites for CO<sub>2</sub> activation. They can activate CO<sub>2</sub> by coordinating to one or two adjacent metal sites through the terminal oxygen atoms of the CO<sub>2</sub> or interaction of the carbon atom of CO<sub>2</sub> with surface oxygen sites. A particularly interesting feature in metal oxides is the oxygen vacancies.

Oxygen vacancies are of great benefits to the overall reaction thermodynamics and kinetics and can greatly enhance the adsorption energy of CO<sub>2</sub> molecules, promoting interaction of CO<sub>2</sub> with the oxide surface. Indeed, oxygen vacancies play vital roles in the overall CO<sub>2</sub> conversion process, ranging from electronic structure modification, selection of reaction pathway, and stabilization of key intermediates to the creation of binding surface, sites for CO<sub>2</sub> adsorption, and dissociation. Although being an integral part of reducible



oxides, the concentration of oxygen vacancies can be increased or created in metal oxide catalysts either in situ during reactions or incorporated by external methods, including thermal annealing at high temperatures, doping, plasma-assisted techniques, photo-irradiation, and solid-state chemical reactions during synthesis or by post-synthesis techniques.

The surface hydroxyl groups, which can be introduced in metal oxide catalysts in the presence of moisture, also present significant CO<sub>2</sub> activation enhancement by facilitating interaction and providing additional binding sites.

Several strategies are applicable to modify metal oxide catalysts for CO<sub>2</sub> activation and conversion. Creating more basic surface sites can stimulate surface reaction with acidic CO<sub>2</sub>. Other strategies include elemental doping and defect engineering. Surface defect sites are good adsorption sites for CO<sub>2</sub> on metal oxides. Doping with low electronegative elements can enrich the surface with electrons to easily transfer to CO<sub>2</sub> upon adsorption. Like the case of basic sites, generating more hydroxyl groups to make the surface hydrophilic can boost the catalytic performance of metal oxides, similar to those of metal hydroxides or layered double hydroxides. Hybrid catalysts, such as metal oxide/carbon material and composite oxide catalysts, tend to improve the performance of the resulting system through the synergism of the individual components. In these processes, it is possible to stabilize the metal surface by forming oxide–metal or oxide–oxide interfaces. The synergetic properties associated with such interfaces can improve the surface chemistry for reactions. In view of the catalysts discussed in this work, metal oxides with large numbers of oxygen vacancies exhibit excellent performance for CO<sub>2</sub> adsorption and activation. In the present, researchers have demonstrated the ability of pure (e.g., In<sub>2</sub>O<sub>3</sub>) or doped (ZnO–ZrO<sub>2</sub>) metal oxides and metal–organic framework to reduce CO<sub>2</sub> to methanol, and of course, some other products. However, challenges remain due to the relatively low catalytic activity and selectivity of these materials. Perhaps, their bulk forms are presented with these limitations. Furthermore, other factors, such as the strong metal–support interactions (SMSI) for supported metal catalysts on the reducible oxide supports, should be considered, as the reduced support oxide can migrate and cover the active metal particles, significantly impacting the electronic and interface structure of the catalysts [195,196].

Specially designing and engineering surface functionalities in these materials, including inserting a controllable amount of oxygen vacancies in the right proportion and surface hydroxyls, is capable of tuning the catalytic properties, in which activation of CO<sub>2</sub> molecule should be a topmost consideration. The future offers great opportunities to develop even more active heterogeneous catalysts for the various CO<sub>2</sub> reduction reactions. The possible structural transformations of the catalysts, which remain elusive, can be unveiled to address the complexities involved in these reactions fully. Identifying the catalyst structural defects, their formation or transformation during the reaction, and their contribution to the overall activity is still a challenging task, yet of significant importance. Theoretical models can provide predictions on the catalyst system, and such methods should be deployed to model new metal oxide catalysts with incorporated functionalities.

**Author Contributions:** U.J.E. and C.Z. wrote the manuscript; U.J.E. organized and revised the manuscript; Z.Z. provided the original thoughts about the content and structure of the manuscript and technical inputs; Z.Z. has structured, modified, and revised the manuscript. All authors have read and agreed to the published version of the manuscript.

**Funding:** 2021 Guangdong Province Key discipline fund, Guangdong Province key Laboratory of Energy Conversion Materials and Technology and 2020 Li Ka Shing Foundation Cross-Disciplinary Research Grant. This work is financially supported by the Guangdong Province Key discipline fund (GTIIT) in 2021, Guangdong Province key Laboratory of Energy Conversion Materials and Technology, by the GTIIT Project KD2000079, and by the 2020 Li Ka Shing Foundation Cross-Disciplinary Research Grant (2020LKSFG09A).

**Institutional Review Board Statement:** Not applicable.

**Informed Consent Statement:** Not applicable.

**Data Availability Statement:** The data presented in this study are available on request from the corresponding author.

**Conflicts of Interest:** The authors declare no conflict of interest.

## References

1. Sun, R.; Liao, Y.; Bai, S.-T.; Zheng, M.; Zhou, C.; Zhang, T.; Sels, B.F. Heterogeneous catalysts for CO<sub>2</sub> hydrogenation to formic acid/formate: From nanoscale to single atom. *Energy Environ. Sci.* **2021**, *14*, 1247–1285. [[CrossRef](#)]
2. Wang, J.; Li, G.; Li, Z.; Tang, C.; Feng, Z.; An, H.; Liu, H.; Liu, T.; Li, C. A highly selective and stable ZnO-ZrO<sub>2</sub> solid solution catalyst for CO<sub>2</sub> hydrogenation to methanol. *Sci. Adv.* **2017**, *3*, e1701290. [[CrossRef](#)] [[PubMed](#)]
3. Ye, R.-P.; Li, Q.; Gong, W.; Wang, T.; Razink, J.J.; Lin, L.; Qin, Y.-Y.; Zhou, Z.; Adidharma, H.; Tang, J. High-performance of nanostructured Ni/CeO<sub>2</sub> catalyst on CO<sub>2</sub> methanation. *Appl. Catal. B Environ.* **2020**, *268*, 118474. [[CrossRef](#)]
4. Lim, E.; Heo, J.; Zhang, X.; Bowen, K.H.; Lee, S.H.; Kim, S.K. Anionic Activation of CO<sub>2</sub> via (Mn-CO<sub>2</sub>)-Complex on Magic-Numbered Anionic Coinage Metal Clusters Mn-(M= Cu, Ag, Au). *J. Phys. Chem. A* **2021**, *125*, 2243–2248. [[CrossRef](#)]
5. Alvarez-Garcia, A.; Flórez, E.; Moreno, A.; Jimenez-Orozco, C. CO<sub>2</sub> activation on small Cu-Ni and Cu-Pd bimetallic clusters. *Mol. Catal.* **2020**, *484*, 110733. [[CrossRef](#)]
6. Álvarez, A.; Borges, M.; Corral-Pérez, J.J.; Olcina, J.G.; Hu, L.; Cornu, D.; Huang, R.; Stoian, D.; Urakawa, A. CO<sub>2</sub> activation over catalytic surfaces. *ChemPhysChem* **2017**, *18*, 3135–3141. [[CrossRef](#)]
7. Nakamura, S.; Hatakeyama, M.; Wang, Y.; Ogata, K.; Fujii, K. A basic quantum chemical review on the activation of CO<sub>2</sub>. In *Advances in CO<sub>2</sub> Capture, Sequestration, and Conversion*; ACS Publications: Washington, DC, USA, 2015; pp. 123–134.
8. Mendes, P.C.; Verga, L.G.; Da Silva, J.L. Ab initio screening of Pt-based transition-metal nanoalloys using descriptors derived from the adsorption and activation of CO<sub>2</sub>. *Phys. Chem. Chem. Phys.* **2021**, *23*, 6029–6041. [[CrossRef](#)]
9. Koppenol, W.; Rush, J. Reduction potential of the carbon dioxide/carbon dioxide radical anion: A comparison with other C1 radicals. *J. Phys. Chem.* **1987**, *91*, 4429–4430. [[CrossRef](#)]
10. Das, S.; Pérez-Ramírez, J.; Gong, J.; Dewangan, N.; Hidajat, K.; Gates, B.C.; Kawi, S. Core-shell structured catalysts for thermocatalytic, photocatalytic, and electrocatalytic conversion of CO<sub>2</sub>. *Chem. Soc. Rev.* **2020**, *49*, 2937–3004. [[CrossRef](#)]
11. Modak, A.; Bhanja, P.; Dutta, S.; Chowdhury, B.; Bhaumik, A. Catalytic reduction of CO<sub>2</sub> into fuels and fine chemicals. *Green Chem.* **2020**, *22*, 4002–4033. [[CrossRef](#)]
12. Etim, U.J.; Semiat, R.; Zhong, Z. CO<sub>2</sub> Valorization Reactions over Cu-Based Catalysts: Characterization and the Nature of Active Sites. *Am. J. Chem. Eng.* **2021**, *9*, 53–78. [[CrossRef](#)]
13. Green, A.E.; Justen, J.; Schöllkopf, W.; Gentleman, A.S.; Fielicke, A.; Mackenzie, S.R. IR Signature of Size-Selective CO<sub>2</sub> Activation on Small Platinum Cluster Anions, Ptn-(n= 4–7). *Angew. Chem.* **2018**, *130*, 15038–15042. [[CrossRef](#)]
14. Xie, S.; Zhang, Q.; Liu, G.; Wang, Y. Photocatalytic and photoelectrocatalytic reduction of CO<sub>2</sub> using heterogeneous catalysts with controlled nanostructures. *Chem. Commun.* **2016**, *52*, 35–59. [[CrossRef](#)]
15. Kumar, B.; Llorente, M.; Froehlich, J.; Dang, T.; Sathrum, A.; Kubiak, C.P. Photochemical and photoelectrochemical reduction of CO<sub>2</sub>. *Annu. Rev. Phys. Chem.* **2012**, *63*, 541–569. [[CrossRef](#)]
16. Fernández-Alvarez, F.J.; Oro, L.A. Homogeneous Catalytic Reduction of CO<sub>2</sub> with Silicon-Hydrides, State of the Art. *ChemCatChem* **2018**, *10*, 4783–4796. [[CrossRef](#)]
17. Jia, C.; Gao, J.; Dai, Y.; Zhang, J.; Yang, Y. The thermodynamics analysis and experimental validation for complicated systems in CO<sub>2</sub> hydrogenation process. *J. Energy Chem.* **2016**, *25*, 1027–1037. [[CrossRef](#)]
18. Aresta, M.; Dibenedetto, A.; Quaranta, E. State of the art and perspectives in catalytic processes for CO<sub>2</sub> conversion into chemicals and fuels: The distinctive contribution of chemical catalysis and biotechnology. *J. Catal.* **2016**, *343*, 2–45. [[CrossRef](#)]
19. Ronda-Lloret, M.; Rothenberg, G.; Shiju, N.R. A critical look at direct catalytic hydrogenation of carbon dioxide to olefins. *ChemSusChem* **2019**, *12*, 3896–3914. [[CrossRef](#)]
20. Radhakrishnan, S.G.; Roduner, E. Carbon dioxide activation. In *Carbon Dioxide Utilization*; Michael, N., Peter, S., Eds.; De Gruyter: Berlin, Germany, 2019; pp. 227–248.
21. Niu, J.; Ran, J.; Ou, Z.; Du, X.; Wang, R.; Qi, W.; Zhang, P. CO<sub>2</sub> dissociation over PtxNi<sub>4-x</sub> bimetallic clusters with and without hydrogen sources: A density functional theory study. *J. CO<sub>2</sub> Util.* **2016**, *16*, 431–441. [[CrossRef](#)]
22. Grice, K.A. Carbon dioxide reduction with homogenous early transition metal complexes: Opportunities and challenges for developing CO<sub>2</sub> catalysis. *Coord. Chem. Rev.* **2017**, *336*, 78–95. [[CrossRef](#)]
23. Taifan, W.; Boily, J.-F.; Baltrusaitis, J. Surface chemistry of carbon dioxide revisited. *Surf. Sci. Rep.* **2016**, *71*, 595–671. [[CrossRef](#)]
24. Freund, H.-J.; Roberts, M.W. Surface chemistry of carbon dioxide. *Surf. Sci. Rep.* **1996**, *25*, 225–273. [[CrossRef](#)]
25. Mondal, B.; Song, J.; Neese, F.; Ye, S. Bio-inspired mechanistic insights into CO<sub>2</sub> reduction. *Curr. Opin. Chem. Biol.* **2015**, *25*, 103–109. [[CrossRef](#)]
26. Nolan, M.; Fronzi, M. Activation of CO<sub>2</sub> at chromia-nanocluster-modified rutile and anatase TiO<sub>2</sub>. *Catal. Today* **2019**, *326*, 68–74. [[CrossRef](#)]
27. Mondal, K.; Banerjee, A.; Ghanty, T.K. Adsorption and activation of C on Zr<sub>n</sub> (n= 2–7) clusters. *Phys. Chem. Chem. Phys.* **2020**, *22*, 16877–16886.
28. Weber, J.M. The interaction of negative charge with carbon dioxide—insight into solvation, speciation and reductive activation from cluster studies. *Int. Rev. Phys. Chem.* **2014**, *33*, 489–519. [[CrossRef](#)]

29. Park, J.; Cho, M.; Rhee, Y.M.; Jung, Y. Theoretical Study on the Degree of CO<sub>2</sub> Activation in CO<sub>2</sub>-Coordinated Ni (0) Complexes. *ACS Omega* **2021**, *6*, 7646–7654. [[CrossRef](#)]
30. Mazheika, A.; Wang, Y.; Valero, R.; Ghiringhelli, L.M.; Vines, F.; Illas, F.; Levchenko, S.V.; Scheffler, M. Ab initio data-analytics study of carbon-dioxide activation on semiconductor oxide surfaces. *arXiv* **2019**, arXiv:1912.06515.
31. Chang, X.; Wang, T.; Gong, J. CO<sub>2</sub> photo-reduction: Insights into CO<sub>2</sub> activation and reaction on surfaces of photocatalysts. *Energy Environ. Sci* **2016**, *9*, 2177–2196. [[CrossRef](#)]
32. Fu, J.; Jiang, K.; Qiu, X.; Yu, J.; Liu, M. Product selectivity of photocatalytic CO<sub>2</sub> reduction reactions. *Mater. Today* **2020**, *32*, 222–243. [[CrossRef](#)]
33. Yang, B.; Wang, L.; Hua, Z.; Guo, L. How CO<sub>2</sub> Chemisorption States Affect Hydrogenation Activity. *Ind. Eng. Chem. Res.* **2019**, *58*, 9838–9843. [[CrossRef](#)]
34. Megha; Mondal, K.; Ghanty, T.K.; Banerjee, A. Adsorption and Activation of CO<sub>2</sub> on Small-Sized Cu–Zr Bimetallic Clusters. *J. Phys. Chem. A* **2021**, *125*, 2558–2572. [[CrossRef](#)]
35. Megha; Banerjee, A.; Ghanty, T.K. Role of metcar on the adsorption and activation of carbon dioxide: A DFT study. *Phys. Chem. Chem. Phys.* **2021**, *23*, 5559–5570. [[CrossRef](#)]
36. Liu, X.; Kunkel, C.; Ramirez de la Piscina, P.; Homs, N.; Vines, F.; Illas, F. Effective and highly selective CO generation from CO<sub>2</sub> using a polycrystalline  $\alpha$ -Mo<sub>2</sub>C catalyst. *ACS Catal.* **2017**, *7*, 4323–4335. [[CrossRef](#)]
37. Ma, Z.; Porosoff, M.D. Development of tandem catalysts for CO<sub>2</sub> hydrogenation to olefins. *ACS Catal.* **2019**, *9*, 2639–2656. [[CrossRef](#)]
38. Zhao, B.; Liu, Y.; Zhu, Z.; Guo, H.; Ma, X. Highly selective conversion of CO<sub>2</sub> into ethanol on Cu/ZnO/Al<sub>2</sub>O<sub>3</sub> catalyst with the assistance of plasma. *J. CO<sub>2</sub> Util.* **2018**, *24*, 34–39. [[CrossRef](#)]
39. Li, Y.; Hui, D.; Sun, Y.; Wang, Y.; Wu, Z.; Wang, C.; Zhao, J. Boosting thermo-photocatalytic CO<sub>2</sub> conversion activity by using photosynthesis-inspired electron-proton-transfer mediators. *Nat. Commun.* **2021**, *12*, 123. [[CrossRef](#)]
40. Liu, L.; Li, Y. Understanding the reaction mechanism of photocatalytic reduction of CO<sub>2</sub> with H<sub>2</sub>O on TiO<sub>2</sub>-based photocatalysts: A review. *Aerosol Air Qual. Res.* **2014**, *14*, 453–469. [[CrossRef](#)]
41. Montoya, J.H.; Seitz, L.C.; Chakthranont, P.; Vojvodic, A.; Jaramillo, T.F.; Nørskov, J.K. Materials for solar fuels and chemicals. *Nat. Mater.* **2017**, *16*, 70–81. [[CrossRef](#)]
42. Chen, S.; Wang, H.; Kang, Z.; Jin, S.; Zhang, X.; Zheng, X.; Qi, Z.; Zhu, J.; Pan, B.; Xie, Y. Oxygen vacancy associated single-electron transfer for photofixation of CO<sub>2</sub> to long-chain chemicals. *Nat. Commun.* **2019**, *10*, 788. [[CrossRef](#)]
43. Sharma, N.; Das, T.; Kumar, S.; Bhosale, R.; Kabir, M.; Ogale, S. Photocatalytic activation and reduction of CO<sub>2</sub> to CH<sub>4</sub> over single phase nano Cu<sub>3</sub>SnS<sub>4</sub>: A combined experimental and theoretical study. *ACS Appl. Energy Mater.* **2019**, *2*, 5677–5685. [[CrossRef](#)]
44. Chu, W.; Zheng, Q.; Prezhd, O.V.; Zhao, J. CO<sub>2</sub> photoreduction on metal oxide surface is driven by transient capture of hot electrons: Ab initio quantum dynamics simulation. *J. Am. Chem. Soc.* **2020**, *142*, 3214–3221. [[CrossRef](#)]
45. Indrakanti, V.P.; Kubicki, J.D.; Schobert, H.H. Photoinduced activation of CO<sub>2</sub> on Ti-based heterogeneous catalysts: Current state, chemical physics-based insights and outlook. *Energy Environ. Sci.* **2009**, *2*, 745–758. [[CrossRef](#)]
46. Yuan, L.; Xu, Y.-J. Photocatalytic conversion of CO<sub>2</sub> into value-added and renewable fuels. *Appl. Surf. Sci.* **2015**, *342*, 154–167. [[CrossRef](#)]
47. Liu, L.; Zhao, C.; Li, Y. Spontaneous Dissociation of CO<sub>2</sub> to CO on Defective Surface of Cu(I)/TiO<sub>2-x</sub> Nanoparticles at Room Temperature. *J. Phys. Chem. C* **2012**, *116*, 7904–7912. [[CrossRef](#)]
48. Liu, L.; Zhao, H.; Andino, J.M.; Li, Y. Photocatalytic CO<sub>2</sub> reduction with H<sub>2</sub>O on TiO<sub>2</sub> nanocrystals: Comparison of anatase, rutile, and brookite polymorphs and exploration of surface chemistry. *ACS Catal.* **2012**, *2*, 1817–1828. [[CrossRef](#)]
49. Rodriguez, M.M.; Peng, X.; Liu, L.; Li, Y.; Andino, J.M. A density functional theory and experimental study of CO<sub>2</sub> interaction with brookite TiO<sub>2</sub>. *J. Phys. Chem. C* **2012**, *116*, 19755–19764. [[CrossRef](#)]
50. He, H.; Zapol, P.; Curtiss, L.A. A theoretical study of CO<sub>2</sub> anions on anatase (101) surface. *J. Phys. Chem. C* **2010**, *114*, 21474–21481. [[CrossRef](#)]
51. Pan, H.; Gu, B.; Zhang, Z. Phase-dependent photocatalytic ability of TiO<sub>2</sub>: A first-principles study. *J. Chem. Theory Comput.* **2009**, *5*, 3074–3078. [[CrossRef](#)]
52. Zhao, Y.; Wei, Y.; Wu, X.; Zheng, H.; Zhao, Z.; Liu, J.; Li, J. Graphene-wrapped Pt/TiO<sub>2</sub> photocatalysts with enhanced photogenerated charges separation and reactant adsorption for high selective photoreduction of CO<sub>2</sub> to CH<sub>4</sub>. *Appl. Catal. B Environ.* **2018**, *226*, 360–372. [[CrossRef](#)]
53. Lu, L.; Wang, B.; Wang, S.; Shi, Z.; Yan, S.; Zou, Z. La<sub>2</sub>O<sub>3</sub>-Modified LaTiO<sub>2</sub>N Photocatalyst with Spatially Separated Active Sites Achieving Enhanced CO<sub>2</sub> Reduction. *Adv. Funct. Mater.* **2017**, *27*, 1702447. [[CrossRef](#)]
54. Xu, F.; Meng, K.; Cheng, B.; Yu, J.; Ho, W. Enhanced Photocatalytic Activity and Selectivity for CO<sub>2</sub> Reduction over a TiO<sub>2</sub> Nanofibre Mat Using Ag and MgO as Bi-Cocatalyst. *ChemCatChem* **2019**, *11*, 465–472. [[CrossRef](#)]
55. Xie, S.; Wang, Y.; Zhang, Q.; Deng, W.; Wang, Y. MgO-and Pt-promoted TiO<sub>2</sub> as an efficient photocatalyst for the preferential reduction of carbon dioxide in the presence of water. *ACS Catal.* **2014**, *4*, 3644–3653. [[CrossRef](#)]
56. Zhao, Y.; Chen, G.; Bian, T.; Zhou, C.; Waterhouse, G.I.; Wu, L.Z.; Tung, C.H.; Smith, L.J.; O’Hare, D.; Zhang, T. Defect-rich ultrathin ZnAl-layered double hydroxide nanosheets for efficient photoreduction of CO<sub>2</sub> to CO with water. *Adv. Mater.* **2015**, *27*, 7824–7831. [[CrossRef](#)]

57. Xiong, Z.; Lei, Z.; Kuang, C.-C.; Chen, X.; Gong, B.; Zhao, Y.; Zhang, J.; Zheng, C.; Wu, J.C. Selective photocatalytic reduction of CO<sub>2</sub> into CH<sub>4</sub> over Pt-Cu<sub>2</sub>O TiO<sub>2</sub> nanocrystals: The interaction between Pt and Cu<sub>2</sub>O cocatalysts. *Appl. Catal. B Environ.* **2017**, *202*, 695–703. [CrossRef]
58. Wang, B.; Wang, X.; Lu, L.; Zhou, C.; Xin, Z.; Wang, J.; Ke, X.-K.; Sheng, G.; Yan, S.; Zou, Z. Oxygen-vacancy-activated CO<sub>2</sub> splitting over amorphous oxide semiconductor photocatalyst. *ACS Catal.* **2018**, *8*, 516–525. [CrossRef]
59. Kim, C.; Hyeon, S.; Lee, J.; Kim, W.D.; Lee, D.C.; Kim, J.; Lee, H. Energy-efficient CO<sub>2</sub> hydrogenation with fast response using photoexcitation of CO<sub>2</sub> adsorbed on metal catalysts. *Nat. Commun.* **2018**, *9*, 3027. [CrossRef]
60. Xie, J.; Huang, Y.; Wu, M.; Wang, Y. Electrochemical carbon dioxide splitting. *ChemElectroChem* **2019**, *6*, 1587–1604. [CrossRef]
61. Nitopi, S.; Bertheussen, E.; Scott, S.B.; Liu, X.; Engstfeld, A.K.; Horch, S.; Seger, B.; Stephens, I.E.; Chan, K.; Hahn, C. Progress and perspectives of electrochemical CO<sub>2</sub> reduction on copper in aqueous electrolyte. *Chem. Rev.* **2019**, *119*, 7610–7672. [CrossRef]
62. Morris, A.J.; McGibbon, R.T.; Bocarsly, A.B. Electrocatalytic Carbon Dioxide Activation: The Rate-Determining Step of Pyridinium-Catalyzed CO<sub>2</sub> Reduction. *ChemSusChem* **2011**, *4*, 191–196. [CrossRef]
63. Yang, P.; Zhao, Z.J.; Chang, X.; Mu, R.; Zha, S.; Zhang, G.; Gong, J. The functionality of surface hydroxy groups on the selectivity and activity of carbon dioxide reduction over cuprous oxide in aqueous solutions. *Angew. Chem.* **2018**, *130*, 7850–7854. [CrossRef]
64. Huang, Q.; Li, Q.; Liu, J.; Wang, R.; Lan, Y.-Q. Disclosing CO<sub>2</sub> activation mechanism by hydroxyl-induced crystalline structure transformation in electrocatalytic process. *Matter* **2019**, *1*, 1656–1668. [CrossRef]
65. Benson, E.E.; Kubiak, C.P.; Sathrum, A.J.; Smieja, J.M. Electrocatalytic and homogeneous approaches to conversion of CO<sub>2</sub> to liquid fuels. *Chem. Soc. Rev.* **2009**, *38*, 89–99. [CrossRef]
66. Zhu, D.D.; Liu, J.L.; Qiao, S.Z. Recent advances in inorganic heterogeneous electrocatalysts for reduction of carbon dioxide. *Adv. Mater.* **2016**, *28*, 3423–3452. [CrossRef]
67. Peterson, A.A.; Abild-Pedersen, F.; Studt, F.; Rossmeisl, J.; Nørskov, J.K. How copper catalyzes the electroreduction of carbon dioxide into hydrocarbon fuels. *Energy Environ. Sci.* **2010**, *3*, 1311–1315. [CrossRef]
68. Kuhl, K.P.; Cave, E.R.; Abram, D.N.; Jaramillo, T.F. New insights into the electrochemical reduction of carbon dioxide on metallic copper surfaces. *Energy Environ. Sci.* **2012**, *5*, 7050–7059. [CrossRef]
69. Xiao, H.; Goddard, W.A.; Cheng, T.; Liu, Y. Cu metal embedded in oxidized matrix catalyst to promote CO<sub>2</sub> activation and CO dimerization for electrochemical reduction of CO<sub>2</sub>. *Proc. Natl. Acad. Sci. USA* **2017**, *114*, 6685–6688. [PubMed]
70. Favaro, M.; Xiao, H.; Cheng, T.; Goddard, W.A.; Yano, J.; Crumlin, E.J. Subsurface oxide plays a critical role in CO<sub>2</sub> activation by Cu (111) surfaces to form chemisorbed CO<sub>2</sub>, the first step in reduction of CO<sub>2</sub>. *Proc. Natl. Acad. Sci. USA* **2017**, *114*, 6706–6711. [PubMed]
71. Li, C.W.; Kanan, M.W. CO<sub>2</sub> reduction at low overpotential on Cu electrodes resulting from the reduction of thick Cu<sub>2</sub>O films. *J. Am. Chem. Soc.* **2012**, *134*, 7231–7234. [CrossRef] [PubMed]
72. Zhang, J.; Yin, R.; Shao, Q.; Zhu, T.; Huang, X. Oxygen vacancies in amorphous InOx nanoribbons enhance CO<sub>2</sub> adsorption and activation for CO<sub>2</sub> electroreduction. *Angew. Chem. Int. Ed.* **2019**, *58*, 5609–5613. [CrossRef] [PubMed]
73. Gu, Z.; Yang, N.; Han, P.; Kuang, M.; Mei, B.; Jiang, Z.; Zhong, J.; Li, L.; Zheng, G. Oxygen vacancy tuning toward efficient electrocatalytic CO<sub>2</sub> reduction to C<sub>2</sub>H<sub>4</sub>. *Small Methods* **2019**, *3*, 1800449.
74. Geng, Z.; Kong, X.; Chen, W.; Su, H.; Liu, Y.; Cai, F.; Wang, G.; Zeng, J. Oxygen vacancies in ZnO nanosheets enhance CO<sub>2</sub> electrochemical reduction to CO. *Angew. Chem.* **2018**, *130*, 6162–6167. [CrossRef]
75. Baruch, M.F.; Pander III, J.E.; White, J.L.; Bocarsly, A.B. Mechanistic insights into the reduction of CO<sub>2</sub> on tin electrodes using in situ ATR-IR spectroscopy. *ACS Catal.* **2015**, *5*, 3148–3156. [CrossRef]
76. Barwa, E.; Pascher, T.F.; Ončák, M.; van der Linde, C.; Beyer, M.K. Carbon Dioxide Activation at Metal Centers: Evolution of Charge Transfer from Mg<sup>+</sup> to CO<sub>2</sub> in [MgCO<sub>2</sub>(H<sub>2</sub>O)<sub>n</sub>]<sup>+</sup>, n = 0–8. *Angew. Chem. Int. Ed.* **2020**, *59*, 7467–7471. [CrossRef]
77. Iskra, A.; Gentleman, A.S.; Cunningham, E.M.; Mackenzie, S.R. Carbon dioxide binding to metal oxides: Infrared spectroscopy of NbO<sub>2</sub><sup>+</sup>(CO<sub>2</sub>)<sub>n</sub> and TaO<sub>2</sub><sup>+</sup>(CO<sub>2</sub>)<sub>n</sub> complexes. *Int. J. Mass Spectrom.* **2019**, *435*, 93–100. [CrossRef]
78. Yin, X.; Moss, J.R. Recent developments in the activation of carbon dioxide by metal complexes. *Coord. Chem. Rev.* **1999**, *181*, 27–59. [CrossRef]
79. Iskra, A.; Gentleman, A.S.; Kartouzian, A.; Kent, M.J.; Sharp, A.P.; Mackenzie, S.R. Infrared spectroscopy of gas-phase M<sup>+</sup>(CO<sub>2</sub>)<sub>n</sub> (M = Co, Rh, Ir) ion–molecule complexes. *J. Phys. Chem. A* **2017**, *121*, 133–140. [CrossRef]
80. Thompson, M.C.; Ramsay, J.; Weber, J.M. Solvent-driven reductive activation of CO<sub>2</sub> by bismuth: Switching from metalloformate complexes to oxalate products. *Angew. Chem. Int. Ed.* **2016**, *55*, 15171–15174. [CrossRef]
81. Knurr, B.J.; Weber, J.M. Solvent-driven reductive activation of carbon dioxide by gold anions. *J. Am. Chem. Soc.* **2012**, *134*, 18804–18808. [CrossRef]
82. Zheng, H.; Kong, X.; Wang, C.; Wang, T.; Yang, D.; Li, G.; Xie, H.; Zhao, Z.; Shi, R.; Han, H. Spectroscopic Identification of Transition-Metal M [η<sup>2</sup>-(O, O) C] Species for Highly-Efficient CO<sub>2</sub> Activation. *J. Phys. Chem. Lett.* **2020**, *12*, 472–477. [CrossRef]
83. Zimmermann, N.; Bernhardt, T.M.; Bakker, J.M.; Barnett, R.N.; Landman, U.; Lang, S.M. Infrared Spectroscopy of Gas-Phase Mn × O<sub>y</sub>(CO<sub>2</sub>)<sub>z</sub> Complexes. *J. Phys. Chem. A* **2020**, *124*, 1561–1566. [CrossRef]
84. Paparo, A.; Okuda, J. Carbon dioxide complexes: Bonding modes and synthetic methods. *Coord. Chem. Rev.* **2017**, *334*, 136–149. [CrossRef]
85. Li, H.; Zhao, J.; Luo, L.; Du, J.; Zeng, J. Symmetry-Breaking Sites for Activating Linear Carbon Dioxide Molecules. *Acc. Chem. Res.* **2021**, *54*, 1454–1464. [CrossRef]

86. Ye, R.-P.; Ding, J.; Gong, W.; Argyle, M.D.; Zhong, Q.; Wang, Y.; Russell, C.K.; Xu, Z.; Russell, A.G.; Li, Q. CO<sub>2</sub> hydrogenation to high-value products via heterogeneous catalysis. *Nat. Commun.* **2019**, *10*, 5698. [[CrossRef](#)]
87. Dietz, L.; Piccinin, S.; Maestri, M. Mechanistic Insights into CO<sub>2</sub> activation via reverse water–gas shift on metal surfaces. *J. Phys. Chem. C* **2015**, *119*, 4959–4966. [[CrossRef](#)]
88. Ko, J.; Kim, B.-K.; Han, J.W. Density functional theory study for catalytic activation and dissociation of CO<sub>2</sub> on bimetallic alloy surfaces. *J. Phys. Chem. C* **2016**, *120*, 3438–3447. [[CrossRef](#)]
89. Wang, S.-G.; Liao, X.-Y.; Cao, D.-B.; Huo, C.-F.; Li, Y.-W.; Wang, J.; Jiao, H. Factors controlling the interaction of CO<sub>2</sub> with transition metal surfaces. *J. Phys. Chem. C* **2007**, *111*, 16934–16940. [[CrossRef](#)]
90. Ding, X.; De Rogatis, L.; Vesselli, E.; Baraldi, A.; Comelli, G.; Rosei, R.; Savio, L.; Vattuone, L.; Rocca, M.; Fornasiero, P. Interaction of carbon dioxide with Ni (110): A combined experimental and theoretical study. *Phys. Rev. B* **2007**, *76*, 195425. [[CrossRef](#)]
91. Eren, B.; Weatherup, R.S.; Liakakos, N.; Somorjai, G.A.; Salmeron, M. Dissociative carbon dioxide adsorption and morphological changes on Cu (100) and Cu (111) at ambient pressures. *J. Am. Chem. Soc.* **2016**, *138*, 8207–8211. [[CrossRef](#)] [[PubMed](#)]
92. Hammami, R.; Dhoub, A.; Fernandez, S.; Minot, C. CO<sub>2</sub> adsorption on (0 0 1) surfaces of metal monoxides with rock-salt structure. *Catal. Today* **2008**, *139*, 227–233. [[CrossRef](#)]
93. Solymosi, F. The bonding, structure and reactions of CO<sub>2</sub> adsorbed on clean and promoted metal surfaces. *J. Mol. Catal.* **1991**, *65*, 337–358. [[CrossRef](#)]
94. Mishra, A.K.; Roldan, A.; de Leeuw, N.H. CuO surfaces and CO<sub>2</sub> activation: A dispersion-corrected DFT+ U study. *J. Phys. Chem. C* **2016**, *120*, 2198–2214. [[CrossRef](#)]
95. Yang, T.; Gu, T.; Han, Y.; Wang, W.; Yu, Y.; Zang, Y.; Zhang, H.; Mao, B.; Li, Y.; Yang, B. Surface orientation and pressure dependence of CO<sub>2</sub> activation on Cu surfaces. *J. Phys. Chem. C* **2020**, *124*, 27511–27518. [[CrossRef](#)]
96. Yu, H.; Cao, D.; Fisher, A.; Johnston, R.L.; Cheng, D. Size effect on the adsorption and dissociation of CO<sub>2</sub> on Co nanoclusters. *Appl. Surf. Sci.* **2017**, *396*, 539–546. [[CrossRef](#)]
97. Etim, U.J.; Song, Y.; Zhong, Z. Improving the Cu/ZnO-Based Catalysts for Carbon Dioxide Hydrogenation to Methanol, and the Use of Methanol As a Renewable Energy Storage Media. *Front. Energy Res.* **2020**, *8*, 545431. [[CrossRef](#)]
98. Fu, S.S.; Somorjai, G.A. Interactions of O<sub>2</sub>, CO, CO<sub>2</sub>, and D<sub>2</sub> with the stepped Cu (311) crystal face: Comparison to Cu (110). *Surf. Sci.* **1992**, *262*, 68–76. [[CrossRef](#)]
99. Rasmussen, P.; Taylor, P.; Chorkendorff, I. The interaction of carbon dioxide with Cu (100). *Surf. Sci.* **1992**, *269*, 352–359. [[CrossRef](#)]
100. Muttaqien, F.; Hamamoto, Y.; Inagaki, K.; Morikawa, Y. Dissociative adsorption of CO<sub>2</sub> on flat, stepped, and kinked Cu surfaces. *J. Chem. Phys.* **2014**, *141*, 034702. [[CrossRef](#)]
101. Pohl, M.; Otto, A. Adsorption and reaction of carbon dioxide on pure and alkali-metal promoted cold-deposited copper films. *Surf. Sci.* **1998**, *406*, 125–137. [[CrossRef](#)]
102. Wang, S.-G.; Cao, D.-B.; Li, Y.-W.; Wang, J.; Jiao, H. Chemisorption of CO<sub>2</sub> on nickel surfaces. *J. Phys. Chem. B* **2005**, *109*, 18956–18963. [[CrossRef](#)]
103. Cao, D.-B.; Li, Y.-W.; Wang, J.; Jiao, H. CO<sub>2</sub> dissociation on Ni (2 1 1). *Surf. Sci.* **2009**, *603*, 2991–2998. [[CrossRef](#)]
104. Illing, G.; Heskett, D.; Plummer, E.; Freund, H.-J.; Somers, J.; Lindner, T.; Bradshaw, A.; Buskotte, U.; Neumann, M.; Starke, U. Adsorption and reaction of CO<sub>2</sub> on Ni {110}: X-ray photoemission, near-edge X-ray absorption fine-structure and diffuse leed studies. *Surf. Sci.* **1988**, *206*, 1–19. [[CrossRef](#)]
105. Heine, C.; Lechner, B.A.; Bluhm, H.; Salmeron, M. Recycling of CO<sub>2</sub>: Probing the chemical state of the Ni (111) surface during the methanation reaction with ambient-pressure X-ray photoelectron spectroscopy. *J. Am. Chem. Soc.* **2016**, *138*, 13246–13252. [[CrossRef](#)] [[PubMed](#)]
106. Roiaz, M.; Monachino, E.; Dri, C.; Greiner, M.; Knop-Gericke, A.; Schlögl, R.; Comelli, G.; Vesselli, E. Reverse water–gas shift or Sabatier methanation on Ni (110)? Stable surface species at near-ambient pressure. *J. Am. Chem. Soc.* **2016**, *138*, 4146–4154. [[CrossRef](#)]
107. Cai, J.; Han, Y.; Chen, S.; Crumlin, E.J.; Yang, B.; Li, Y.; Liu, Z. CO<sub>2</sub> activation on Ni (111) and Ni (100) surfaces in the presence of H<sub>2</sub>O: An ambient-pressure X-ray photoelectron spectroscopy study. *J. Phys. Chem. C* **2019**, *123*, 12176–12182. [[CrossRef](#)]
108. Silaghi, M.-C.; Comas-Vives, A.; Coperet, C. CO<sub>2</sub> Activation on Ni/γ-Al<sub>2</sub>O<sub>3</sub> catalysts by first-principles calculations: From ideal surfaces to supported nanoparticles. *ACS Catal.* **2016**, *6*, 4501–4505. [[CrossRef](#)]
109. Liu, Z.; Zhou, Y.; Solymosi, F.; White, J. Spectroscopic study of K-induced activation of CO<sub>2</sub> on Pt (111). *Surf. Sci.* **1991**, *245*, 289–304. [[CrossRef](#)]
110. Ricart, J.M.; Habas, M.P.; Clotet, A.; Curulla, D.; Illas, F. Theoretical study of CO<sub>2</sub> activation on Pt (111) induced by coadsorbed K atoms. *Surf. Sci.* **2000**, *460*, 170–181. [[CrossRef](#)]
111. Huang, M.; Adnot, A.; Suppiah, S.; Kaliaguine, S. XPS observation of surface interaction between H<sub>2</sub> and CO<sub>2</sub> on platinum foil. *J. Mol. Catal. A: Chem.* **1995**, *104*, L131–L137. [[CrossRef](#)]
112. Su, H.; Ye, Y.; Lee, K.-J.; Zeng, J.; Mun, B.S.; Crumlin, E.J. Probing the surface chemistry for reverse water gas shift reaction on Pt (1 1 1) using ambient pressure X-ray photoelectron spectroscopy. *J. Catal.* **2020**, *391*, 123–131. [[CrossRef](#)]
113. Víctor, A.; González, S.; Illas, F.; Fierro, J.L. Evidence for spontaneous CO<sub>2</sub> activation on cobalt surfaces. *Chem. Phys. Lett.* **2008**, *454*, 262–268.

114. Jia, J.; Qian, C.; Dong, Y.; Li, Y.F.; Wang, H.; Ghossoub, M.; Butler, K.T.; Walsh, A.; Ozin, G.A. Heterogeneous catalytic hydrogenation of CO<sub>2</sub> by metal oxides: Defect engineering—perfecting imperfection. *Chem. Soc. Rev.* **2017**, *46*, 4631–4644. [[CrossRef](#)]
115. Seiferth, O.; Wolter, K.; Dillmann, B.; Klivenyi, G.; Freund, H.-J.; Scarano, D.; Zecchina, A. IR investigations of CO<sub>2</sub> adsorption on chromia surfaces: Cr<sub>2</sub>O<sub>3</sub> (0001)/Cr (110) versus polycrystalline α-Cr<sub>2</sub>O<sub>3</sub>. *Surf. Sci.* **1999**, *421*, 176–190. [[CrossRef](#)]
116. Gao, P.; Li, S.; Bu, X.; Dang, S.; Liu, Z.; Wang, H.; Zhong, L.; Qiu, M.; Yang, C.; Cai, J. Direct conversion of CO<sub>2</sub> into liquid fuels with high selectivity over a bifunctional catalyst. *Nat. Chem.* **2017**, *9*, 1019–1024. [[CrossRef](#)]
117. Liu, L.; Fan, W.; Zhao, X.; Sun, H.; Li, P.; Sun, L. Surface dependence of CO<sub>2</sub> adsorption on Zn<sub>2</sub>GeO<sub>4</sub>. *Langmuir* **2012**, *28*, 10415–10424. [[CrossRef](#)]
118. Rodriguez, J.A.; Liu, P.; Stacchiola, D.J.; Senanayake, S.D.; White, M.G.; Chen, J.G. Hydrogenation of CO<sub>2</sub> to methanol: Importance of metal–oxide and metal–carbide interfaces in the activation of CO<sub>2</sub>. *ACS Catal.* **2015**, *5*, 6696–6706. [[CrossRef](#)]
119. Hezam, A.; Namratha, K.; Drmosh, Q.A.; Ponnamm, D.; Wang, J.; Prasad, S.; Ahamed, M.; Cheng, C.; Byrappa, K. CeO<sub>2</sub> nanostructures enriched with oxygen vacancies for photocatalytic CO<sub>2</sub> reduction. *ACS Appl. Nano Mater.* **2019**, *3*, 138–148. [[CrossRef](#)]
120. Bu, Y.; Weststrate, C.; Niemantsverdriet, J.; Fredriksson, H.O. Role of ZnO and CeO<sub>x</sub> in Cu-Based Model Catalysts in Activation of H<sub>2</sub>O and CO<sub>2</sub> Dynamics Studied by in Situ Ultraviolet–Visible and X-ray Photoelectron Spectroscopy. *ACS Catal.* **2016**, *6*, 7994–8003. [[CrossRef](#)]
121. Chen, S.; Cao, T.; Gao, Y.; Li, D.; Xiong, F.; Huang, W. Probing surface structures of CeO<sub>2</sub>, TiO<sub>2</sub>, and Cu<sub>2</sub>O nanocrystals with CO and CO<sub>2</sub> chemisorption. *J. Phys. Chem. C* **2016**, *120*, 21472–21485. [[CrossRef](#)]
122. Wang, Y.; Zhao, J.; Wang, T.; Li, Y.; Li, X.; Yin, J.; Wang, C. CO<sub>2</sub> photoreduction with H<sub>2</sub>O vapor on highly dispersed CeO<sub>2</sub>/TiO<sub>2</sub> catalysts: Surface species and their reactivity. *J. Catal.* **2016**, *337*, 293–302. [[CrossRef](#)]
123. Di, J.; Zhu, C.; Ji, M.; Duan, M.; Long, R.; Yan, C.; Gu, K.; Xiong, J.; She, Y.; Xia, J. Defect-rich Bi<sub>12</sub>O<sub>17</sub>Cl<sub>2</sub> nanotubes self-accelerating charge separation for boosting photocatalytic CO<sub>2</sub> reduction. *Angew. Chem. Int. Ed.* **2018**, *57*, 14847–14851. [[CrossRef](#)]
124. Yan, S.C.; Ouyang, S.X.; Gao, J.; Yang, M.; Feng, J.Y.; Fan, X.X.; Wan, L.J.; Li, Z.S.; Ye, J.H.; Zhou, Y. A room-temperature reactive-template route to mesoporous ZnGa<sub>2</sub>O<sub>4</sub> with improved photocatalytic activity in reduction of CO<sub>2</sub>. *Angew. Chem.* **2010**, *122*, 6544–6548. [[CrossRef](#)]
125. Guo, J.; Ouyang, S.; Kako, T.; Ye, J. Mesoporous In(OH)<sub>3</sub> for photoreduction of CO<sub>2</sub> into renewable hydrocarbon fuels. *Appl. Surf. Sci.* **2013**, *280*, 418–423. [[CrossRef](#)]
126. Cao, A.; Wang, Z.; Li, H.; Nørskov, J.K. Relations between Surface Oxygen Vacancies and Activity of Methanol Formation from CO<sub>2</sub> Hydrogenation over In<sub>2</sub>O<sub>3</sub> Surfaces. *ACS Catal.* **2021**, *11*, 1780–1786. [[CrossRef](#)]
127. Staudt, T.; Lykhach, Y.; Tsud, N.; Skála, T.S.; Prince, K.C.; Matolín, V.R.; Libuda, J.R. Electronic structure of magnesia–ceria model catalysts, CO<sub>2</sub> adsorption, and CO<sub>2</sub> activation: A synchrotron radiation photoelectron spectroscopy study. *J. Phys. Chem. C* **2011**, *115*, 8716–8724. [[CrossRef](#)]
128. Graciani, J.; Mudiyansele, K.; Xu, F.; Baber, A.E.; Evans, J.; Senanayake, S.D.; Stacchiola, D.J.; Liu, P.; Hrbek, J.; Sanz, J.F. Highly active copper–ceria and copper–ceria–titania catalysts for methanol synthesis from CO<sub>2</sub>. *Science* **2014**, *345*, 546–550. [[CrossRef](#)] [[PubMed](#)]
129. Cheng, Z.; Sherman, B.J.; Lo, C.S. Carbon dioxide activation and dissociation on ceria (110): A density functional theory study. *J. Chem. Phys.* **2013**, *138*, 014702. [[CrossRef](#)]
130. Yang, C.; Bebensee, F.; Chen, J.; Yu, X.; Nefedov, A.; Wöll, C. Carbon dioxide adsorption on CeO<sub>2</sub> (110): An XPS and NEXAFS study. *ChemPhysChem* **2017**, *18*, 1874–1880. [[CrossRef](#)]
131. Hahn, K.R.; Iannuzzi, M.; Seitsonen, A.P.; Hutter, J.R. Coverage effect of the CO<sub>2</sub> adsorption mechanisms on CeO<sub>2</sub> (111) by first principles analysis. *J. Phys. Chem. C* **2013**, *117*, 1701–1711. [[CrossRef](#)]
132. Inoue, T.; Fujishima, A.; Konishi, S.; Honda, K. Photoelectrocatalytic reduction of carbon dioxide in aqueous suspensions of semiconductor powders. *Nature* **1979**, *277*, 637–638. [[CrossRef](#)]
133. Thompson, T.L.; Diwald, O.; Yates, J.T. CO<sub>2</sub> as a probe for monitoring the surface defects on TiO<sub>2</sub> (110) temperature-programmed desorption. *J. Phys. Chem. B* **2003**, *107*, 11700–11704. [[CrossRef](#)]
134. Funk, S.; Burghaus, U. Adsorption of CO<sub>2</sub> on oxidized, defected, hydrogen and oxygen covered rutile (1 × 1)-TiO<sub>2</sub> (110). *Phys. Chem. Chem. Phys.* **2006**, *8*, 4805–4813. [[CrossRef](#)]
135. Suriye, K.; Praserttham, P.; Jongsomjit, B. Control of Ti<sup>3+</sup> surface defect on TiO<sub>2</sub> nanocrystal using various calcination atmospheres as the first step for surface defect creation and its application in photocatalysis. *Appl. Surf. Sci.* **2007**, *253*, 3849–3855. [[CrossRef](#)]
136. Suriye, K.; Jongsomjit, B.; Satayaprasert, C.; Praserttham, P. Surface defect (Ti<sup>3+</sup>) controlling in the first step on the anatase TiO<sub>2</sub> nanocrystal by using sol–gel technique. *Appl. Surf. Sci.* **2008**, *255*, 2759–2766. [[CrossRef](#)]
137. Sorescu, D.C.; Al-Saidi, W.A.; Jordan, K.D. CO<sub>2</sub> adsorption on TiO<sub>2</sub> (101) anatase: A dispersion-corrected density functional theory study. *J. Chem. Phys.* **2011**, *135*, 124701. [[CrossRef](#)]
138. Liao, L.-F.; Lien, C.-F.; Shieh, D.-L.; Chen, M.-T.; Lin, J.-L. FTIR study of adsorption and photoassisted oxygen isotopic exchange of carbon monoxide, carbon dioxide, carbonate, and formate on TiO<sub>2</sub>. *J. Phys. Chem. B* **2002**, *106*, 11240–11245. [[CrossRef](#)]
139. Lee, J.; Sorescu, D.C.; Deng, X. Electron-induced dissociation of CO<sub>2</sub> on TiO<sub>2</sub> (110). *J. Am. Chem. Soc.* **2011**, *133*, 10066–10069. [[CrossRef](#)]

140. Nolan, M. Adsorption of CO<sub>2</sub> on heterostructures of Bi<sub>2</sub>O<sub>3</sub> nanocluster-modified TiO<sub>2</sub> and the role of reduction in promoting CO<sub>2</sub> activation. *ACS Omega* **2018**, *3*, 13117–13128. [[CrossRef](#)]
141. Pavelec, J.; Hulva, J.; Halwidl, D.; Bliem, R.; Gamba, O.; Jakub, Z.; Brunbauer, F.; Schmid, M.; Diebold, U.; Parkinson, G.S. A multi-technique study of CO<sub>2</sub> adsorption on Fe<sub>3</sub>O<sub>4</sub> magnetite. *J. Chem. Phys.* **2017**, *146*, 014701. [[CrossRef](#)]
142. Hakim, A.; Marliza, T.S.; Abu Tahari, N.M.; Wan Isahak, R.W.; Yusop, R.M.; Mohamed Hisham, W.M.; Yarmo, A.M. Studies on CO<sub>2</sub> adsorption and desorption properties from various types of iron oxides (FeO, Fe<sub>2</sub>O<sub>3</sub>, and Fe<sub>3</sub>O<sub>4</sub>). *Ind. Eng. Chem. Res.* **2016**, *55*, 7888–7897. [[CrossRef](#)]
143. Li, X.; Paier, J. Vibrational properties of CO<sub>2</sub> adsorbed on the Fe<sub>3</sub>O<sub>4</sub> (111) surface: Insights gained from DFT. *J. Chem. Phys.* **2020**, *152*, 104702. [[CrossRef](#)]
144. Mirabella, F.; Zaki, E.; Ivars-Barcelo, F.; Schauermaun, S.; Shaikhutdinov, S.; Freund, H.-J. CO<sub>2</sub> adsorption on magnetite Fe<sub>3</sub>O<sub>4</sub> (111). *J. Phys. Chem. C* **2018**, *122*, 27433–27441. [[CrossRef](#)]
145. Su, T.; Qin, Z.; Huang, G.; Ji, H.; Jiang, Y.; Chen, J. Density functional theory study on the interaction of CO<sub>2</sub> with Fe<sub>3</sub>O<sub>4</sub> (111) surface. *Appl. Surf. Sci.* **2016**, *378*, 270–276. [[CrossRef](#)]
146. Tang, Q.-L.; Hong, Q.-J.; Liu, Z.-P. CO<sub>2</sub> fixation into methanol at Cu/ZrO<sub>2</sub> interface from first principles kinetic Monte Carlo. *J. Catal.* **2009**, *263*, 114–122. [[CrossRef](#)]
147. Fisher, I.A.; Bell, A.T. In-situ infrared study of methanol synthesis from H<sub>2</sub>/CO<sub>2</sub> over Cu/SiO<sub>2</sub> and Cu/ZrO<sub>2</sub>/SiO<sub>2</sub>. *J. Catal.* **1997**, *172*, 222–237. [[CrossRef](#)]
148. Jin, X.; Lv, C.; Zhou, X.; Ye, L.; Xie, H.; Liu, Y.; Su, H.; Zhang, B.; Chen, G. Oxygen vacancy engineering of Bi<sub>24</sub>O<sub>31</sub>Cl<sub>10</sub> for boosted photocatalytic CO<sub>2</sub> conversion. *ChemSusChem* **2019**, *12*, 2740–2747. [[CrossRef](#)]
149. Wu, J.; Li, X.; Shi, W.; Ling, P.; Sun, Y.; Jiao, X.; Gao, S.; Liang, L.; Xu, J.; Yan, W. Efficient visible-light-driven CO<sub>2</sub> reduction mediated by defect-engineered BiOBr atomic layers. *Angew. Chem.* **2018**, *130*, 8855–8859. [[CrossRef](#)]
150. Huygh, S.; Bogaerts, A.; Neyts, E.C. How oxygen vacancies activate CO<sub>2</sub> dissociation on TiO<sub>2</sub> anatase (001). *J. Phys. Chem. C* **2016**, *120*, 21659–21669. [[CrossRef](#)]
151. Pan, Y.-x.; Liu, C.-J.; Mei, D.; Ge, Q. Effects of Hydration and Oxygen Vacancy on CO<sub>2</sub> Adsorption and Activation on β-Ga<sub>2</sub>O<sub>3</sub>(100). *Langmuir* **2010**, *26*, 5551–5558. [[CrossRef](#)]
152. Ye, J.; Liu, C.; Mei, D.; Ge, Q. Active oxygen vacancy site for methanol synthesis from CO<sub>2</sub> hydrogenation on In<sub>2</sub>O<sub>3</sub> (110): A DFT study. *ACS Catal.* **2013**, *3*, 1296–1306. [[CrossRef](#)]
153. Sarkar, A.; Khan, G.G. The formation and detection techniques of oxygen vacancies in titanium oxide-based nanostructures. *Nanoscale* **2019**, *11*, 3414–3444. [[CrossRef](#)] [[PubMed](#)]
154. Ye, H.; Na, W.; Gao, W.; Wang, H. Carbon-Modified CuO/ZnO Catalyst with High Oxygen Vacancy for CO<sub>2</sub> Hydrogenation to Methanol. *Energy Technol.* **2020**, *8*, 2000194. [[CrossRef](#)]
155. Jiang, D.; Wang, W.; Zhang, L.; Zheng, Y.; Wang, Z. Insights into the surface-defect dependence of photoreactivity over CeO<sub>2</sub> nanocrystals with well-defined crystal facets. *ACS Catal.* **2015**, *5*, 4851–4858. [[CrossRef](#)]
156. Wang, F.; Li, C.; Zhang, X.; Wei, M.; Evans, D.G.; Duan, X. Catalytic behavior of supported Ru nanoparticles on the {1 0 0}, {1 1 0}, and {1 1 1} facet of CeO<sub>2</sub>. *J. Catal.* **2015**, *329*, 177–186. [[CrossRef](#)]
157. Bielz, T.; Lorenz, H.; Jochum, W.; Kaindl, R.; Klausner, F.; Klötzer, B.; Penner, S. Hydrogen on In<sub>2</sub>O<sub>3</sub>: Reducibility, Bonding, Defect Formation, and Reactivity. *J. Phys. Chem. C* **2010**, *114*, 9022–9029. [[CrossRef](#)]
158. Rui, N.; Wang, Z.; Sun, K.; Ye, J.; Ge, Q.; Liu, C.-J. CO<sub>2</sub> hydrogenation to methanol over Pd/In<sub>2</sub>O<sub>3</sub>: Effects of Pd and oxygen vacancy. *Appl. Catal. B: Environ.* **2017**, *218*, 488–497. [[CrossRef](#)]
159. Wang, M.; Shen, M.; Jin, X.; Tian, J.; Li, M.; Zhou, Y.; Zhang, L.; Li, Y.; Shi, J. Oxygen vacancy generation and stabilization in CeO<sub>2-x</sub> by Cu introduction with improved CO<sub>2</sub> photocatalytic reduction activity. *ACS Catal.* **2019**, *9*, 4573–4581. [[CrossRef](#)]
160. Li, X.; Liu, Q.; Jiang, X.; Huang, J. Enhanced photocatalytic activity of Ga-N Co-doped anatase TiO<sub>2</sub> for water decomposition to hydrogen. *Int. J. Electrochem. Sci* **2012**, *7*, 11519–11527.
161. Wang, P.; Qi, C.; Wen, P.; Hao, L.; Xu, X.; Agathopoulos, S. Synthesis of Si, N co-doped nano-sized TiO<sub>2</sub> with high thermal stability and photocatalytic activity by mechanochemical method. *Nanomaterials* **2018**, *8*, 294. [[CrossRef](#)]
162. Qiu, M.; Tian, Y.; Chen, Z.; Yang, Z.; Li, W.; Wang, K.; Wang, L.; Wang, K.; Zhang, W. Synthesis of Ti<sup>3+</sup> self-doped TiO<sub>2</sub> nanocrystals based on Le Chatelier's principle and their application in solar light photocatalysis. *RSC Adv.* **2016**, *6*, 74376–74383. [[CrossRef](#)]
163. Zhu, K.; Shi, F.; Zhu, X.; Yang, W. The roles of oxygen vacancies in electrocatalytic oxygen evolution reaction. *Nano Energy* **2020**, *73*, 104761. [[CrossRef](#)]
164. Guo, S.; Di, J.; Chen, C.; Zhu, C.; Duan, M.; Lian, C.; Ji, M.; Zhou, W.; Xu, M.; Song, P. Oxygen vacancy mediated bismuth stannate ultra-small nanoparticle towards photocatalytic CO<sub>2</sub>-to-CO conversion. *Appl. Catal. B Environ.* **2020**, *276*, 119156. [[CrossRef](#)]
165. Santara, B.; Giri, P.; Imakita, K.; Fujii, M. Evidence of oxygen vacancy induced room temperature ferromagnetism in solvothermally synthesized undoped TiO<sub>2</sub> nanoribbons. *Nanoscale* **2013**, *5*, 5476–5488. [[CrossRef](#)]
166. Wang, Z.; Zhang, Y.; Neyts, E.C.; Cao, X.; Zhang, X.; Jang, B.W.-L.; Liu, C.-J. Catalyst preparation with plasmas: How does it work? *ACS Catal.* **2018**, *8*, 2093–2110. [[CrossRef](#)]
167. Feng, W.-H.; Yu, M.-M.; Wang, L.-J.; Miao, Y.-T.; Shakouri, M.; Ran, J.; Hu, Y.; Li, Z.; Huang, R.; Lu, Y.-L. Insights into Bimetallic Oxide Synergy during Carbon Dioxide Hydrogenation to Methanol and Dimethyl Ether over GaZrO<sub>x</sub> Oxide Catalysts. *ACS Catal.* **2021**, *11*, 4704–4711. [[CrossRef](#)]

168. Tabatabaei, J.; Sakakini, B.; Waugh, K. On the mechanism of methanol synthesis and the water-gas shift reaction on ZnO. *Catal. Lett.* **2006**, *110*, 77–84. [[CrossRef](#)]
169. Singh, R.; Tripathi, K.; Pant, K.K. Investigating the role of oxygen vacancies and basic site density in tuning methanol selectivity over Cu/CeO<sub>2</sub> catalyst during CO<sub>2</sub> hydrogenation. *Fuel* **2021**, *303*, 121289. [[CrossRef](#)]
170. Rhodes, M.D.; Bell, A.T. The effects of zirconia morphology on methanol synthesis from CO and H<sub>2</sub> over Cu/ZrO<sub>2</sub> catalysts: Part I. Steady-state studies. *J. Catal.* **2005**, *233*, 198–209. [[CrossRef](#)]
171. Martin, O.; Mondelli, C.; Cervellino, A.; Ferri, D.; Curulla-Ferré, D.; Pérez-Ramírez, J. Operando synchrotron X-ray powder diffraction and modulated-excitation infrared spectroscopy elucidate the CO<sub>2</sub> promotion on a commercial methanol synthesis catalyst. *Angew. Chem. Int. Ed.* **2016**, *55*, 11031–11036. [[CrossRef](#)]
172. Kattel, S.; Yan, B.; Chen, J.G.; Liu, P. CO<sub>2</sub> hydrogenation on Pt, Pt/SiO<sub>2</sub> and Pt/TiO<sub>2</sub>: Importance of synergy between Pt and oxide support. *J. Catal.* **2016**, *343*, 115–126. [[CrossRef](#)]
173. Wang, F.; He, S.; Chen, H.; Wang, B.; Zheng, L.; Wei, M.; Evans, D.G.; Duan, X. Active site dependent reaction mechanism over Ru/CeO<sub>2</sub> catalyst toward CO<sub>2</sub> methanation. *J. Am. Chem. Soc.* **2016**, *138*, 6298–6305. [[CrossRef](#)]
174. Srinivas, B.; Shubhamangala, B.; Lalitha, K.; Anil Kumar Reddy, P.; Durga Kumari, V.; Subrahmanyam, M.; De, B.R. Photocatalytic Reduction of CO<sub>2</sub> over Cu-TiO<sub>2</sub>/Molecular Sieve 5A Composite. *Photochem. Photobiol.* **2011**, *87*, 995–1001. [[CrossRef](#)]
175. Liu, B.-J.; Torimoto, T.; Matsumoto, H.; Yoneyama, H. Effect of solvents on photocatalytic reduction of carbon dioxide using TiO<sub>2</sub> nanocrystal photocatalyst embedded in SiO<sub>2</sub> matrices. *J. Photochem. Photobiol. A Chem.* **1997**, *108*, 187–192. [[CrossRef](#)]
176. Baltrusaitis, J.; Schuttlefield, J.; Zeitler, E.; Grassian, V.H. Carbon dioxide adsorption on oxide nanoparticle surfaces. *Chem. Eng. J.* **2011**, *170*, 471–481. [[CrossRef](#)]
177. Li, H.; Rameshan, C.; Bukhtiyarov, A.V.; Prosvirin, I.P.; Bukhtiyarov, V.I.; Rupprechter, G. CO<sub>2</sub> activation on ultrathin ZrO<sub>2</sub> film by H<sub>2</sub>O co-adsorption: In situ NAP-XPS and IRAS studies. *Surf. Sci.* **2019**, *679*, 139–146. [[CrossRef](#)]
178. Zhu, M.; Chen, J.; Shen, L.; Ford, M.E.; Gao, J.; Xu, J.; Wachs, I.E.; Han, Y.-F. Probing the surface of promoted CuO-Cr<sub>2</sub>O<sub>3</sub>-Fe<sub>2</sub>O<sub>3</sub> catalysts during CO<sub>2</sub> activation. *Appl. Catal. B: Environ.* **2020**, *271*, 118943. [[CrossRef](#)]
179. Posada-Borbón, A.; Grönbeck, H. CO<sub>2</sub> adsorption on hydroxylated In<sub>2</sub>O<sub>3</sub> (110). *Phys. Chem. Chem. Phys.* **2019**, *21*, 21698–21708. [[CrossRef](#)] [[PubMed](#)]
180. Ghuman, K.K.; Hoch, L.B.; Wood, T.E.; Mims, C.; Singh, C.V.; Ozin, G.A. Surface analogues of molecular frustrated Lewis pairs in heterogeneous CO<sub>2</sub> hydrogenation catalysis. *ACS Catal.* **2016**, *6*, 5764–5770. [[CrossRef](#)]
181. Martin, O.; Martin, A.J.; Mondelli, C.; Mitchell, S.; Segawa, T.F.; Hauert, R.; Drouilly, C.; Curulla-Ferre, D.; Perez-Ramirez, J. Indium Oxide as a Superior Catalyst for Methanol Synthesis by CO<sub>2</sub> Hydrogenation. *Angew. Chem. Int. Ed.* **2016**, *55*, 6261–6265. [[CrossRef](#)] [[PubMed](#)]
182. Tian, P.; Gu, M.; Qiu, R.; Yang, Z.; Xuan, F.; Zhu, M. Tunable Carbon Dioxide Activation Pathway over Iron Oxide Catalysts: Effects of Potassium. *Ind. Eng. Chem. Res.* **2021**, *60*, 8705–8713. [[CrossRef](#)]
183. Aziz, M.A.A.; Jalil, A.A.; Wongsakulphasatch, S.; Vo, D.-V.N. Understanding the role of surface basic sites of catalysts in CO<sub>2</sub> activation in dry reforming of methane: A short review. *Catal. Sci. Technol.* **2020**, *10*, 35–45. [[CrossRef](#)]
184. Nie, X.; Meng, L.; Wang, H.; Chen, Y.; Guo, X.; Song, C. DFT insight into the effect of potassium on the adsorption, activation and dissociation of CO<sub>2</sub> over Fe-based catalysts. *Phys. Chem. Chem. Phys.* **2018**, *20*, 14694–14707. [[CrossRef](#)]
185. Miao, L.; Wang, J.; Zhang, P. Review on manganese dioxide for catalytic oxidation of airborne formaldehyde. *Appl. Surf. Sci.* **2019**, *466*, 441–453. [[CrossRef](#)]
186. Peng, Y.; Wang, L.; Luo, Q.; Cao, Y.; Dai, Y.; Li, Z.; Li, H.; Zheng, X.; Yan, W.; Yang, J. Molecular-level insight into how hydroxyl groups boost catalytic activity in CO<sub>2</sub> hydrogenation into methanol. *Chem* **2018**, *4*, 613–625. [[CrossRef](#)]
187. Stacchiola, D.J.; Senanayake, S.D.; Liu, P.; Rodriguez, J.A. Fundamental studies of well-defined surfaces of mixed-metal oxides: Special properties of MO<sub>x</sub>/TiO<sub>2</sub> (110){M= V, Ru, Ce, or W}. *Chem. Rev.* **2013**, *113*, 4373–4390. [[CrossRef](#)]
188. Witton, T.; Numpilai, T.; Phongamwong, T.; Donphai, W.; Boonyuen, C.; Warakulwit, C.; Chareonpanich, M.; Limtrakul, J. Enhanced activity, selectivity and stability of a CuO-ZnO-ZrO<sub>2</sub> catalyst by adding graphene oxide for CO<sub>2</sub> hydrogenation to methanol. *Chem. Eng. J.* **2018**, *334*, 1781–1791. [[CrossRef](#)]
189. Ma, Q.; Geng, M.; Zhang, J.; Zhang, X.; Zhao, T.S. Enhanced Catalytic Performance for CO<sub>2</sub> Hydrogenation to Methanol over N-doped Graphene Incorporated Cu-ZnO-Al<sub>2</sub>O<sub>3</sub> Catalysts. *ChemistrySelect* **2019**, *4*, 78–83. [[CrossRef](#)]
190. Qi, Y.; Jiang, J.; Liang, X.; Ouyang, S.; Mi, W.; Ning, S.; Zhao, L.; Ye, J. Fabrication of black In<sub>2</sub>O<sub>3</sub> with dense oxygen vacancy through dual functional carbon doping for enhancing photothermal CO<sub>2</sub> hydrogenation. *Adv. Funct. Mater.* **2021**, *31*, 2100908. [[CrossRef](#)]
191. Tomboc, G.M.; Tesfaye Gadisa, B.; Jun, M.; Chaudhari, N.K.; Kim, H.; Lee, K. Carbon Transition-metal Oxide Electrodes: Understanding the Role of Surface Engineering for High Energy Density Supercapacitors. *Chem.—Asian J.* **2020**, *15*, 1628–1647. [[CrossRef](#)]
192. Chatterjee, D.P.; Nandi, A.K. A review on the recent advances in hybrid supercapacitors. *J. Mater. Chem. A* **2021**, *9*, 15880–15918. [[CrossRef](#)]
193. Yang, Y.; White, M.G.; Liu, P. Theoretical study of methanol synthesis from CO<sub>2</sub> hydrogenation on metal-doped Cu (111) surfaces. *J. Phys. Chem. C* **2012**, *116*, 248–256. [[CrossRef](#)]
194. Surnev, S.; Fortunelli, A.; Netzer, F.P. Structure–property relationship and chemical aspects of oxide–metal hybrid nanostructures. *Chem. Rev.* **2013**, *113*, 4314–4372. [[CrossRef](#)] [[PubMed](#)]



- 
195. Wang, H.; Wang, L.; Lin, D.; Feng, X.; Niu, Y.; Zhang, B.; Xiao, F.-S. Strong metal–support interactions on gold nanoparticle catalysts achieved through Le Chatelier’s principle. *Nat. Catal.* **2021**, *4*, 418–424. [[CrossRef](#)]
  196. Meng, C.; Zhao, G.; Shi, X.-R.; Chen, P.; Liu, Y.; Lu, Y. Oxygen-deficient metal oxides supported nano-intermetallic InNi<sub>3</sub>C<sub>0.5</sub> toward efficient CO<sub>2</sub> hydrogenation to methanol. *Sci. Adv.* **2021**, *7*, 1–11. [[CrossRef](#)] [[PubMed](#)]